Ministry of Higher Education and

Scientific Research

University of Diyala

College of Science

Department of Chemistry

Spectroscopic and surface study of deactivated and Nano catalysts

A Thesis Submitted to Council of the College of Science, University of Diyala in Partial Fulfillment of the Requirements for the Degree of Master of

Science in Chemistry

by

Baraa Asaad Latoof

B.Sc. In Chemistry Science

College of Science - University of Diyala

Supervised by

Prof. Dr. Karim Henikish Hassan

2021 AD **IRAQ** **1443 AH**

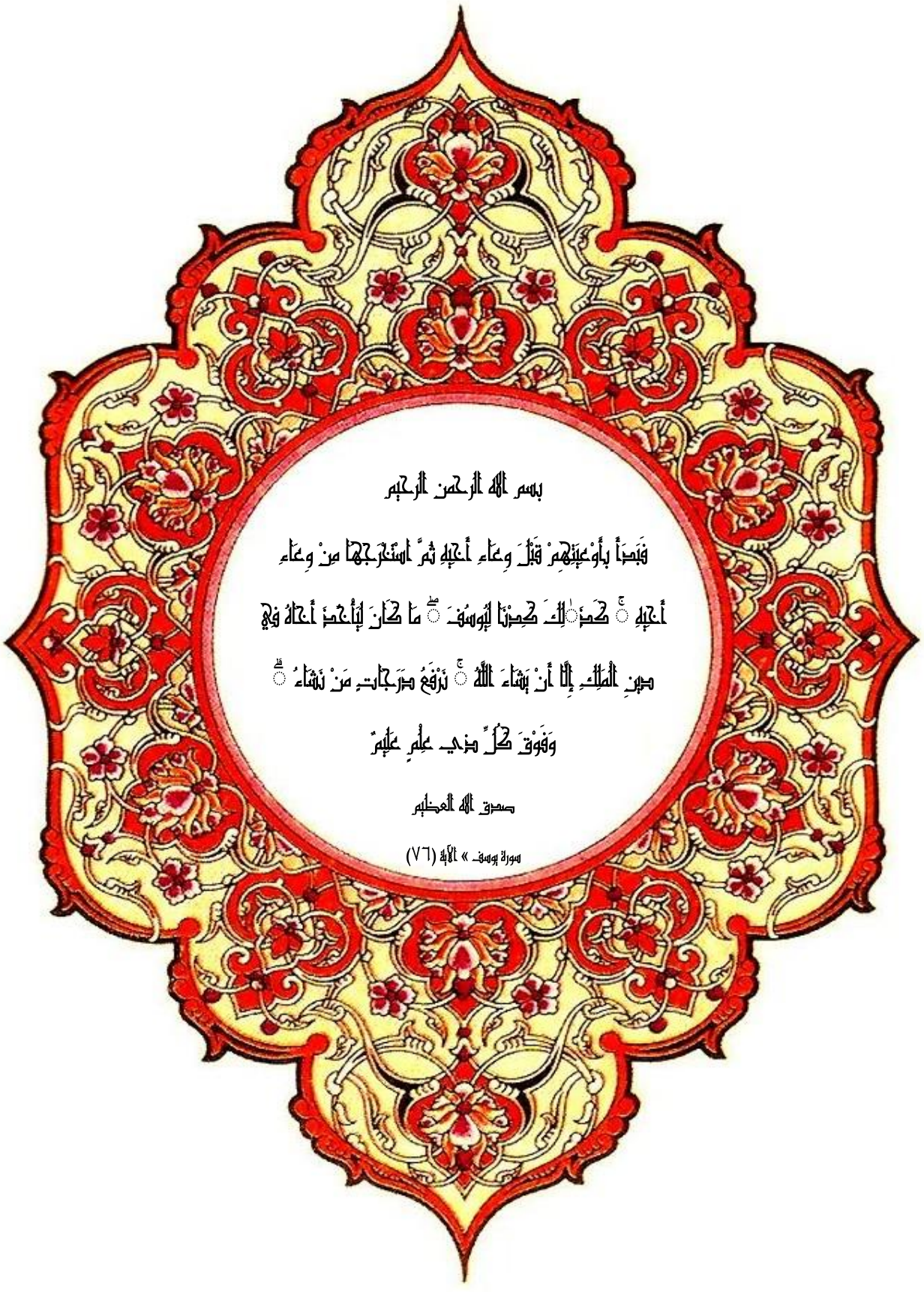

بسم الله الرحمن الرحيم

فَبَدَأَ بِأَوْعِيَتِهِمْ قَبْلَ وِعَاءِ أَخِيهِ ثُمَّ اسْتَخْرَجَهَا مِنْ وِعَاءِ
أَخِيهِ ۚ كَذَٰلِكَ كِدْنَا لِيُوسُفَ ۖ مَا كَانَ لِيَأْخُذَ أَخَاهُ فِي
دِينِ الْمَلِكِ إِلَّا أَنْ يَشَاءَ اللَّهُ ۚ نَرْفَعُ دَرَجَاتٍ مَنْ نَشَاءُ ۗ
وَفَوْقَ كُلِّ ذِي عِلْمٍ عَلِيمٌ

صدق الله العظيم

سورة يوسف » الآية (٧٦)

Dedication

To my strength in life my dearest Father

To the symbol of goodness ,kindness and sacrifice, My mother, To the luminous stars who shine in my dark night , my Sisters and Brothers.

To everyone who loved me and wished me well my dearest friends.

BARAA ...

Acknowledgment

I thank Allah who helped me to complete this work I would like to express my sincere gratitude, thanks to my supervisor prof. Dr. Karim Henikish Hassan for the support in my M.SC. study and also for patience, constant encouragement and valuable assistance through the whole research period.

Special thanks are extended to the Dean and President of the Chemistry Department and staff , College of Science, Diyala University. Thanks also to all postgraduate unit staff, dean assistant for scientific affairs staff.

Finally, I would thanks everyone who helped me directly or indirectly in this work

BARAA

ABSTRACT

This work, we present the physical and chemical studies and comparison of the new and spent NiMo/γ-Al_2O_3 catalysts. The investigation of deactivated catalysts phenomena was done using different characterizations including, Thermo gravimetric analysis (TGA) , X-ray diffraction (XRD) Energy Dispersion X-ray (EDX) , Field Emission Scanning Electron Microscopy (FESEM) , Atomic Force Microscopy (AFM), Fourier Transform Infrared Spectroscopy (FTIR) and Raman analysis . The comparison study between the new and spent NiMo/γ-Al_2O_3 catalysts show that the particle's size and shape were changed due to the consumption process.

The nano NiMo/ γ-Al_2O_3 catalyst was prepared based on impregnation method of nickel chloride (as a source of nickel) and ammonium molybdate (as a source of molybdenum) on the alumina with calcination at a temperature of 500 ºC for (6 hours). The results of characterizations showed that, the particle size of the prepared nano NiMo/ γ-Al_2O_3 catalyst was around 11.903 nm. The spent NiMo/ γ-Al_2O_3 catalyst was activated first by washing it with benzene and toluene at 25ºC, then the dried catalyst was exposed to carbon disulfide (CS_2) for 12 hours. Afterward, the catalyst was calcined at 450 ºC to completely remove all the carbon and sulfur compounds.

The amount of metals present was determined in the new and spent catalysts. It was found that there is a clear increase in the metals or elements content in the spent catalysts that come from both the feed and the reactants in addition to those that come from corrosion of reactor due to harsh operating conditions and time.

It was observed also that there are clear changes in the physical properties such as the density and porosity of the primary catalysts due to deposition of carbon, sulfur and some minerals and the change in their structure composition.

The kinetic study of the carbon removal process was carried out on spent $NiMo/Al_2O_3$ catalysts at different calcinated temperatures (723, 773, 823 and 873 K) and at a different period of time (30, 60 , 90 and 120 minutes). From calculating the values of the thermodynamic functions for the kinetics of removing carbon (E_a, ΔH, ΔS), it was found that it is an endothermic reaction, two kinetic equations were used, a first-order equation and a second-order equation. The results show that the kinetics of the carbon removal was fit with the first order equation because the correlation coefficient (R^2) gave the highest value compared to the second order model.

List of Contents

List of Tables

List of Figure

List of Symbols and Abbreviations

Symbol or Abbreviation	Definition
K	absolute reaction temperature
E_a	apparent activation energy
AAS	Atomic absorption spectrophotometer
AFM	Atomic force microscopy
Ra	Average roughness
K_b	Boltzmann constant
d_b	bulk density
DTA	Differential thermal analysis
EDX	Energy-dispersive X-ray spectroscopy
ΔH^*	enthalpy of activation
ΔS^*	entropy of activation
EPA	Environmental Protection Agency
A	Factor in the Arrhenius equation
FESEM	Field Emission Scanning Electron Microscopy
FCC	Fluid catalytic cracking process.
FTIR	Fourier transform infrared spectroscopy
FWHM	Full width at half maximum
$t_{1/2}$	half-life
HDM	Hydrodemetallization

HDS	***Hydrodesulfurization Process***
HDT	***hydrotreating***
$NiMo/Al_2O_3$	***Nickel molybdenum/ alumina***
d_p	***Particle density***
h	***Plank constant***
θ	***Porosity***
K_1	***Pseudo-First Order Constant***
K_2	***Pseudo-Second Order Constant***
RMS	***Root mean square***
d_s	***Skeletal Density***
R_{ku}	***Surface kurtosis***
R_{sk}	***Surface skewenss***
$[C]_t$	***The carbon weight at any time***
$[C]_o$	***The initial carbon weight***
TGA	***Thermo gravimetric analysis spectroscopy***
K	***transmission coefficient***
R	***universal gas constant***
ε	***Void fraction***
XRD	***X-Ray Diffraction***

CHAPTER ONE

Introduction

1.1 General Introduction

The catalysts were widely used in refining and chemical processing industries for many years. With nearly 75% of catalysis chemical processes, the catalyst market increases by 5% in a year. Used alumina, zeolite, carbon, silica, zirconia or clay materials as support for catalysts . like nickel, platinum, barium, molybdenum, cobalt, copper, iron , etc. [1] .

The amount of catalysts consumed with mineral pollution from water treatment units has increased widely in recent years due to the rapid growth in the upgrading capacity of residual oil and heavy treatment through the hydrotreating process [2,3]. Due to constant changes in legislative requirements for transportation fuels, the process of hydrodisulfurization (HDS) is currently receiving increased attention. Oil refineries face the challenge of achieving new specifications by improving hydrotreating performance . Although conventional (NiMo and CoMo) catalysts have been widely used in commercial hydrotreating for several decades already ,but only little is known about the deactivation mechanism of these catalysts [4]. Up to (50%) of the initial activity may be lost from the catalyst within a few days on stream . It is important to investigate this phenomenon in more detail using various quasi in situ techniques. If answers can be found to the question why the catalyst deactivates initially ,disabled its performance can be improved by changing the catalyst characteristics or operating conditions. There are many possible reasons for the catalyst to deactivate [5].

The dispersion loss may be due to the loss of the active phase (sintering). Also, the active sites may change during the reaction, resulting in reduced activity, active sites may be poisoned or blocked by coke. Finally, the catalysts may be blocked by coke deposition, resulting in a loss of accessible pore volume and surface area, in the long term, regeneration of these catalysts will become impossible due to irreparable disruption, and spent catalysts will be disposed of as solid waste [6, 7].

When used, these catalysts are depleted due to loss of surface area, sintering and formation of surface deposits of carbon and sulfur, etc. After a certain period, new catalysts must be loaded into the reactors and such replacement, expensive costs are a major expenditure component in the chemical and allied industries. Spent catalysts also contribute to a large amount of solid waste generated in process industries [1].

With the exponential increase in the use of catalyst worldwide, sulfur, one of the most dangerous air pollutants from burning transportation fuels, has become a major environmental concern [8]. In recent years, many countries have launched new environmental legislation aimed at reducing the release of sulfur into the atmosphere. For example, the United States Environmental Protection Agency (EPA) has adopted a strict list to reduce the sulfur level in gasoline from 500 to 30 parts per million in 2007. The new regulation has presented a technical challenge to existing commercial desulfurization operations [9].

Additionally, petroleum contains many molecules that include heterogeneous atoms such as sulfur, nitrogen, and vanadium. The most common heteroatom containing molecules are thiophene type compounds. These sulfur-containing materials are indispensable in industry, agriculture and medicine, but also caused most problems in the oil recovery industry. In particular, the required level for desulfurization of petroleum products is gradually increased [4].

Many types of (HDS) catalyst are now utilized in the oil industry depending on the feed properties and reaction conditions . The most important factor in hydrotreating process is the catalyst [10-12] CoMo / Al_2O_3 and NiMo / Al_2O_3 are widely used to remove sulfur, nitrogen, oxygen, metals and other pollutants from crude oil part under operating conditions. In these mixed catalysts , metals uses by working as an active component and their activity is enhanced by presence of cobalt (Co) or nickel (Ni) [12,13]. A regenerated (HDS) catalyst is also increasing estimated at more than 30,000 tons every year worldwide [14].

Spent catalysts from are classified as hazardous waste by (USEPA). May emit toxic gases, prone to spontaneous ignition, and contain heavy metals and carcinogenic compounds. Even after high temperatures metals such as nickel, vanadium, cobalt, and molybdenum can be filtered out through many processes [15] . Until now, Al_2O_3 has been the most widely used support material in HDS catalysts because it has reasonably high surface area and porosity, easily forming into desired forms with excellent mechanical strength and hydrothermal stability [16-20].

The amount of spent catalysts discharged from different process units depends largely on the amount of new catalysts used, their age, and their components during use in the reactors . Due to increasing cost of disposal and transportation of spent catalysts, increase in the cost of metals, increasing environmental concerns and legislation regarding the disposal of hazardous spent catalysts, companies and countries are being forced to process their own waste products and residues. The metal recovery depends on several factors: sample nature (chemical composition), processed raw materials, metal price, environmental guidance, and the distance between the operating plant , recycling industry, and operating costs [1].

1.2. Literature survey

(Kaluža & Zdražil , 2007) synthesis ($CoO-MoO_3/\gamma-Al_2O_3$, $NiO-MoO_3/\gamma-Al_2O_3$) catalysts by the reaction of the α-boehmite (α-AlOOH) with MoO_3 in aqueous paste, followed by the interaction of (MoO_3/α-AlOOH) catalyst with ($Co(OH)_2 \cdot CoCO_3$) or ($2NiCO_3 \cdot 3Ni(OH)_2 \cdot 4H_2O$) in aqueous paste and by subsequent drying and calcination .The deposited MoO_3 worked as a thermal stabilizer inhibiting the sintering of the (Al_2O_3) phase during calcination. The deposited (Co and Ni) were efficient activity promoters in benzo thiophene (HDS) [21].

(Guichard,et.al,2009) were characterized deposits of the spent catalysts in order to compare its behavior in terms of quantity, molecular order and interaction between a cobalt and nickel configuration catalyst. (TGA), (RAMAN), (NMR), (^{13}C spectroscopy). It was used to evaluate coke interaction. All observed characteristics are related to three-phase disabling system. In the first phase, Alumina is assumed to be covered quickly by coke, while active sites remain protected through their high hydrogenation activity. The nickel is separated from MoS_2 molecules during aging and the graphite-like crystallite extends significantly . In the last step of the development of coke, can be assumed that some organization occurs in molecular structure of coke [22].

(Vakros ,et.al,2010) were prepared four CoMo catalysts supported on Al_2O_3-SiO_2 mixed materials of varying SiO_2 content (1.5, 10, 20 and 30% SiO2 w/w) following the co-EDF methodology , The catalysts were characterized using various techniques (BET, potentiometric mass titrations, XRD, DRS, XPS, LRS, TPR, TPD of ammonia and NO chemisorption). Two additional catalysts were prepared and characterized following the conventional impregnation procedure. The following activity trend was obtained over the catalysts, 20Si > 30Si > 1.5Si > 10Si, which indicates that the activity is maximized over the catalyst [23].

(Karim Henikish ,et.al,2018) studied the rejuvenated for spent NiMo/γ-Al_2O_3 hydrodesulfurizaion catalyst was using n-hexane to remove the soluble coke and the oxalic acid to remove the foulant elements and insoluble coke. Characterized by AFM techniques, and , the lead ion was separated from its aqueous solution via the adsorption batch method with varying concentrations of the lead ions, and then, the absorption efficiency was calculated. The results indicated that the removal efficiency of more than 99% was resulted when the rejuvenated NiMo/Al_2O_3 catalysts were used, compared with 51 % removal when a none rejuvenated one was used. [24].

(Kubicka & Horácek,2011) studied deactivation of HDS catalysts in deoxygenation of vegetable oils, Several rapeseed oils used as feedstocks for deoxygenation over sulfided CoMo/γ-Al_2O_3 catalyst. Refined rapeseed oils were converted to hydrocarbons more efficiently than neat rapeseed oil, The high concentration of phospholipids in trap grease ,the main reason for the deactivation is coke. The high concentration of alkalis in waste rapeseed oil was the main reason for increased deactivation in comparison with neat rapeseed oil [25].

(Karim, et.al, 2011), studied preparation of alumina by sol-gel technique and using urea in aqueous media. The resulting sol composed of $Al(OH)_3$ particles was heated at 280°C to get alumina particles. The γ-Alumina powder is characterized by (FTIR, XRD and BET) techniques. Electron micrograph shows that the particles are nano sized having non-spherical shape [26].

(Pacheco, et.al, 2011) studied kinetic approach in order to observe the impact of accelerated deactivation conditions upon catalyst performances during hydrodesulfurization (HDS), hydrodenitrogenation (HDN), and aromatic hydrogenation (HDA) reactions. Results obtained with a reference catalyst indicate that the proposed methodology is able to deactivate the catalyst effectively, leading to proper representation of actual industrial deactivation at the end of a catalyst life cycle [27].

(Zhang, et.al, 2011) studied the catalyst deactivation and the regeneration method by (XRD), N_2 adsorption-desorption, (IR), and (IR-NH_3). These characterizations indicated that coke formation was the main reason for the catalyst deactivation. To regenerate the deactivated catalyst, two methods, i.e. ,calcination and methanol leaching, were used. (IR and IR-NH_3) characterizations showed that both methods can eliminate coke deposited on the catalyst and make the catalyst reactivated. (XRD) showed that the structure of the catalyst did not change after regeneration [28].

(Luiz de souza ,et.al,2011) studied a three-step pre-treatment route for processing spent commercial NiMo/Al_2O_3 catalysts. Extraction of soluble coke with n-hexane and leaching of foulant elements with oxalic acid. Oxidized catalysts were leached with 9 mol L^{-1} sulfuric acid. Iron was the only foulant element partially leached by oxalic acid .The amount of insoluble matter in sulfuric acid was drastically reduced. Losses of active phase metals (Ni, Mo) during leaching with oxalic acid were compensated by the increase of their recovery in the sulfuric acid leached [29].

(Yudong, et.al ,2012) studied the element compositions of spent catalyst ($NiMo/Al_2O_3$) from a commercial fixed-bed residue hydrotreating unit and investigate the reasons for the catalyst deactivation .Depositions of C, H, S, N, Ni and V on the spent catalysts were studied , The deposition amount of elements was mainly related to local reaction conditions and catalyst loading states in the fixed-bed, The catalysts with high metal depositions have low contents of coke, high contents of sulfur and high H/C, which indicates that residue hydrotreating is an autocatalytic process. Metal sulfides deposited on catalysts have a hydrogenation activity in residue hydrotreating. The coke on residue hydrotreating catalysts mainly comes from some specific condensed ring structures containing nitrogen existed in asphaltene which is difficult to hydrotreat [30].

(Rahmanpour, et.al, 2012), studied a new way to synthesis the nano size (γ-Al_2O_3) by precipitation methods under ultrasonic vibration mixing dehydration of methanol to dimethyl ether . The shaped alumina is characterized by using SEM, XRD, BET and TPD technologies. The materials in the nano-scale show different characteristics in comparison with their bulk state [31].

(Behnejad, et. al, 2019) were synthesized a bimetallic nickel–molybdenum catalyst supported on γ-alumina by the two-step incipient wetness impregnation technique. The activity of the prepared Ni–Mo/γ-alumina catalyst was evaluated in a down flow fixed-bed micro-reactor. In this way, hydrodesulfurization (HDS) and hydrodenitrogenation (HDN) reactions of the main distillate fractions of crude oil were assessed. XRD, SEM, TPR, ICP-OES, BET–BJH and nitrogen adsorption/desorption methods were used for characterizing the synthesized Ni–Mo/γ-alumina catalyst. [32].

(Bleken, et.al,2013) studied the deactivation behaviors of a regular, commercial ZSM-5 catalyst and its mesoporous, desilicated counterpart have been investigated and compared, After partial deactivation in the conversion of methanol to hydrocarbons at high pressure and characterized by several spectroscopic techniques, gas adsorption measurements, thermo gravimetry , remarkable differences between the desilicated and the parent H-ZSM-5 catalysts are seen [33].

(Ahn, et.al,2014) ,studied mesoporous cobalt oxide (Co_3O_4) prepared through the template-replicating method by using the templating material of KIT-6 , and its catalytic activity for CO hydrogenation to hydrocarbons by the Fischer–Tropsch (FT).Different deactivation phenomena were observed during the (FT) reaction due to collapse of the pore structure and carbon deposition on mesoporous Co_3O_4 , The different catalytic performance and deactivation behavior of the two Co_3O_4 catalysts were mainly due to the variation of surface morphologies and the types of coke formed [34].

(Xiaodong Yi,et.al,2017) were studied a simple and solvent-free solid-state method to prepare NiMo–Al_2O_3 (HDS) catalyst using $Ni(NO_3)_2.6H_2O$, $(NH_4)6Mo_7O_{24}.4H_2O$, and $AlCl_{l3}.6H_2O$ as the solid raw materials and polyethylene glycol (PEG) as an additive and characterized by it nitrogen adsorption–desorption measurements, powder X-ray diffraction (XRD), thermogravimetric analysis/differential scanning calorimetry (TGA/DSC), H_2 temperature-programmed reduction (H_2-TPR), X-ray photoelectron spectroscopy (XPS), scanning electron microscopy (SEM) and high resolution transmission electron microscopy (HRTEM). The results are visible that excess polyethylene glycol (PEG) leads to the decrease in specific surface area and pore volume attributed to the metal sintering caused by the strong heat release during thermal decomposition [35] .

(Tavizón-Pozos,et.al,2016) studied effect of Mixed Al_2O_3-TiO_2 oxide (Al / Ti = 2, named AT2) support on metal reaction in the case of oxide state and its effect on MoS_2 dispersion and it's the impact on the hydro deoxy genating of phenol reaction , the sulfided (CoMo/AT2) catalyst reached (85%) higher catalytic activity on the hydro deoxy genation of phenol than ($CoMo/Al_2O_3$) [36].

(Kim,et.al,2016) prepared the ($CoMo/Al_2O_3$, $CoMo/CeO_2$, $CoMo/TiO_2$) catalysts using the ultrasonic spray pyrolysis and activities of the synthesized catalysts toward the (HDS) of (4, 6-dimethyldibenzothiophene) were examined using a flow reactor . Measurement results using (XRD), (SEM) field emission gun ,electron probe micro analyzer and the transmission electron microscope , the analysis of surface properties raman spectroscopy , identified the characteristic phases such as ($Ce_2Mo_3O_{13}$, MoO_3, and $CoMoO_4$) of each synthesized catalyst . the evaluation of catalytic activity showed that the order of (HDS) activity is ($CoMo/CeO_2$ > $CoMo/Al_2O_3$ > $CoMo/TiO_2$) . In particular a ($CoMo/CeO_2$) catalyst exhibits the utmost catalytic activity toward (HDS), reducing the amount of (4,6-dimethyldibenzothiophene)from (10 ppm) to about (0.1 ppm) at 350 ^oC [37].

(Mohamed & Atta , 2016) prepared Nano γ- Al_2O_3 support by coprecipitation method using different calcination temperatures (550,650, and 750) ^oC and prepared Nano NiMo/ γ-Al_2O_3 catalyst by impregnation method with nickel carbonate and ammonium paramolybdate with Nano γ-Al_2O_3 support at calcination temperature of 550 ^oC . It was characterized by utilizing X-ray diffraction, X-ray fluorescent, AFM, SEM, BET surface area, and pore volume [38].

(Hassan, et.al, 2017) studied prepared copper oxide nanoparticles by sol-gel method and then use to remove the Cd (II) and Ni (II) from aqueous solution by it . Copper oxide nanoparticles characterized by XRD, SEM, TEM, and AFM . The XRD explain that the average size of CuO was around 21.11 nm [39].

(Jbara,et.al, 2017) prepared γ-Al_2O_3 by co-precipitation under annealing temperature effect, structural characterization using XRD analysis indicated that the particle diameter ranging from 6 to 24 nm of gamma phase alumina .The surface area of the prepared nano powders is in the range of (109 to 367)., the morphology analysis indicates that γ-Al_2O_3 nanopowders are consisted of grains almost spherical in shape [40].

(Tabesh ,et.al,2018) prepared γ-Al_2O_3 by using modified sol–gel method where aluminium nitrate, ethylene glycol (EG), citric acid and triethanol amine (TEA) were used as an Al^{+3} source, gel, chelating and surfactant agents, respectively. Structural characterization using X-ray diffraction (XRD), scanning electron microscopy (SEM), thermo gravimetric analysis (TGA) and infrared spectroscopy (IR). Then, the removal efficiency of heavy metal ions (lead and cadmium) in the adsorption process by the as-synthesized alumina nanoparticle has been investigated in pH (5) ,contact time of the 20 min and 30 min for Pb^{+2} and Cd^{+2} respectively [41].

(Munguía-Guillén ,et.al,2018) Prepared series of CoMo/γ-Al_2O_3 catalysts by a reverse micro emulsion method using 1-butanol as organic agent and cetyl trimethyl ammonium bromide as surfactant, The materials were prepared at different solution concentrations in order to obtain different metal contents ,Samples were characterized by X-ray diffraction, Raman spectroscopy, nuclear magnetic resonance and nitrogen physisorption, . All samples with the exception of that with the highest metal content were amorphous as shown by X-ray diffraction. By Raman

spectroscopy, Mo-O-Mo and MoO_2 species were observed in all calcined samples. Mo-O-Co , Al-O-Mo , monomers and hetero poly molybdates were observed for the lower metal content samples, and the formation of $CoMoO_4$ and aluminum molybdate species for the higher metal contents. These results suggest that the materials with lower metal loading have species that are easily sulfidable and provide high activity in hydrodesulfurization reactions. A model for the interaction of the species in the aqueous phase of the micelle is presented [42] .

(Pimerzina, et.al,2018) studied a reactivation of industrial $CoMo/Al_2O_3$ hydrotreating (HDT) catalysts. are used for about 2.5 years. It was oxidatively regenerated and rejuvenated by organic acids. characterized by the elemental analysis, N_2 physisorption ,(XRD),(XPS),(TGA),(HRTEM). It was found that oxidative regeneration allowed restoring about 70–85% , of initial activity. .Resulting catalytic activity of the reactivated catalysts depended on the properties of the formed active phase species [43].

(Stummann, et.al, 2019) studied deactivation of a sulfided $CoMo/MgAl_2O_4$ catalyst during fluid bed catalytic hydropyrolysis of biomass (beech wood). A secondary hydrotreating reactor with a sulfided $NiMo/Al_2O_3$ catalyst was used, the results shown that potassium, a known catalyst poison, is transferred from the beech wood to the catalyst, and the effect of doping the catalyst with 1.9 wt % potassium was therefore also investigated , Doping the catalyst with potassium also increased the char and coke yield Catalyst deal with Potassium also increased the yield of coal and coke from 13.3 to 14.6% dry weight, indicating that potassium could act as a catalyst pyrolysis vapors polymerization [44].

(Liu,et.al,2020) were prepared a series of NiMo/γ-Al_2O_3 hydrodesulfurization (HDS) catalysts with different metal–support interactions by a conventional impregnation method through changing the calcination temperature. Catalysts were characterized by X-ray fluorescence spectroscopy, X-ray diffraction, N_2 adsorption–desorption ,ultra violet–visible spectroscopy, Raman spectroscopy, H_2 temperature-X-ray photoelectron spectroscopy, and high resolution transmission electron microscopy. These results suggest that the Ni–Al_2O_3 interaction imposes a more dominant influence on the HDS catalysts. The (HDS) performance was evaluated using dibenzothiophene as the model reactant, and through correlating the catalyst structures with the activity, an original suggestion about the effects of the Ni-Al_2O_3 interaction on HDS performance was given the Ni–Al_2O_3 interaction not only enhances the availability of surface nickel atoms to form more Ni-Mo–S active sites, but also improves the microstructures of MoS_2, i.e., shorter nanoslabs and higher stacking layers, which together enhance the apparent activity and intrinsic activity of Ni–Mo catalysts [45].

(kohli,et.al,2020), was demonstrated The effect of various stents such as silica and activated carbon (AC) and Alumina mesoporous (Al_2O_3) on the catalyst activities of hydrotreating nickel molybdenum (NiMo) to improve nitrogen absorption-desorption analysis shown the silica and the (NiMo) stream-backed with a very high surface area. Analysis (XRD) showed that active minerals were dispersed in catalysts. Detection analysis (TEM) for the presence of active MoS_2 sites in the NiMo /Al_2O_3 catalyst. The results supported that the catalyst that has a large pore diameter, high pore volume, and better active metals dispersion is highly desirable for upgrading of a vacuum residue [46].

(Hamidi, et.al, 2020) were synthesized alumina supported NiMo nanocatalysts through ultrasonic-assisted combustion method with various organic additives, including citric acid, ethylene glycol, glycine and urea using in hydrodesulfurization of thiophene at atmospheric pressure. The samples were characterized by XRD, TGA, FESEM, EDX, BET-BJH and TPR analysis. The results indicated that the type of organic compound has a noticeable effect on phase structure, surface morphology and reducibility potential as a consequence of different amount of heat and gaseous products released during combustion reaction [47].

1.3 Aim of the present study

The aim of the present study can be summarized in:

1-Investigate the phenomenon of deactivation of catalysts in more detail using different techniques.

2- Comparison the Physical and chemical study for the new and spent NiMo/γ-Al_2O_3 catalysts .

3 – Synthesis nano NiMo/γ-Al_2O_3 using the impregnation method (one-pot synthesis.

4- Regeneration of spent NiMo/γ-Al_2O_3 catalyst.

5- Determination of the amount of metals present in new and spent catalysts.

6- Determine of some physical properties such as (density, Pore volume, porosity and void fractions).

7- kinetic study of carbon removal process from spent NiMo/Al_2O_3 catalysts**.**

8- determination of thermodynamic potential such as ΔH , ΔS , Ea

CHAPTER TWO

Theoretical Part

2.1.Catalyst and catalysis

2.1.1. Definition

Catalyst can be defined as a substance that increases the rate of the reaction in which a chemical reaction approaches equilibrium without permanently interfering with the reaction and can return to its original form without being destroyed or consumed at the end of the reaction. It has several industrial and environmental uses and applications and this is done by reducing the activation energy , (E_a) of the reaction as shown in figure (2.1) [5] .

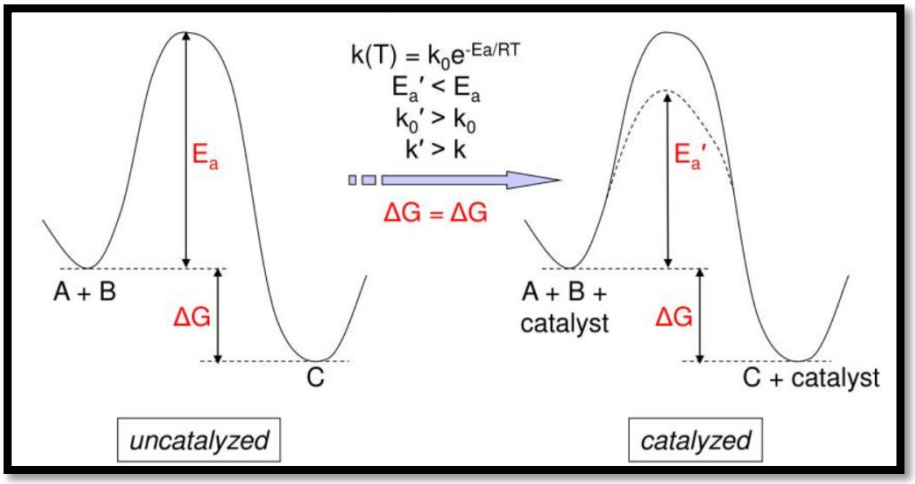

Fig (2.1)Potential energy diagram of a heterogeneous catalytic reaction[5].

Requirements for a good catalyst is activity ,selectivity and stability ,the solid catalyst should have reasonably large surface area needed for reaction (active sites). The catalyst plays a major role in chemical transformations and lies in the heart of countless chemical protocols, from academic research at the laboratory level to the chemical industry level [48]. Catalysis contributes the mechanism by which chemical transformations take place thus enabling the commercially viable creation of desired materials . By using catalysts manufacturing protocols can be made thus more economic and sustainable [49].

Among three well-known catalysis categories for example (homogeneous , heterogeneous and enzymatic catalysis) enzymatic catalysis is the most efficient and greenest catalysis found in nature. Both the homogeneous and heterogeneous catalysis has its own merits and demerits due to which there is urgent need of a new catalytic system as shows in **table (2.1)** which should be active like homogeneous catalysis, and should also easily be recoverable like heterogeneous catalyst [50].

Table (2.1) Comparative efficiency of homogeneous, heterogeneous .

Homogeneous Catalysis	Heterogeneous Catalysis
Merits:	**Merits:**
1. single phase	1. multiphase
2. typically liquid	2. mostly solid-liquid and solid-gas
3. low temperature	3. high temperature
4. High activity	4. Excellent stability
5.High chemo-and region selectivity	5. Easy accessibility
Demerits:	**Demerits:**
1.separation are tricky	1.design and optimization tricky
2.Cumbersom product purification and difficulty in catalyst recovery	2.Inferior catalytic activity relative to their counterpart homogeneous and requires more reaction time

Nano catalysts has collected the advantages of homogeneous and heterogeneous catalyst systems. The Nano catalytic system allows rapid and selective chemical transformations with an excellent product yield as well as easily catalyst and recovery . However, the distributions of wide pore size is not useful for effective catalytic reactions [51].

Further integration of different metal oxides (NiO , V_2O_5, CeO_2, and CaO) into arranged medium porous alumina channels resulted in novel catalysts with high catalytic activities in various reactions [53].

2.1.2.Catalyst classification according to phase.

1.Homogeneous Catalysis

The catalyst is the same phase as the reactants and products, examples are hydrolysis of esters by acids (liquid-liquid), oxidation of SO_2 by NO_2 (vapor-vapor), and decomposition of potassium chlorate by MnO_2 (solid-solid). Usually, the liquid phase is most common, with both catalyst [54].

2.Heterogeneous Catalysis

In these systems the reactants and catalyst exist in different phases. Most commonly, solid catalysts are used with gaseous or liquid reactants, sometimes both. Other permutations are possible but less often encountered. Phase here refers not only to solid, liquid, gas, but also immiscible liquids, for example, oil and water. The great majority of practical heterogeneous catalysts are solids and the great majority of reactants are gases or liquids. Heterogeneous catalysis is of paramount importance in many areas of the chemical and energy industries [55,56].

3.Enzyme Catalysis

Enzymes are protein molecules of colloidal size, somewhere between the molecular homogeneous and the macroscopic heterogeneous catalyst. There is great interest in harnessing enzyme catalysis for industrial use ,for several reasons, it has the ability to withstand extreme conditions [55] .

2.2 Catalyst composition

Most catalysts have three type of easily distinguished component :

• **Active phase** : Active components are responsible for the principal chemical reaction. Selection of the active component is the first step in catalyst design. As knowledge of catalytic mechanisms on various materials advances, methods for selection are becoming more scientific, if perhaps still empirical [57].

• **Promoter :** A promoter is some third agent when added, often in small amounts results in desirable activity, selectivity or stability effects [57].

• **Support /carrier** : Supports, or vectors, perform many functions, but the most important is maintain a high surface area for the active ingredient. Another set of support is porous materials, especially porous alumina. Alumina is widely used in HDS process due to high surface area, high thermal stability, low prices [58,59].

A promoter is some third agent when added often in small amounts, leads to desired activity ,selectivity and stability effect .Promoters are designed to assist either the support or the activity component. One important example of support promotion is control of stablity. However, most often promoters, are added to hydrotreating process in order to increase Hydrodesulfurization (HDS), Hydrodemetallization (HDM) and inhibit undesirable activity ,such as coke formation [60]. Examples of the components and types of catalysts are given in the **table (2.2) .**

Table (2.2) components of a typical heterogeneous catalyst.

Component	Material types	examples
Active phase:	Metals	Noble metal(Pt , Pd , Ni, Fe)
	Metals oxides	Transition metal oxides (MoO4 ,CuO)
	Metals sulfides	Transition metal sulfides(MoS_2 , Ni_3S_2)
Carrier or Support	Stable , high surface area	Croup IIIA, alkaline earth and transition .
	Metal oxides , carbons	metal oxides e.g.(Al_2O_3 , SiO_2 , TiO_2 , MgO , zeolites and carbon.
Promoter	Textural(metal oxides)	(Al_2O_3 , SiO_2 , MgO, BaO , TiO_2 , ZrO_2)
	Chemical(metal oxides)	Alkali or alkaline earth (K_2O , PbO)

Definitely, for the reaction to proceed , the catalyst must have a chemical activity. After that, there can be a growing activity several benefits:

1. Higher rates for the same conditions.

2. Equivalent rates but with higher or smaller reactors.

In low temperatures or pressures, where increased balance, yields increases, processes become easier, reduced disorder, or selective improvement. Mechanical strength and thermal stability of catalyst articles are always a source of concern for designers [60]. Different support for hydrotreating catalysts has been studied. The most widely used support remains alumina because of its excellent mechanical and dispersing properties . As a rule, the active components are loaded on the support using cobalt (nickel) nitrates and ammonium heptamolybdate solutions [61,62]. As shown in the **figure (2.2)** , Pt support on Al_2O_3 these points represent the catalytic sites (the active site) spread over the alumina surface. Alumina can be considered a sponge with small pores and different sizes and shapes in which the reactants can flow and interact with the materials spread on the surface.

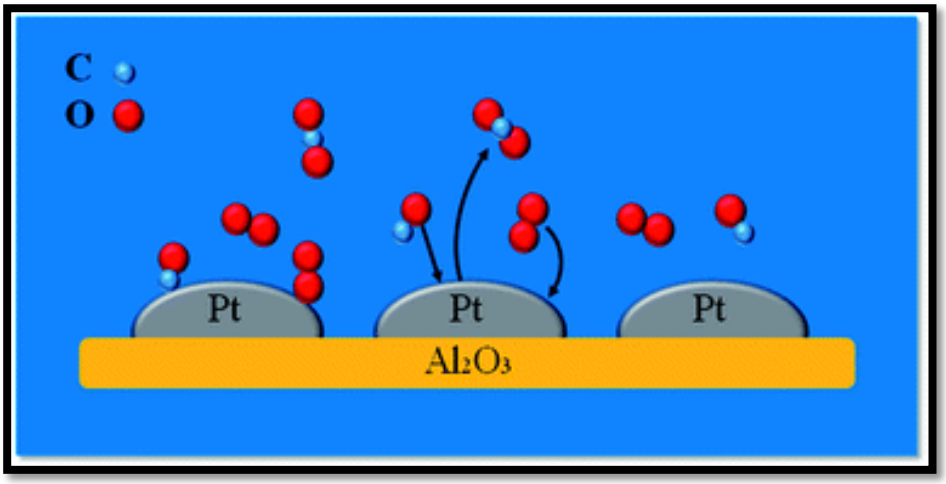

Fig (2.2) dispersed Pt on a high-surface-area Al_2O_3 [63].

2.3 Nano material and nanocatalysts .

Nanomaterial's are defined as those which have structured components with at least one dimension less than (1-100) nm (1nm = 10^{-9} m) [55]. Catalysis is one of the pioneer applications of nanoparticles. Various elements and materials like aluminium, iron, titanium dioxide, clays, and silica all have been used as catalysts in nanoscale for many years. Thus the question here is how the physical properties of nanoparticles affect their catalytic properties, and how fabrication parameters can in turn affect those physical properties, By better understanding of these, a scientist can design nanocatalysts which are highly active, highly selective, and highly resilient. All these advantages will enable industrial chemical reactions to become more resource efficient, consume less energy, and produce less waste which help to counter the environmental impact caused by our reliance on chemical process [62].

Nanomaterials are experiencing a rapid development in recent years due to their existing or potential applications in a wide variety of technological areas such as electronics, catalysis, ceramics, magnetic data storage, structural components etc. To meet the technological demands in these areas [64,65].

2.4 Catalyst design and engineering

Systematic scientific methods for catalyst design have been pursued by researchers for many years. After the design stage, the exploratory stimuli are applied to the test ,although small preparations using colloidal laboratory procedures to be used , this not only protects patents but it helps future reproduction and scale-up by manufacturers [57]. An important feature at this stage is the improvement of important properties. The design defines only active ingredients, supports and promoters . Design process catalyst development is extremely important. After a long term period for commercial use, the trigger may return as a different need is faced loss of activity for example, is potassium in high pressure steam reforming. were discovered, this potassium, added to reduce carbon pollution in the repair of

naphtha, easily volatile from the catalyst. To counter this, catalyst designers incorporate proper amount of soluble potassium silicate compound.

which only slowly degrades and thus maintains effective levels alkali volatile at all times. High activity and selectivity are designed by selecting the correct chemical Components, using methods of preparation to give the required surface area, and formulation of granules to ensure good access to active sites. Investigation activity alone is not sufficient unless balanced with these other requirements [57].This innovative time release capsule was exactly the drug required to extend the life of the catalyst. In catalyst design several factors need to be consider and this is shown clearly in **figure (2.3)**

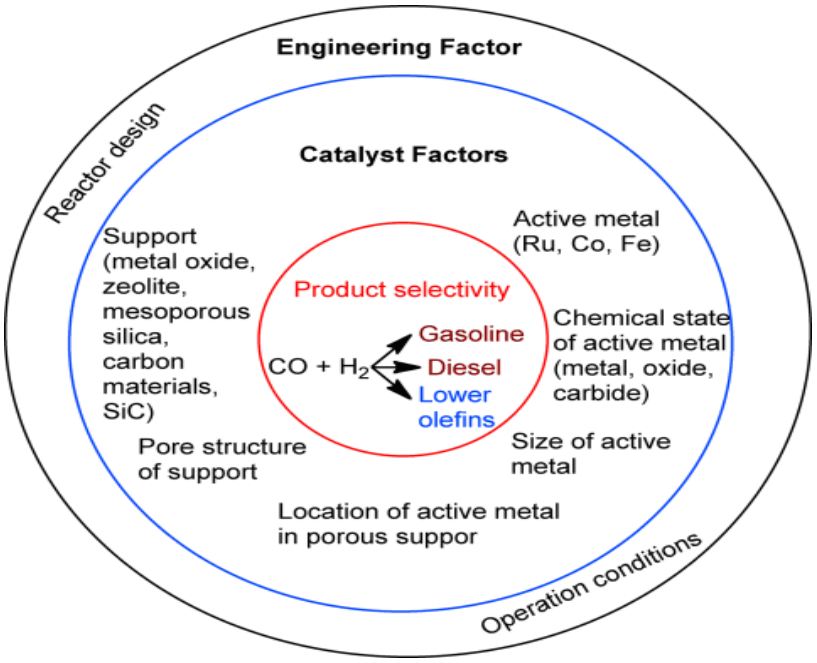

Fig. (2.3) Engineering features of the catalyst [67].

2.5 Fluid catalytic cracking and Hydrodesulfurization processes

2.5.1.Fluid catalytic cracking (FCC) process.

(FCC) Is one of the most important conversion used in petroleum refineries. There is a global demand for low sulfur, improving improved fuel oils and fuel and hydrocracking is continually increasing, while the available heavy crudes are becoming heavier [66-68]. Crude oils contain a significant number of extremely poor-quality heavy compounds , Therefore, refining processes that turn heavier oils into high value products are critical to refinement. However, the heavier cuts, known as vacuum residue, contain a large amount of impurities such as metal, nitrogen, sulfur and polyaromatic compounds. These are characterized as boiling above (550^{o}C), having high viscosity and specific gravity, and having high carbon residues and asphaltenes [67].

2.5.2. chemistry of the (HDS) process

Hydrodesulfurization (HDS) or hydrotreating is a catalytic chemical process widely used to remove sulfur compounds from refined petroleum products such as gasoline or petrol, jet fuel, diesel fuel, and fuel oils [69,70]. One purpose for removing the sulfur is to reduce the sulfur dioxide emissions resulting from using those fuels in automotive vehicles, aircraft, railroad , ships, or oil burning power plants and industrial furnaces, and other forms of fuel combustion [71-74]. Another important reason for removing sulfur from the intermediate product naphtha streams within a petroleum refineries that sulfur, even in extremely low concentrations, poisons the noble metal catalysts platinum and rhenium in the catalytic reforming units that are subsequently used to upgrade the naphtha streams [74].

for example , the hydrodesulfurization reaction can be expressed as:

Ethanethiol + Hydrogen ⇒ Ethane + Hydrogen Sulfide

$$C_2H_5SH + H_2 \Rightarrow C_2H_6 + H_2S \quad \ldots\ldots(2.1)$$

Due to increasingly stringent environmental regulations for the sulfur content in fuel oils, catalytic hydrodesulfurization (HDS) is widely used to remove sulfides in petroleum refning. Many approaches have been employed to improve metal dispersion of the catalysts for high HDS activity. The commonly used HDS catalyst preparation methods include simultaneous or sequential impregnation, hydrothermal deposition and sol–gel synthesis. For these methods, a complicated and time consuming process is always required and active metal components on the support surface tend to agglomerate into large crystallites [54].

Hydroprocessing catalysts are quite versatile, exhibiting activity for a number of important reactions. These great attention in hydroprocessing are removal of heteroatoms , hydrodesulfurization (HDS) , hydrodenitrogenation (HDN) , and for coal derived liquids , hydrodeoxygenation (HDO). These reactions involve hydrogenolysis of C-heteroatom bonds. An important attendant reaction is hydrogenation of aromatics (HYD). Hydrogenolysis of C=C bonds is generally minor, except when hydrocracking catalysts are employed [75].

Hydrotreating (HDT) is a widely used technology for scary removal (S, N) metal of diesel , and in this process the heteroatom-containing compounds react with hydrogen on the catalyst surface under high temperature and pressure, thus to eliminate heteroatoms [76,77]. The basic hydrogenolysis reaction has a number of uses other than hydrodesulfurization. The hydrogenolysis reaction is also used to reduce the nitrogen content of a petroleum stream and, in that case, is referred to as hydrodenitrification (HDN). The process flow scheme is the same as for an HDS unit. In fact, units may be designed for both hydrodesulfurization and hydrodenitrification, and many are so designed [69,72]. Using pyridine (C_5H_5N), a

nitrogen compound present in some petroleum fractionation products, as an example, the hydro denitrification reaction has been postulated as occurring in three steps:

Pyridine + Hydrogen ⇒ Piperdine + Hydrogen ⇒ Amylene + Hydrogen ⇒ Pentane + Ammonia

$$C_5H_5N + 5H_2 \Rightarrow C_5H_{11}N + 2H_2 \Rightarrow C_5H_{11}NH_2 + H_2 \Rightarrow C_5H_{12} + NH_3 \quad \text{....(2.2)}$$

and the overall reaction may be expressed as:

Pyridine + Hydrogen ⇒ Pentane + Ammonia

$$C_5H_5N + 5H_2 \Rightarrow C_5H_{12} + NH_3 \quad \text{.....(2.3)}$$

The hydrogenolysis reaction may also be used to saturate or convert olefins (alkenes) into paraffins (alkanes). The process used is the same as for an HDS unit. As an example, the saturation of the olefin, pentene, can be expressed as:

Pentene + Hydrogen ⇒ Pentane

$$C_5H_{10} + H_2 \Rightarrow C_5H_{12} \quad \text{....(2.4)}$$

The food industry uses hydrogenation to completely or partially saturate the unsaturated fatty acids in liquid vegetable fats and oils to convert them into solid or semi-solid fats, such as those in margarine and shortening.

2.6 HDS catalyst

HDS catalyst is the core hydrotreating catalyst used in the hydrotreater, which typically includes catalysts for hydrodesulfurization, hydrodenitrogenation , hydrogenation of aromatics, and hydrodemetallization [78]. The alkali metals, alkali earth metals and rare earth metals) are used in the preparation of hydrotreating catalysts for better dispersion of the types of active metals and to reduce the reaction of the metal support somewhat, thus improving their sulfurization, forming more NiMoS-II phases of high activity and selectivity [16].

Many metals catalyst HDS reaction but that are most active is those at the middle of the transition metal series , but binary combinations of cobalt and molybdenum are also highly active. In practice, most HDS units in petroleum refineries use catalysts based on cobalt-modified molybdenum disulfide (MoS_2) together with smaller amounts of other metals. Apart from MoS_2 catalysts, nickel and tungsten are also used, depending on the nature of feed [79] . For example, (Ni-W) catalysts are more effective for (HDN) which is also desired in many HDS units. Metal sulfides are supported on materials with high surface areas. A typical support for HDS catalyst is alumina [79] . Support allows the most expensive catalytic distribution, leading to a larger part of MoS_2 active motivational. (HDT) There is constantly increasing demand for HDT catalysts due to increased low-sulfur fuel consumption and tendency to process heavy distillated fractions [80].

2.7 Description of hydrodesulfurization unit .

In an industrial hydrogenation desulfurization unit, as in a petroleum refinery, the hydrogenation desulfurization reaction takes place in a stationary bed reactor at elevated temperatures ranging from 300 to 400°C and a high pressure of 30 to 130 atm of absolute pressure, usually in the presence of a catalyst consisting of a base impregnated with cobalt and molybdenum. The **figure (2.4)** below is a schematic diagram of the equipment and process flow in a typical HDS refinery [20].

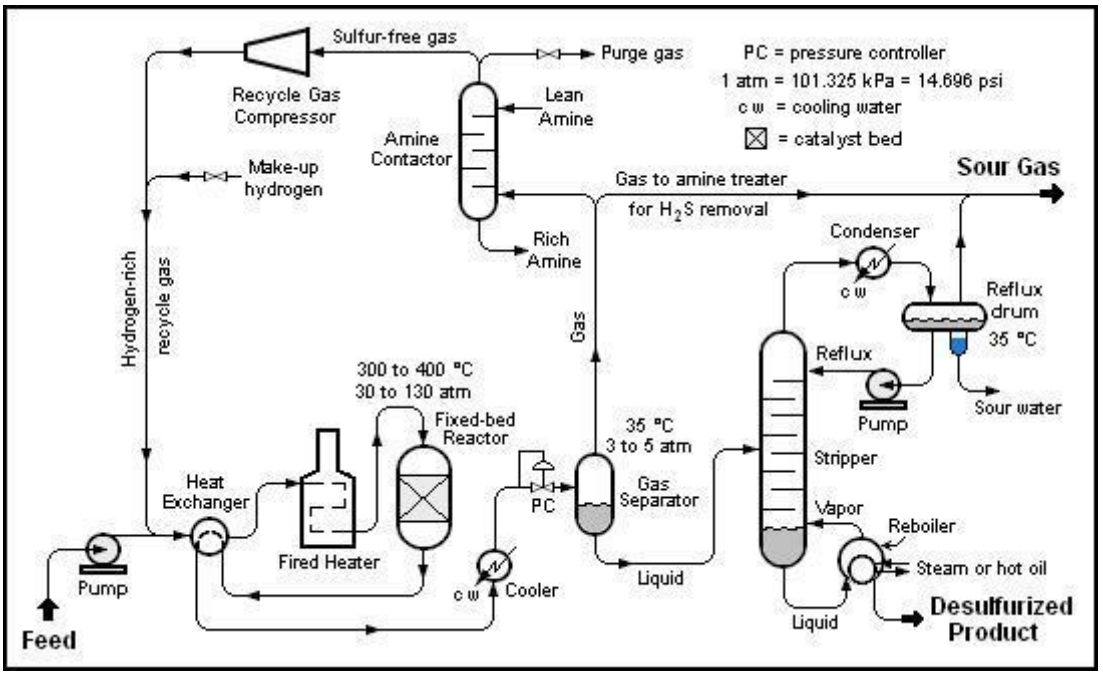

Fig(2.4) Schematic diagram of a typical hydrodesulfurization (HDS) unit in a petroleum refinery [20].

The liquid feed (at the bottom left in the diagram) is pumped up to the required elevated pressure and is joined by a stream of hydrogen-rich recycle gas. The resulting liquid-gas mixture is preheated by flowing through a heat exchanger. The preheated feed then flows through a fuel-fired heater where the feed is totally vaporized and heated to the required elevated temperature before entering the reactor and flowing through a fixed-bed of catalyst where the hydrodesulfurization reaction takes place. The hot reaction products are partially cooled by flowing through the heat exchanger where the reactor feed was preheated and then flows through a water-cooled heat exchanger before it flows through the pressure controller (PC) and undergoes a pressure reduction down to about three to five atmospheres [79].

The resulting mixture of liquid and gas enters the gas separator vessel at about 35 °C and three to five atmospheres of absolute pressure. Most of the hydrogen-rich gas from the gas separator vessel is recycle gas which is routed through an amine

contactor for removal of the reaction product hydrogen sulfide gas (H_2S) that it contains. The H_2S-free hydrogen-rich gas is then recycled back for reuse in the reactor section. Any excess gas from the gas separator vessel joins the sour gas (i.e., gas containing H_2S) from the stripping of the reaction product liquid .

The liquid from the gas separator vessel is routed through a reboiled stripper distillation tower. The bottoms product from the stripper is the final desulfurized liquid product from the hydrodesulfurization unit. The overhead sour gas from the stripper contains hydrogen, methane, ethane, hydrogen sulfide, propane and perhaps some butane and heavier components (i.e., higher molecular weight components).

That sour gas is sent to the refinery's central gas processing plant for removal of the hydrogen sulfide in the refinery's main amine gas treating unit and through a series of distillation towers for recovery of propane, butane and pentane or heavier components. The residual hydrogen, methane, ethane and some propane is used as refinery fuel gas [81,82].

The hydrogen sulfide removed and recovered by the amine gas treating unit is subsequently converted to elemental sulfur in a Claus process unit. Note that the above description assumes that the HDS unit feed contains no olefins. If the feed does contain olefins (for example, the feed is a naphtha derived from a refinery fluid catalytic cracker (FCC) unit), then the overhead gas from the HDS stripper may also contain some ethene, propene, butenes and pentenes or heavier olefins. It should also be noted that the amine solution to and from the recycle gas contactor comes from and is returned to the refinery's main amine gas treating unit [81].

2.8 Necessity of hydrotreating process

The hydrotherapy process plays an important role in improving the quality of products , it is derived from petroleum raw materials. Some of the key factors that require the hydrotreating process in the petroleum refinery is below:

2.8.1 Environmental Concerns

The main factor that necessitates hydrotreating is the pollution associated with sulphur compounds that produces SO_x emissions in the atmosphere. Short term exposure to SO_2 can result in asthma symptoms as well as other respiratory problems , it can exacerbate respiratory problems and exacerbate cardiovascular disease [83].

2.8.2 Efficient operation of downstream units

Sulphur compounds are serious poisons to many catalysts used in the downstream processing units. For example, a naphtha desulphurization unit is required to protect the noble metal catalyst used in the catalytic reforming unit (CRU) that produces high octane gasoline [84].

2.8.3 Corrosion concerns

Sulphur compounds can produce H_2S in the downstream process units, which can cause corrosion. This will necessitate increased capital cost affecting the profitability of the process [84].

2.8.4 Improvement of product quality

Presence of oxygenated compounds in petroleum feedstocks can pose challenges to product stability due to the formation of derivatives that can solidify and create blockings in the downstream process equipment. Hydrotreating can effectively remove such compounds thereby increasing the product stability on storage [84].

2.9 Catalyst properties

2.9.1 Densities

2.9.1.1 Theoretical Density

This is defined as the ratio of the mass of a collection of discrete pieces of solid to the sum of the volumes of each piece, if the solid has an ideal regular arrangement at the atomic level. Theoretical volumes are determined from (XRD) unit cell measurements, so this density is also known as the x-ray or unit cell density. Ideal volumes are of little use in catalysis, and this term has hardly any applicability [85].

2.9.1.2 Particle Density.

Here the volume is the sum of the solid, closed pores, and accessible pores within the particle. It is essentially the volume of the particle, but should not be found by measuring dimensions. A displacement psychometer is used but with a fluid that does not penetrate the interior pores of the pellet. One approach is to fill these pores with the fluid prior to displacement, for example, with methanol. A more satisfactory method is to use mercury,which does not penetrate pores smaller than (1.2 x 103 nm) at atmospheric pressure. For this reason particle density is also called mercury density [85].

2.9.1.3 Packing Density

Also called bulk or bed density, the volume in this case includes the void space between particles. It was defined as the mass of many particles of a substance divided by the total volume they occupy.The total volume includes particle size, interparticle space size, and internal pore size [85].

2.9.1.4. Skeletal Density

In this density, volume is defined as the sum of the volume of the solid material and any closed pores within. the solid. These pores cannot be penetrated by any fluid and become part of the powder volume. A mass of catalyst is placed in a flask of known volume, and the amount of helium needed to fill the flask measured, giving the powder volume by difference. Care should be taken to dehydrate all pores thoroughly. Because helium is used as the displacing fluid, this density is sometimes called the helium density [85] .

2.9.2 Particle Size

Measurement of particle size of macroscopic pellets, extrudates, and spheres presents no problems. Dimensions can be determined directly or sample material sieved for irregular particles. Smaller distributions in powders, such as cracking catalysts, require specialized procedures: optical and electrical imaging, light scattering, light shadowing, elutriation, sedimentation, electrical resistance, impaction, and nozzle pressure drop [85].

2.9.3 Pore size distribution

Measuring pore size distribution is now essential a feature of particle characterization. Pore spread resistance, poisoning of the mouth pores, and the disruption of control . Large pores have been measured over with mercury borosymmeters and mesopores with nitrogen isothermal adsorption desorption [85].

2.9.4 Porosity

Is a measure of the void (i.e. "empty") spaces in a material, and is a fraction of the volume of voids over the total volume, between 0 and 1, or as a percentage between 0% and 100% , some tests measure the "accessible void", the total amount of void space accessible from the surface [86].

A value for porosity can alternatively be calculated from the bulk density[85]:

$$\theta = \frac{p_{paticle} - p_{bulk}}{p_{particle} - p_{fluid}} \dots\dots (2.5)$$

There is a relationship between particle and skeletal densities, dp and ds and porosity, θ, given by equation (2.6) [85] :

$$\theta = (1 - \frac{dp}{ds}) \dots\dots (2.6)$$

2.9.5 Void fraction

The void fraction which is defined a measure of the void (i.e. empty) spaces in a material, and is a fraction of the volume of voids over the total volume , can be calculated from (bulk density) and (particle density) [85] , using the following equation[85] :

$$\varepsilon = \left(1 - \frac{db}{dp}\right) \dots\dots\dots (2.7)$$

2.9.6 Loss on Ignition

Is a test used in inorganic analytical chemistry and soil science, particularly in the analysis of minerals and the Chemical composition of soil. It consists of strongly heating ("igniting") a sample of the material at a specified temperature, allowing volatile substances to escape, until its mass ceases to change. A variant of the test in which mass change is continually monitored as the temperature is changed by (TGA) [87] .

2.10 Catalyst deactivation

2.10.1 Problem of catalyst deactivation

Catalyst deactivation, the loss over time of catalytic activity or selectivity, is a problem of great economical concern in application of commercial catalytic processes. Catalyst deactivation is attributed to interaction between the catalyst and the impurities present in process effluent in which the catalyst is used. Any chemical or physical interaction that reduces catalyst activity or selectivity is classified as catalyst deactivation phenomena. In general, deactivation leads to a shortened catalyst lifetime, and the replacement of an aged catalyst to a new one is determined by the industrial processes for which the catalyst is used. Industrial catalytic deactivation can range from short term to several years. reduced catalyst lifetime has a strong negative impact on the process economics and improved catalyst lifetime is of great commercial value [88] . Depending on the type of deactivation process, activity loss can be temporary or permanent. Reasons for disruption include coke formation, poisoning, mineral deposition and sintering [89-91].

In an industrial reactor, constant conversion levels are maintained by an increase the reaction temperature that can offset the deactivation effect [88]. The first principle is deactivation mainly due to coke formation followed by slow deactivation, mainly due to mineral precipitation .The final loss is attributed to the increase in the generated coke and the change in the pore structure, as well as the pollution with different chemicals absorbed in the active sites [88] . A higher reaction temperature increases not only the conversion rate, but also the amounts of coke. Therefore, catalysts and hydrogen are used to inhibit coke formation [86]. Additionally, coke deposition occurs in the pores or on the surface of catalysts, reducing activity and product selectivity , since coke deposition is generally believed to be the primary cause for catalyst deactivation, the first remedy for deactivation has always been linked to coking behavior on catalysts [75,92,93].

2.10.2 Reasons for catalyst deactivation

2.10.2.1 Deactivation by coke

Coke formation can occur in the hydrotreating reactor through polymerization, dehydrogenation, or thermal reactions as described below :

$$\text{Hydrocarbon} \underset{\text{Hydrogenation}}{\overset{\text{Dehydrogenation}}{\rightleftharpoons}} \text{Coke precursors} \xrightarrow[\text{polymerization}]{\text{Condensation}} \text{Coke} \quad \text{.....(2.8)}$$

Coke is carbon deficient material and stays on the surface of the catalysts, blocking the active sites. Coke built up is seen to increase with increase in molecular weight/boiling range of feedstock [66,75]. Coke disruption leads to catastrophic loss of activity, pore constriction and eventual pore blockage as shown in **figure (2.5)**.

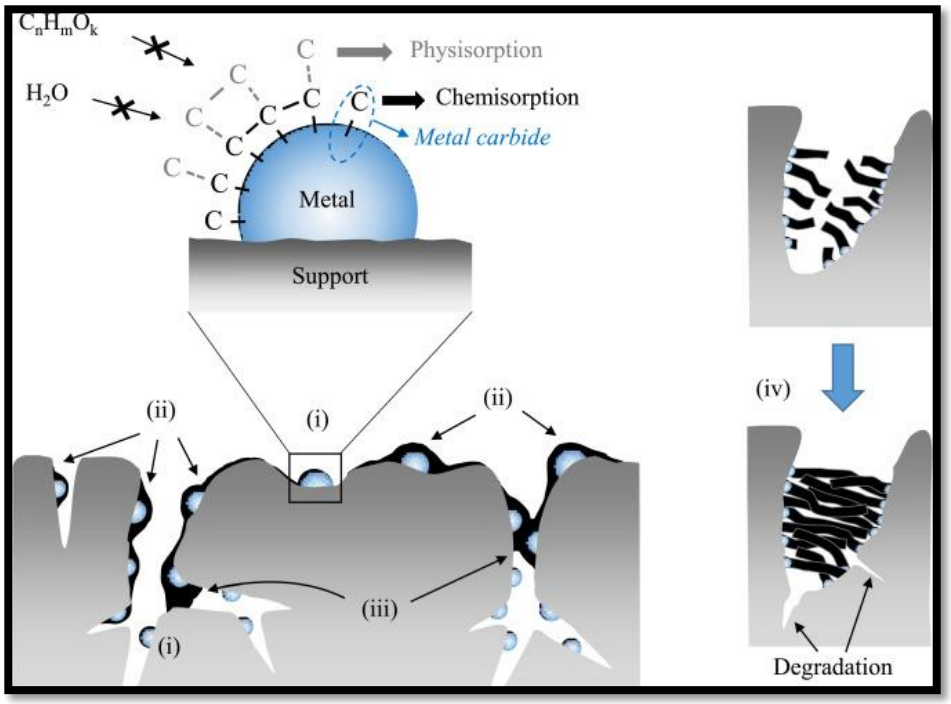

Fig(2.5) closing pores due to formation of coke [94] .

2.10.2.2 Coking propensity: Carbon vs. Alumina

One of the primary methods of catalyst deactivation is by the formation of coke, which is generally attributed to the presence of polynuclear aromatic compounds and olefins in gas oil feeds . Coking propensity of Mo/C catalysts found to decrease with increase in hydrogen partial pressure due to minimization of dehydrogenation (and hence minimum polymerization) reactions. At a pressure of 6.9 MPa the coking tendency of Mo/C supports was three times lower than that of their γ-Al_2O_3 counterparts [88].

2.10.2.3 Deactivation by poisons

A toxin is a substance that absorbs onto the sites of an active catalyst, causing either site disruption or competition with the reactants for a specific reaction. The toxin may be due to the reactant, intermediates, or products, as well as from the extraneous compounds present in the feed. The net result is a decrease in the activity of the catalyst. It is assumed that during in toxication, the basic structure of the active sites does not change [75]. It is of two types :

1-Selective poisoning:- a chemical directly reacts with the active site or the carrier, rendering it less or completely inactive. When the carrier reacts with a constituent in the gas stream to form a new compounds, as in the case of $Al_2(SO_4)_3$, pores are generally partially blocked, resulting in increased diffusion resistance. This will cause a decrease in the activation energy. Using nonsulfating carriers such as ZrO_2 or SiO_2 leads to a faster rate of deactivation since no reservoir is available for spillover or by using nonsulfating carriers .

2-Nonselective poisoning :- deposition of fouling agents onto or into the catalyst carrier, masking sites and pores, resulting in a loss in performance .Types of poisoning are shown in **figure (2.6).** High molecular weight material from upstream equipment physically deposit onto the surface of the support to cause deactivation is

referred to as "fouling" or "masking" as shown in **fig (2.7).** Reactor-scale metals (Fe, Ni, Cr, etc.) resulting from corrosion, silica/alumina-containing dusts, phosphorous from lubricating oils, and similar compounds are good examples .

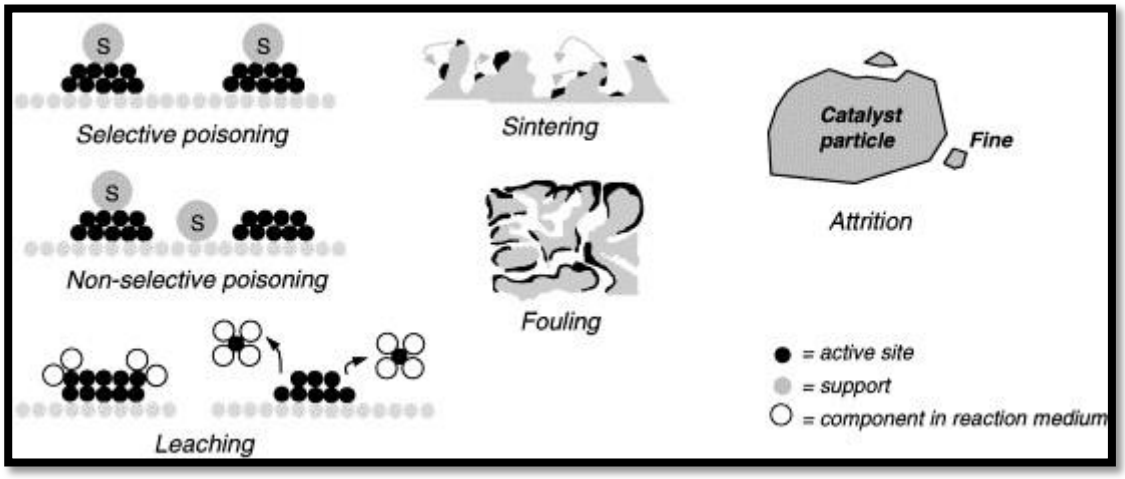

Fig(2.6) selective and non-selective poisoning of the catalytic sites[95].

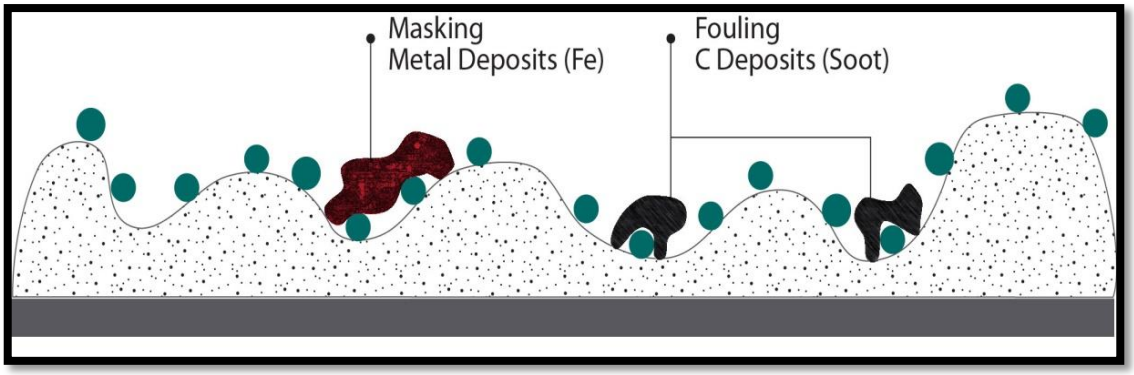

Fig (2.7) masking and fouling in catalyst [96].

2.10.2.4 Poisoning by nitrogen compounds

In the case of hydroprocessing, nitrogen containing compounds are the most common poisons by virtue of their strong adsorption on catalyst sites. Because of their basic nature, they adsorb on catalyst acidic sites, may adsorb reversibly or irreversibly, depending on reaction conditions. Most of the nitrogen in petroleum is in the form of 5- and 6-membered heteroatom rings and aniline [75].

2.10.2.5 Deactivation by metal deposits

During hydroprocessing, part of the metals present in the feed will deposit on the catalyst surface and cause deactivation. The nature of the metals deposited depends on the origin of the feed. V and Ni are prevalent metals in petroleum crudes, heavy oils and oil shale- derived liquids, while Fe and Ti are the main metals coal-derived liquids. Heavy oils derived from tar sands (V, Ni, Ti and Fe) and small amounts of other metals [57]. Slow declining was mainly linked to disabled metals on catalysts. Metals are deposited in nutrition stocks on the internal and external surfaces of the catalyst and disable catalyst by blocking mouth pores [97].

It is reported that the deposited metals poisoned active sites and the poisoning rate was controlled by the diffusion of metal complexes through the pores filled with liquid. Besides these two main causes of catalyst deactivation, HDS catalysts are also deactivated by the agglomeration of active metals and the sintering of support which can occur in the catalyst treated at high temperatures [98] . While the properties of disabling and stability have been linked to the loss of active metal Ni through solid state reactions (composition $NiAl_2O_4$, or another nickel contains mixed types of oxide [99,100].

2.10.2.6 Fouling

fouling means the deposition of reactor debris on the particles. Additionally, scale, rust, and other corrosion products are all possibilities to the chemical components of the units of current. Reactors often have iron oxide scales that are red-brown on the outside. Calcium compounds are also found. The most severe cases occur in coal processing and liquids derived from charcoal, which contain large amounts of inorganic minerals [85] .

2.10.2.7 Component volatization and sintering

High temperatures can lead to a loss of active ingredients or catalysts through fumigation. It follows loss of activity and function of the promoter, With additional complications of corrosive deposits in the bottom steam plant equipment. Events of this type are easily detected in laboratory operations.

Sintering is the loss of surface area of the deserved catalyst for crystal growth. The stability of the hydrotreating catalyst is affected by prolonged exposure to higher temperatures have been observed the Ni-Mo-S phase was decomposed by pre-asphalt during coal processing derived fluids. This is observed upon entry into the catalyst layer but not at exit .Whereas, the deactivation was found due to MoS_2 clustering. a 470 °C temperature flight resulted in nickel sintering, which eventually it resulted in losing the active phase [85].

2.11 Deactivation and regeneration

2.11.1 Deactivation in industrial process

The size of these solid waste has increased significantly around the world and in petroleum refining industries due to the steady increase in the upgrading of raw materials or distillation outcomes to meet the low-sulfur fuel environmental regulations. Several alternative methods such as disposal in landfills, reclamation of metals, regeneration, reuse, and utilization as raw materials to produce other useful products are available to the refiners to deal with the spent catalyst problem. The choice between these options depends on technical feasibility and economic considerations [101].The reduction of the sulfur content in gasoline and diesel fractions is still receiving increasing interest due to the requirement for clean fuels production for environmental production.

At present, hydrodesulfurization removal (HDS) is the most common technique in the refining industry to remove the vehicles containing sulfur. The main point of HDS is the design and development of new catalysts with activity and high selectivity [16].

2.11.2 Regeneration of hydroprocessing catalyst for restore activity

regeneration can re-activate somewhat efficiently for different refining or petrochemical catalysts. An oxidizing atmosphere can be used at 450-550°C, carbonaceous species can be eliminated. For example, in the case of hydroprocessing catalysts, regeneration converts a sulfide phase, which could have partially sintered, back to an oxide phase quite similar to the original of the fresh catalyst [102-104].

The deep removal of sulfur compounds from diesel fuel gasoline is an important issue in environmental catalysis [105,106]. Processing the new generation resulted in either the formation of $CoMoO_4$ or $NiMoO_4$ if the regeneration temperature was too high or to insufficient oxidation of S and C if the temperature was too low [107].

Chemical treatment after oxidative regeneration is the most common method of consumer catalyst regeneration. Several acidic or alkaline solutions such as oxalic acid, mineral acids, potassium hydroxide, acetic acid, and citric acid are used to recover spent catalysts. The regeneration mechanism and the effects of different chemicals, concentrations and operating conditions on regeneration of the catalyst differ depending on the catalyst consumed and the reliable information in the open literature is very limited [108-113] .

In some cases it is possible to restore much of the original catalytic activity by removing the deactivation agent and/or reversing its effects on the active phase. This is only possible when deactivation is reversible (as coke fouling). Coke removal via oxidation is a delicate task and requires a careful temperature control. The reaction is highly exothermic and can easily result in overheating and in thermal reorganization of the sample. The end result is the loss of surface area (sintering) and formation thermal compounds. Many contaminants can be found in spent HDT catalysts. It may come from raw materials (V, Ni, Ca, As, Fe, Na), and additives in some refining operations (Si), or corrosion (Fe) [15].

Active sites are poisoned with elements such as S, V, and sintering is essentially irreversible in catalysts. Depending on the process, this expendable catalysts containing more than 1-3% and 0.2-0.4% by weight as are not recommended. It does not allow items such as Na and Si to fully recover after regeneration. V destroys the mechanical strength of the alumina support granules. Even after removing the coke, some V and Ni remain in the treated catalyst. It acts as a diffusion barrier for the reactants , Fe as a physical blocker to the active sites [114].

2.12 Spectroscopy in Catalysis.

Catalytic spectroscopy is a group of analytical techniques used today in catalysis and in catalytic surface chemistry, and the catalytic surface properties are determined by their composition and structure at the atomic scale. Hence, it is not sufficient to know that the surface is composed of a metals and a catalyst, but it is necessary to know the exact composition of the metal surface, and the microscopic plane is the level of basic studies, dealing with details of adsorption on surfaces, reaction mechanisms, theoretical modeling and surface science, including any defects. Thus, from a fundamental point of view the catalyst aim of characterizing a catalyst should be to examination of a surface atom of a substance, and to develop techniques to characterize catalytic systems in situ during their development in time with an environmentally changing chemical is a very difficult task [115].

The many aspects that we need to study in order to properly understand supported catalysts on a fundamental level are shown schematically in **Figure (2.8)**.

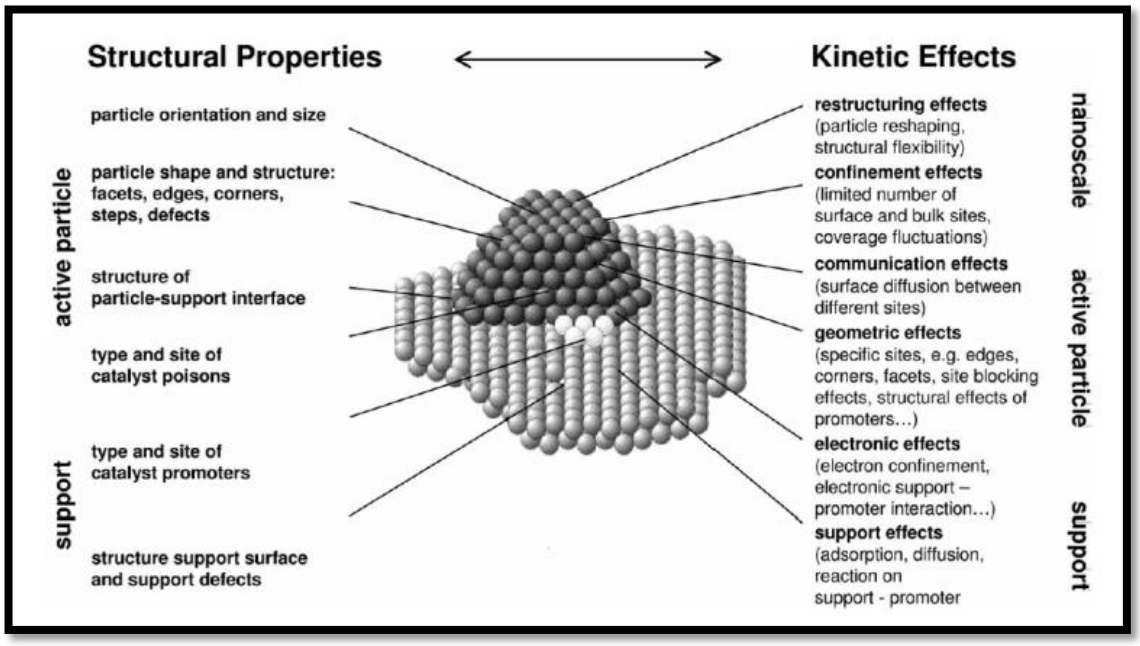

Fig (2.8) Many aspects of supported catalyst Characterization at the molecular level [115] .

The industrial view on catalyst characterization is different, however. The emphasis is placed mainly on developing an active, selective, stable and mechanically robust catalyst. the catalyst characterization in industrial research deals with the materials science of catalysts on a more or less mesoscopic scale, whereas the ultimate goal of fundamental catalytic research is to characterize the surface of a catalyst at the microscopic level mon the atomic scale [116].

2.13 Spectroscopic Techniques.

Catalysis is a complex multidisciplinary science that cannot be fully understood without applied spectroscopy. Spectroscopy is thus the enabling tool for knowledge-based design of highly efficient and stable catalysts. There are many ways to obtain information on the physico-chemical properties of materials, For example, the catalyst can be measured by X-ray and study how x-rays are deflected X-ray diffraction (XRD), or one can study the energy distribution of electrons emitted from the catalyst (X-ray optical spectroscopy, XPS) **.**One can also heat up a spent catalyst and examination of the absorbing temperatures of the intermediates and the products of the reaction from the surface (temperature programmed absorption) [115].

Another point that concerns the relevance of spectroscopic research in catalysis is the following. Both catalysis and spectroscopy are disciplines that demand considerable expertise. For instance, the state of a catalyst often depends critically on the method of preparation, its pretreatment, or its environment. It is therefore essential to investigate a catalyst under carefully chosen, relevant conditions, and after the proper treatment. Catalytic scientists recognize these requirements precisely[115].

On the other hand, spectroscopy is not simple, fast and easy where there are experiments to characterize the catalyst. Correct interpretation spectra requires practice-based expertise, with sound theory and background in spectroscopy, In conclusion, investigate motivational problems using a combination of spectroscopy

techniques, it offers the best perspectives for successful research into catalysts. Many of the existing techniques focus only on examining the properties of the catalyst, while others are better suited for studying the surface chemistry associated with the reaction process [116].

2.13.1 X-Ray Diffraction(XRD) .

X-ray diffraction (XRD) is a useful tool to characterize catalytic materials . the technique discriminates between amorphous and crystalline samples. For crystalline materials, it allows for the determination of the component phases. Furthermore, it allows for the determination of particle size and other characteristics of the component crystallites. In most cases, it also allows for the determination of the atomic arrangement of the atoms in the crystallographic unit cell, XRD is used for determine the size of the particles. In catalyst characterization, diffraction patterns are mainly used to identify the crystallographic phases that are present in the catalyst[116].

2.13.2 Fourier transform infrared spectroscopy (FTIR).

Fourier-transform infrared spectroscopy (FTIR) is a technique used to obtain an infrared spectrum of absorption or emission of a solid, liquid or gas. An FTIR spectrometer simultaneously collects high-resolution spectral data over a wide spectral range. The technique is able to probe the chemical and geometric structures of (adsorbed) molecules (molecular vibrational/rotational modes) and solids (lattice vibrations/acoustic modes or phonons). Nowadays pricewise, the FTIR spectrometer is comparatively inexpensive and, as such, is one of the workhorses in both academic and industrial heterogeneous catalysis laboratories [117].

2.13.3 Raman spectroscopy

Is a spectroscopic technique typically used to determine vibrational modes of molecules, although rotational and other low-frequency modes of systems may also be observed. Raman spectroscopy is commonly used in chemistry to provide a structural fingerprint by which molecules can be identified. Raman spectroscopy relies upon inelastic scattering of photons, known as Raman scattering. A source of monochromatic light, usually from a laser in the visible, near infrared, or near ultraviolet range is used, although X-rays can also be used [118].

2.13.4 Thermo gravimetric analysis (TGA) spectroscopy.

Thermogravimetric analysis or thermal gravimetric analysis (TGA) is a method of thermal analysis in which the mass of a sample is measured over time as the temperature changes. This measurement provides information about physical phenomena, such as phase transitions, absorption, adsorption and desorption; as well as chemical phenomena including chemisorptions, thermal decomposition, and solid-gas reactions (e.g., oxidation or reduction). Thermogravimetric analysis (TGA) is conducted on an instrument referred to as a thermogravimetric analyzer. A thermogravimetric analyzer continuously measures mass while the temperature of a sample is changed over time. Mass, temperature, and time are considered base measurements in thermogravimetric analysis while many additional measures may be derived from these three base measurements [119].

2.13.5 Atomic Absorption Spectrometer (AAS).

Atomic absorption spectroscopy (AAS) and atomic emission spectroscopy (AES) is a spectroanalytical procedure for the quantitative determination of chemical elements using the absorption of optical radiation (light) by free atoms in the gaseous state. Atomic absorption spectroscopy is based on absorption of light by free metallic ions. In analytical chemistry the technique is used for determining the concentration

of a particular element (the analyte) in a sample to be analyzed. AAS can be used to determine over 70 different elements in solution, or directly in solid samples via electrothermal vaporization, and is used in pharmacology, biophysics, archaeology and toxicology research [120].

2.13.6 Field Emission Scanning Electron Microscopy (FESEM)

(FESEM) is a type of electron microscope produces sample images by scanning the surface with a concentrated package of electrons. The electrons interact with atoms in the sample, different signals contain information about the surface and sample configuration information.The electron beam is scanned in a raster scan pattern, and the position of the beam is combined with the intensity of the detected signal to produce an image. In the most common (FESEM) mode, secondary electrons emitted by atoms excited by the electron beam are detected using a secondary electron detector (Everhart-Thornley detector). The number of secondary electrons that can be detected, and thus the signal intensity, depends, among other things, on specimen topography. Some (FESEM) can achieve resolutions better than (1 nm). The signals used by an (FESEM) to produce an image result from interactions of the electron beam with atoms at various depths within the sample [121].

2.13.7 Energy-dispersive X-ray spectroscopy(EDX).

Energy-dispersive X-ray spectroscopy (EDS,EDX, EDXS, XEDS), sometimes called (EDXA or EDAX) , is an analytical technique used to analysis the elements or chemical characterization of a sample. It relies on an interaction of some source of X-ray excitation and a sample. Its characterization capabilities are due in large part to the basic principle that each element has a unique atomic structure that allows for a unique set of peaks on its electromagnetic emission spectrum. EDS can be used to identify the chemical elements present in a sample, and can be used to estimate their

relative abundance. EDS also helps to measure the thickness of the multi-layer coating of metallic coatings and to analyze different alloys [122].

2.13.8 Atomic Force Microscopy (AFM)

Atomic force microscopy (AFM) or scanning force microscopy (SFM) is a high-resolution type of scanning probe microscopy (SPM) , with a resolution shown in nanometer fractions, over 1,000 times that of optical diffraction-limit .Applications in the field of solid state physics include:

(a) the identification of atoms at a surface

(b) the evaluation of interactions between a specific atom and its neighboring atoms.

(c) the study of changes in physical properties arising from changes in an atomic arrangement through atomic manipulation. In molecular biology, AFM can be used to study the structure and mechanical properties of protein complexes and assemblies. For example, AFM has been used to image microtubules and measure their stiffness [123].

CHAPTER THREE

Experimental Part

3.1. Instruments and apparatus

3.1.1 The Instruments used

The instruments that are used in this study are tabulated with their details , origin , and location in **table (3. 1).**

Table (3.1): The instrument used in this study .

No.	Instruments name	Details & Origin	Location
1	**Electric Balance**	KERN & Shone GmbH, Type ACS 120-40 ,WB 12 AE 0308,MAX 120 g , d = 0.1 mg , **(Germany)**	The Laboratories of Chemistry Department , College of Science , University of Diyala , Iraq
2	**Oven**	BINDER , Hotline International (20-360 °C) , **(Germany)**	
3	**pH meter**	pH/Ion Benchtop WTW inolab pH meter 7110 benchtop meter , **(Germany)**	
4	**Hot plate magnetic stirrer**	MS-H280-pro ISO LAB Laboratory GmbH , **(Germany)**	
5	**Electrical Furnace**	Type -Nabertherm , Max Temperature 1300 °C ,400 V ,15.0 A ,50/60 Hz , **(Germany)**	

3.1.2. Apparatus used

The apparatus used are shown in **table (3.2)** with their details , origin , and location .

Table (3.2) : Apparatus used in characterization .

No.	Apparatus names	Details & Origin	Place of measurement
1	**X-ray Diffraction Spectroscopy (XRD)**	XRD-6000 CuKα (λ=1.5406 A◦), 220/50,HZ , SHIMADZU, (Japan)	Lab.of X-Ray Diffraction ,ministry of science and technology , Iraq
2	**Atomic Absorption Spectrometer (AAS)**	Perkins elmer AA-7000 (USA)	Lab . of Atomic Absorption Flame in Molecular bioly,Nano technology ,Tissue Culture ,Iraq
3	**Atomic Force Microscope (AFM)**	AA3000 Angstrom Advanced.Inc.USA	Service Lab Ibn Al-Haitham University of Baghdad
4	**Field Emission Scanning Electron Microscope (FESEM)**	MIRA3 TESCAN-Czech	Research lab Centre Mashhad University - Iran
5	**Thermo Gravimetric Analysis (TGA)**	SDT Q600 V20.9 Build 20	Research lab Centre Mashhad University - Iran
6	**Energy dispersion X-ray (EDX)**	MIRA3 TESCAN-Czech	Research lab Centre Mashhad University - Iran
9	**RAMAN**	Teksan Co Tak ram N1-541: iran	Research lab Centre Mashhad University - Iran
10	**Fourier transform, infrared spectroscopy (FTIR)**	SHIMADZU (IR PRESTIGE 21)	Chemistry Department College of Education for pure Sciences / Diyala University

3.2 Materials

3.2.1 The chemical materials

The properties of chemicals used in this work are shown in **table (3.3):**

Table (3.3) The chemicals used .

No.	Chemicals	Formula	Purity%	Molecular Weight g/mol	Source
1	Ammonium hepta molybdate	$(NH_4)_6Mo_7O_{24}.4H_2O$	99	1235.86	Thomas baker (chemicals) Pvt.Ltd.
2	Nickel nitrate hexa hydrate	$Ni(NO_3)_2.6H_2O$	99.5	290.79	Central Drug House (P)Ltd.
3	Gamma alumina	$\gamma -Al_2O_3$	99.5	101.961	Changsha Santech Co. , Ltd.
4	Absolute ethanol	C_2H_5OH	99	46.069	ALPHA CHEMIKA Made in INDIA
5	Benzene	C_6H_6	99.5	78.11	ALPHA CHEMIKA Made in INDIA
6	Toluene	$C_6H_6CH_3$	99.8	92.14	ALPHA CHEMIKA Made in INDIA
7	carbon disulfide	CS_2	99.5	76.14	Central Drug House (P)Ltd

3.2.2. HDS catalysts used in Characterization

1. New NiMo/γ-Al_2O_3 (supplied from Baji refinery company).

2. Spent NiMo/γ-Al_2O_3 (supplied from Baji refinery company ministry of oil , Iraq . it was purchased from BASF company and the spent one was being in operation for about 6 years).

3. Prepared NiMo/γ-Al_2O_3 .

4. Regenerated NiMo/γ-Al_2O_3

3.3. Preparation of nano NiMo/γ-Al_2O_3 using impregnation / incipent wetness method

The catalyst NiMo/γ-Al_2O_3 was prepared by (1.946 g) of $(Ni(NO_3)_2.6H_2O)$ was dissolved in (20 ml) ethanol with dissolve (1.226g)of $(NH_4)_6Mo_7O_{24}.4H_2O)$ in a glass beaker in (20 ml) ethanol at the conditions surrounding. These were mixed in a beaker with vigorous stirred . After that. alumina was added to blend solutions as shown in **figure (3.1.A and B)** The beaker was then covered with a polyethylene film and stirring at room temperature for at least (6 hours) as shown in **figure (3.1.C and D)**, and then transferred to drying oven for ethanol evaporation at (60 ^oC). After aging for two days, the prepared material becomes a solid, resembling green foam . The product was calcined at (500 ^oC) for (7 hours) to obtain the desired material shown in **figure (3.1.E and F)** [78].

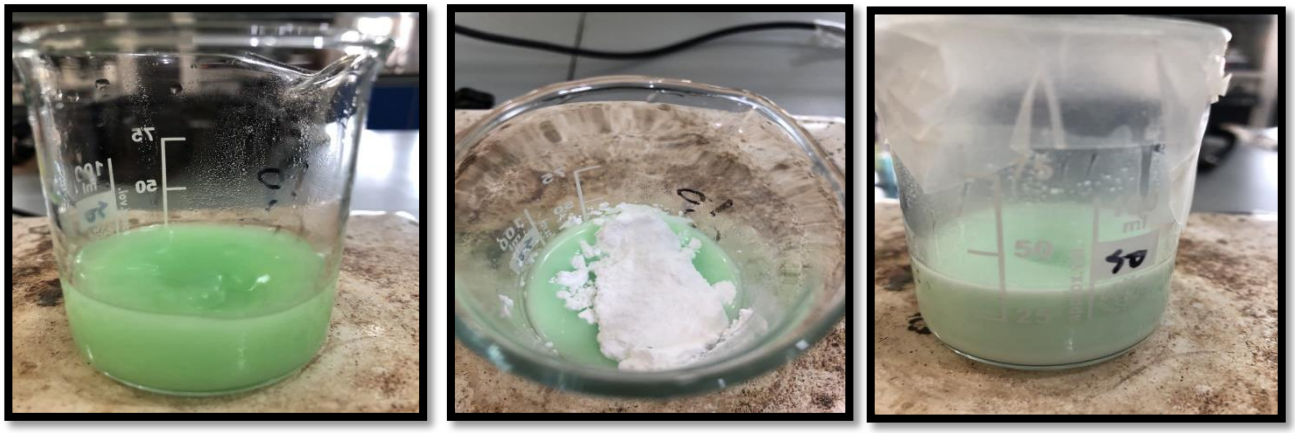

(A) **(B)** **(C)**

(D) **(E)** **(F)**

Fig (3.1) Steps of the preparation of NiMo/γ-Al_2O_3 .

3.4. The Regeneration of Spent Catalyst .

The spent NiMo/ γ-Al_2O_3 HDS catalysts was being in operation for about 6 years. The spent NiMo/γ-Al_2O_3 catalyst in cylindrical form (2.5mm x 1.5mm) contains oil residue resulting from use as shown in **figure (3.2)**. It washed with distilled water and dried in an oven maintained at (100 °C) for (2 hour) and then used in the treatment and regeneration process .

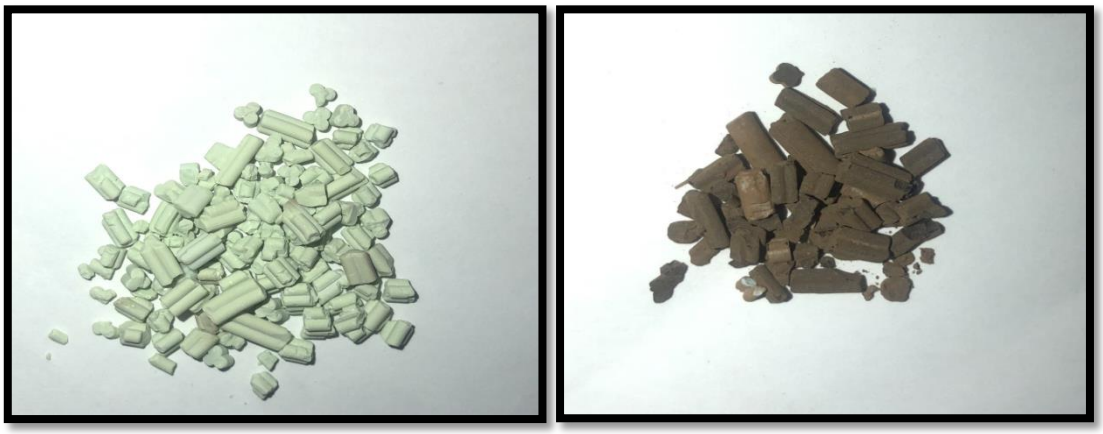

Fig (3.2) New and spent catalysts (Real image).

A five grams of the catalyst obtained from the previous step is taken ,the contaminated residual lube oil is removed by washing the catalyst well with benzene first and then with toluene by refluxing at temperature (25 °C) for 4 hours with fixed stirring (200 rpm) as shown in **fig (3.3.A) .** The clean catalyst containing coke, sulfur and minerals was dried in an oven at (120 °C) for 6 hours as shown in **fig (3.3.B).** The dried catalyst was exposed to carbon disulfide (100 ml) with continuous stirring in closed flask for 12 hours at room temperature as shown in **fig (3.3.C and D).** Then it was filtered and dried in air at room temperature as shown in **fig (3.3.E)** and calcined at (450 °C) in electric oven at constant temperature for 4 hours to remove all carbon and residual sulfur and then measure the remain weight of it as shown in **fig (3.3.F)** .

(A) (B) (C)

(D) (E) (F)

Fig (3.3) Steps of the regeneration of spent catalyst NiMo/γ-Al_2O_3 .

3.5. Determination of metals in catalysts

To find out the quantity of elements in the catalyst, aqua regia was prepared by adding nitric acid (conc=16 M) to hydrochloric acid (conc = 12 M) in a ratio of (1:3) . A known weight of virgin and spent catalyst was mixed with aqua regia solution and heated and digested at (100 °C) for 4 hours with continuous addition of distilled water whatever necessary until it is completely dissolved.

The produced solution are then completed to a known volume with distilled water and then the metal content was determined by atomic absorption method .

3.6. Catalyst properties

3.6.1. The bulk density or packing density

The bulk density (d_b) is determined by placing a known weight of catalyst in graduated cylinder and measure the volume of it and then the density is calculated. Based on weight/ volume ratio .The bulk density was determined using the equation below :

$$\textbf{Bulk density} = \frac{W}{V} \quad \textbf{……(3.1)}$$

In which :

W = weight of catalyst in the cylinder .

V = volume of the catalyst in the cylinder .

3.6.2. Particle density

For the particle density (d_p) several extrudates particles were weight and their volumes were also calculated by considering them as cylinders and then from weight and volume the particle density is evaluated .

3.6.3. Skeletal density

To estimate the skeletal density (d_s),a volume of known weight of catalysts was determined by subtracting the volume of pores present from pore volume measurement ,and then the density is calculated from the weight/ volume ratio **.**

3.6.4. Pore volume

The size of the pores was estimated by impregnation method to find the volume of water required to fill the pores with a quantity of weight of the catalyst. A known weight of the catalyst is placed in the beaker, then the volume of water from the burette, which covers the sample, is calculated, and the size of the pores is determined using the equation below [85]:

$$\textbf{Pore volume} = \frac{V}{W} \quad \textbf{.....(3.2)}$$

In which :

V = The volume of water that filled the pores

W= weight of sample

3.6.5. Porosity

Porosity can be calculated from the relationship between particle (d_p) and skeletal (d_s) densities and porosity (θ) is given by [85,86]:

$$\theta = \left(\frac{1-dp}{ds}\right) \quad \textbf{.....(3.3)}$$

In which :

θ = porosity

d_p = particle density

d_s = skeletal density

3.6.6. Void fraction

The void fraction (ε)can be calculated from bulk density and particle density using the following equation [85] :

$$\varepsilon = [1- (d_b / d_p)] \ldots\ldots\ldots\ldots (3.4)$$

In which :

ε = Void fraction

d_b = bulk density

d_p = particle density

3.6.7. loss on ignition

The mass loss of ignition was determined with a weight of 10 g of the catalyst and put inside the oven at a constant temperature of 800 ° C for 3-4 hours. After roasting, the sample was removed and put in desiccator for cooling.

Then the The remaining product is weighed and the mass difference is the mass of organic matter present in the sample. The loss weight percent was calculated using the equation below [87]:

$$\text{loss on ignition } \% = \frac{W1-W2}{w1} \ldots\ldots\ldots (3.5)$$

In which :

W_1 = Weight before burning

W_2 = Weight after burning

3.6.8. pH determination

The pH of the samples was determined by a weight of (1 gm) of the catalyst, boiled in a beaker contains (10 ml) distilled water for 5 minutes, Cooled at room temperature, the pH was measured with a pH meter .

CHAPTER FOUR

Results and Discussion

4.1 Spectroscopic Studies of New and Spent NiMo/γ-Al_2O_3 Catalyst .

4.1.1 Structural Techniques

4.1.1.1 X-Ray Diffraction

X-ray diffraction is used to examination and determine the crystalline phase of materials. The X-ray diffraction data due to the strongest three peaks of the prepared catalyst NiMo/γ-Al_2O_3 as shown in **table (4.1).** there are three main wide diffraction peaks at 2θ values of (37°, 46°, 67°) the x-ray diffraction pattern is shown in **figure (4.1)**. The appearance of these peaks can be attributed to the presence of Mo species and varying degree of the peaks are the result of the difference in the degree of crystallinity, as well as the effect of calcination at high temperatures which depends on the crystallinity of the nanoparticles.

The most common oxides of nickel, NiO and Ni_2O_3 may also be present in the amorphous phase or microcrystals [124]. Moreover, it has been noted that both (Al_2O_3) and $NiAl_2O_4$ have a characteristic peak at (2θ = 37.7) . but this peak for the former is broad and weak, while for the latter it is relatively narrow and sharp [125]. As the calcination temperature increases, some Ni atoms enter the surface of the Al_2O_3 internal structure to form $NiAl_2O_3$ [45].

The peaks position and intensities are in a good agreement with those reported in Join committee on power diffraction standards (JCPDS) file No.(20-0776) for prepared (NiMo/γ-Al_2O_3).

The particle sizes were calculated from Deby-Sherrer formula given below [126] :

$$D = \frac{0.9\,\lambda}{\beta cos\theta} \quad \text{.....} \quad (4.1)$$

In which :

D: is the crystallite size.

λ: is the wave length of radiation.

θ: is the Bragg's angle.

β: is the full width at half maximum (FWHM).

The estimated particle size of the prepared NiMo/γ-Al_2O_3 is (11.903) nm. The presence of sharp peaks in XRD pattern and particle size being less than (100) nm refers to the nano-crystalline nature of the prepared materials .

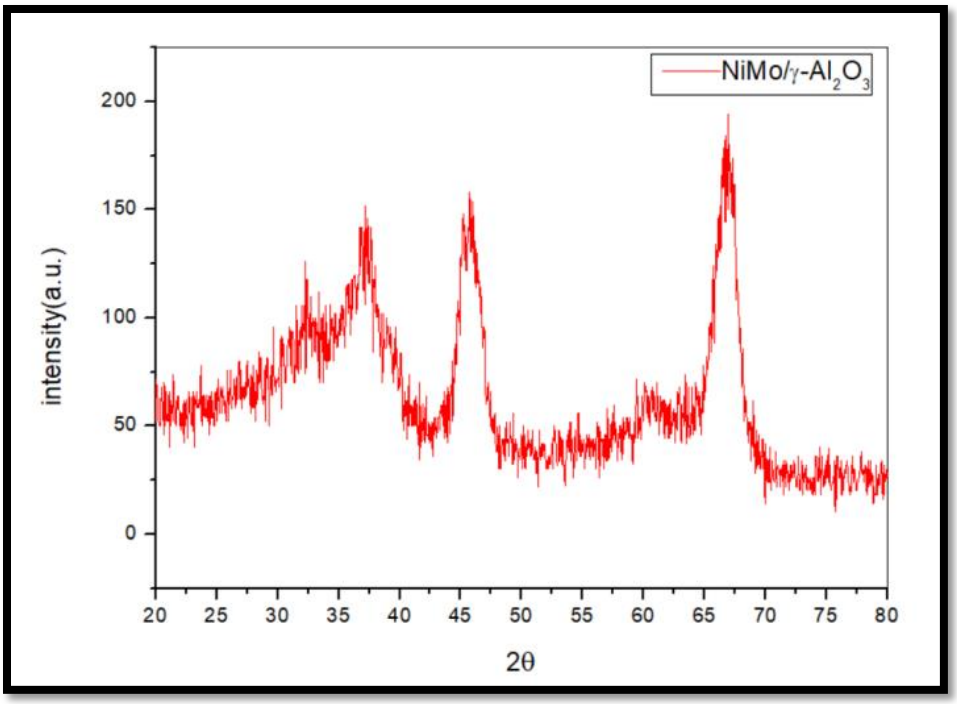

Fig (4.1): X-ray diffraction for prepared (NiMo/γ-Al_2O_3) catalyst with calcined at (500 °C) for (7 hours).

Table (4.1) The three strongest peaks in the XRD pattern of perpared $NiMo/Al_2O_3$ catalyst.

No. peak	2 Theta (deg)	d (A°)	FWHM (deg)	Intensity (counts)
1	37.2609	2.41123	1.55000	29
2	46.7720	1.98072	2.05000	58
3	67.7722	1.39984	1.80000	81

4.1.1.2 Raman spectroscopy

Figure (4.2) and **(4.3)** show the raman spectra of new and spent $NiMo/Al_2O_3$ catalyst . there is several bands , at (501 cm^{-1}) for the MoS_2 crystal [127] . The band at (922 and 780 cm^{-1}) attributed to $NiMoO_4$ precursor phases . the Broad band in (1070.5 to 1570 cm^{-1}) is associated to the Mo=O stretching vibrations [128] . Spectra can also be observed to be very similar to pure graphite . Whereas, the difference in intensity is due to an increase in intensity when the volume of graphite decreases . This assumption applies and confirm to the coke being present in spent catalyst[127].

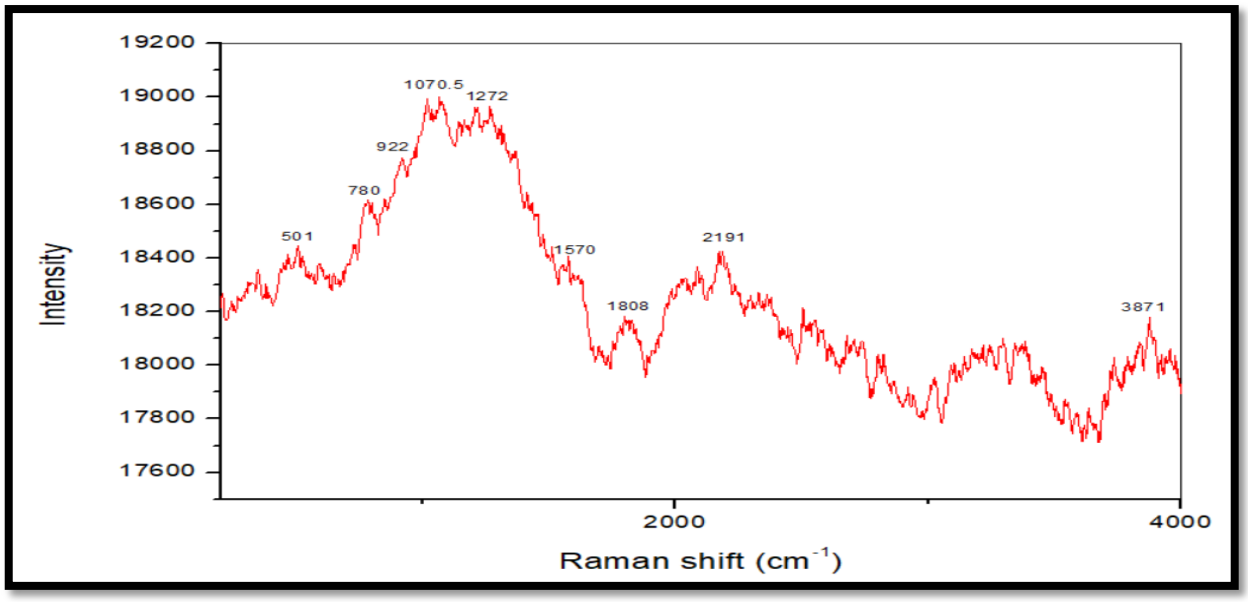

Fig (4.2) Raman spectrum of new NiMo/γ-Al_2O_3 catalyst

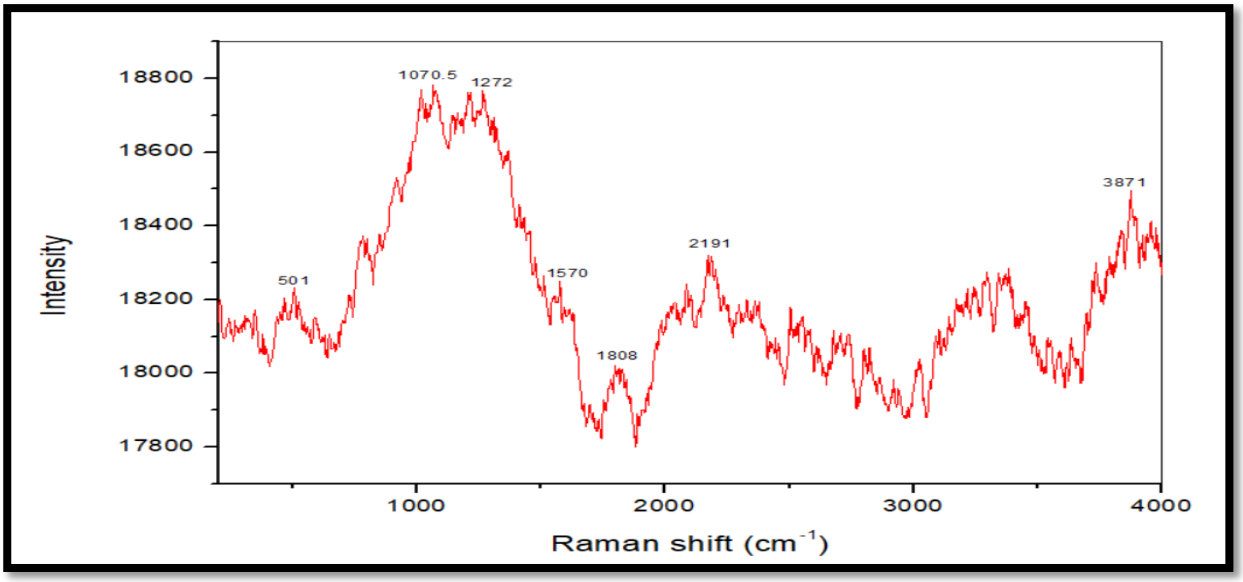

Fig (4.3) Raman spectrum of spent NiMo/ γ-Al_2O_3 catalyst

4.1.1.3 Fourier transform infrared spectroscopy (FTIR).

Although the spectra in **Figures.(4.4)** and **(4.5)** of both new and spent catalysts are similar in general, there are some slight differences in vibrational frequencies of metal-metal bonds and Ni-O, MoO_4 and Al-O structuers and this is attributed to interaction of precuser catalysts components with carbon, hydrogen and sulfur compounds in the oil feed used at high temperature and pressure, the disapperance of low intensity bands in 1200 to 1700 cm^{-1} region is due to removal and decline of boron and phosphorous compounds promoters in the spent catalyst. These results are in agreement with the FTIR spectrum of $NiMo/Al_2O_3$ reported previously [78].

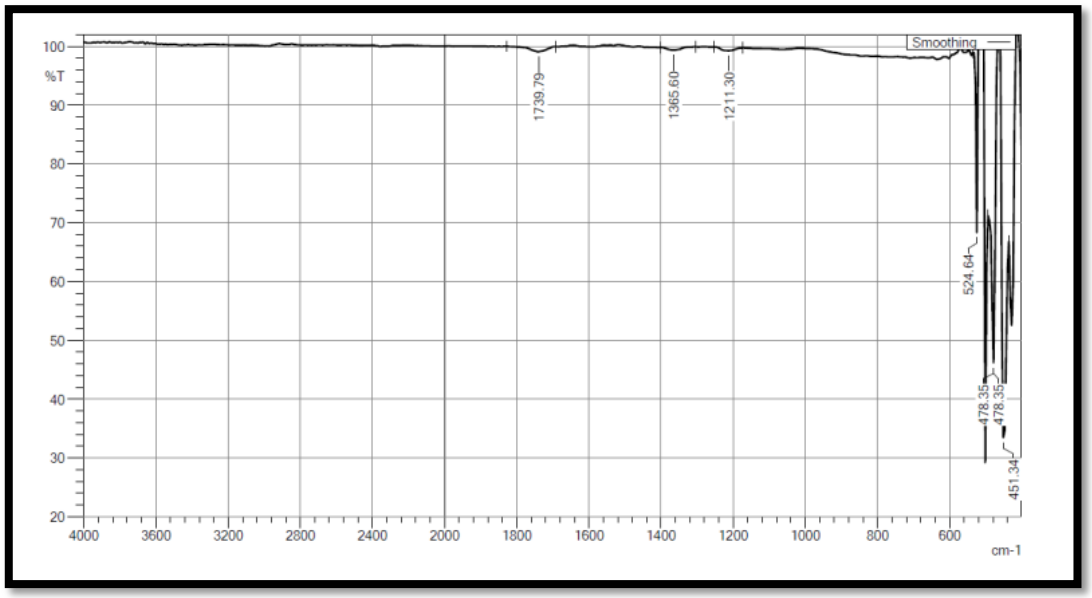

Fig (4.4) FTIR spectrum of new NiMo/γ- Al_2O_3 catalyst .

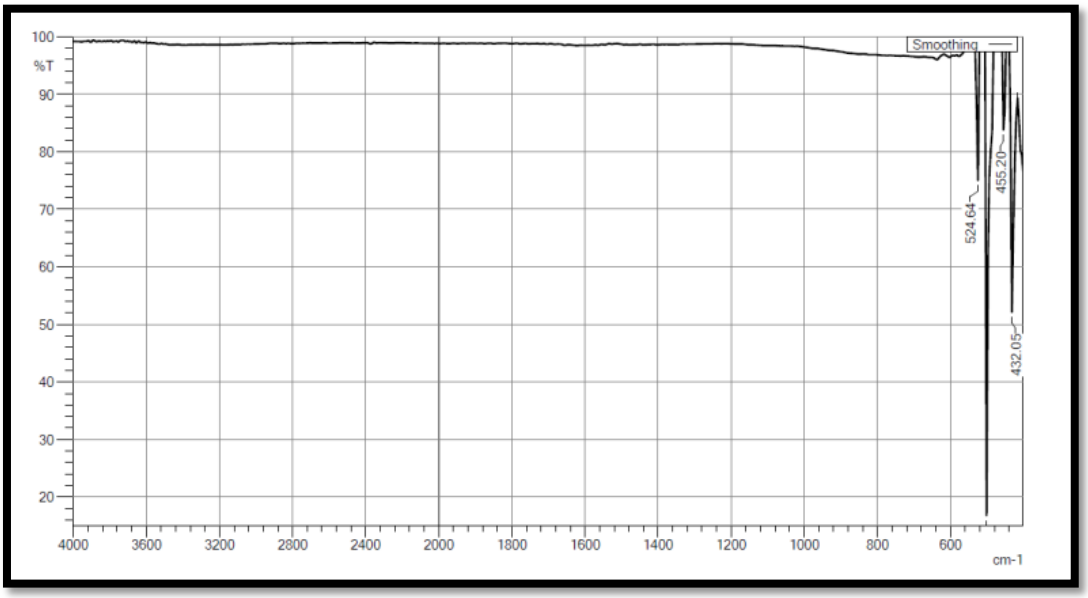

Fig (4.5) FTIR spectrum of spent NiMo/γ-Al_2O_3 catalyst .

The FTIR spectra of the prepared catalyst are shown in **Figure (4.6) .** Peak in the region (400-1050 cm^{-1}) corresponds to MoO_3 in (815.12). The absorption bands assigned to the Al-O vibration in (575.46 and 751.21) represent the aluminum ions octahedral and tetrahedral respectively . These value found in fingerprint region under 1000 cm-1 arising from inter-atomic vibrations .These results are in agreement with NiMo/Al2O3 the previously reported FTIR spectrum[78]

The values in FTIR spectra for regenerated NiMo/γ-Al_2O_3 catalyst shown in **figure (4.7)** are approximate to the prepared catalyst. These results are in agreement with NiMo/Al_2O_3 previously reported FTIR spectrum [26 ,129].

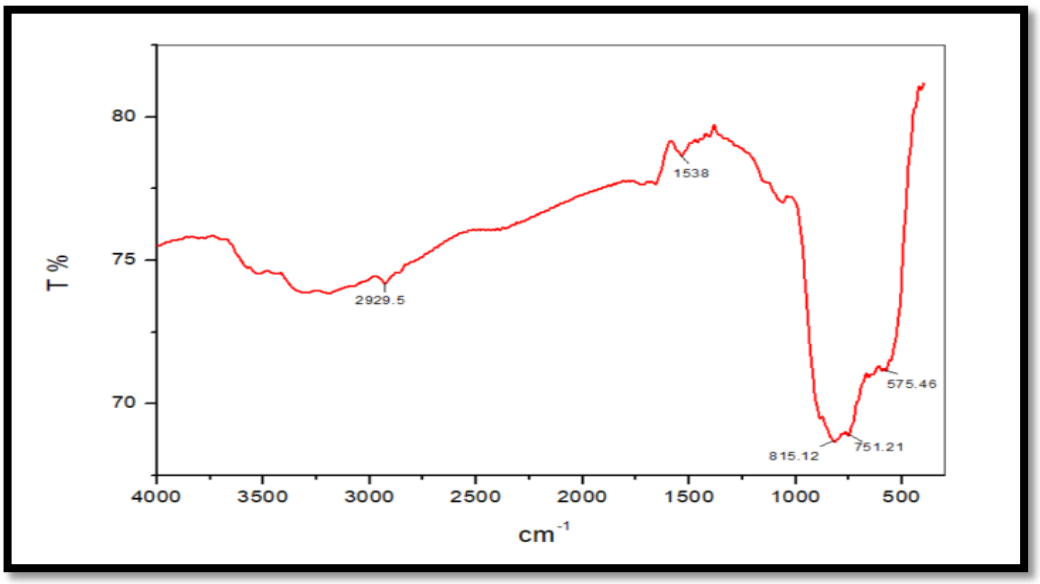

Fig (4.6) FTIR spectrum of prepared NiMo/γ-Al_2O_3 catalyst

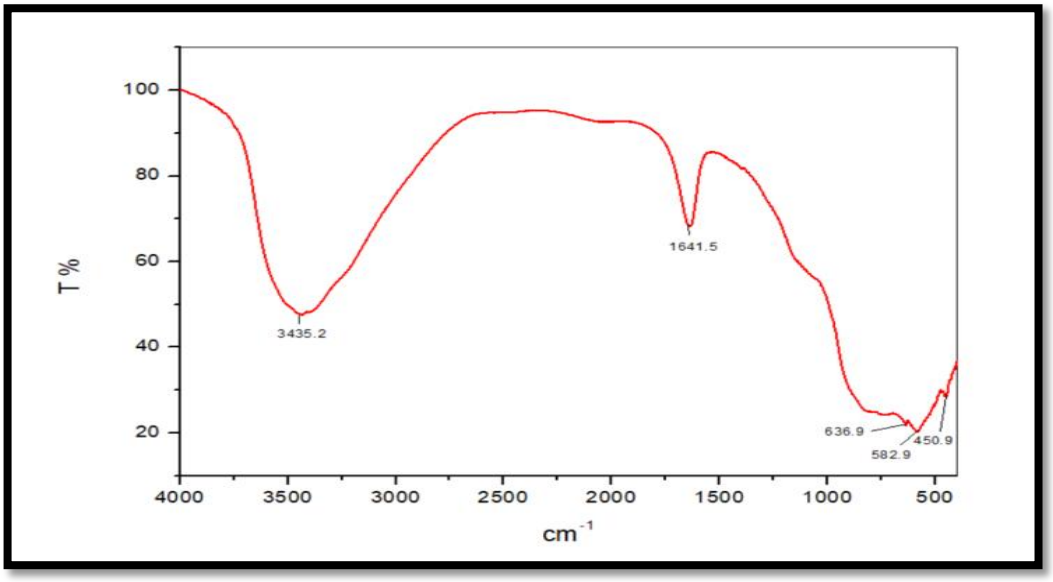

Fig (4.7) FTIR spectrum of regenerated NiMo/γ-Al_2O_3 catalyst

4.1.1.4 Energy dispersion X-ray (EDX)

Energy dispersive X-ray (EDX) spectra were used to provide both qualitative and quantitative information about the surface composition of the studied catalysts. The EDX profiles of virgin and spent catalysts in **figures (4.8)** and **(4.9)** identified the elements that present as (O, Al, Ni and Mo) which are the main components of the virgin catalysts with their atomic and weight percent given in **table (4.2)** .

There is a decrease in the values of the elements content (Ni , Mo) as a result of consumption and use over time, whereas (O) increase is due to oxidation of the catalyst with long term use .The apparition of new materials such as (C and S) in the spent catalyst as shown **figure (4.9)** Which comes as a result of catalysts consumption and use over time, in desulfurization processes .

While the appearance of some minerals such as (Fe , K) that comes from both the feed and the reactants as well as those that come from the corrosion of reactor materials in processes with time .

EDX of prepared and regenerated NiMo/γ-Al_2O_3 catalysts as shown in **figures (4.10)** and **(4.11)** are approximate to the new NiMo/Al_2O_3 catalyst .

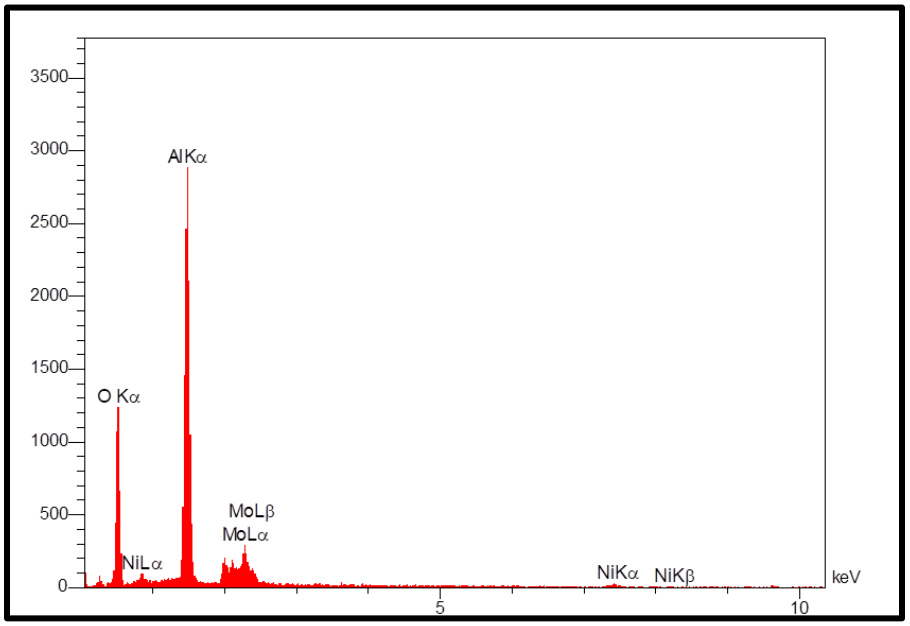

Fig (4.8) . EDX analysis for new $NiMo/Al_2O_3$

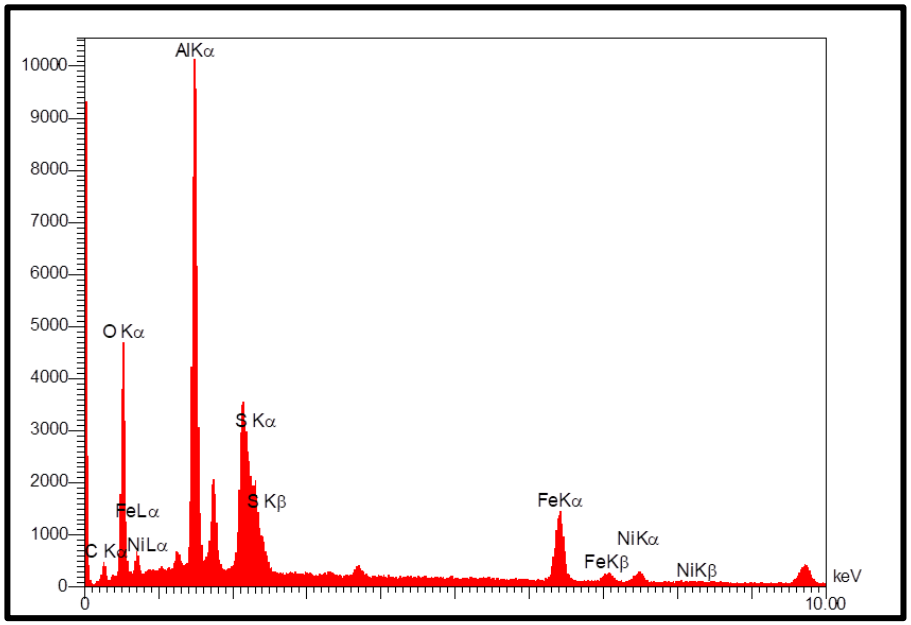

Fig (4.9) . EDX analysis for spent $NiMo/Al_2O_3$

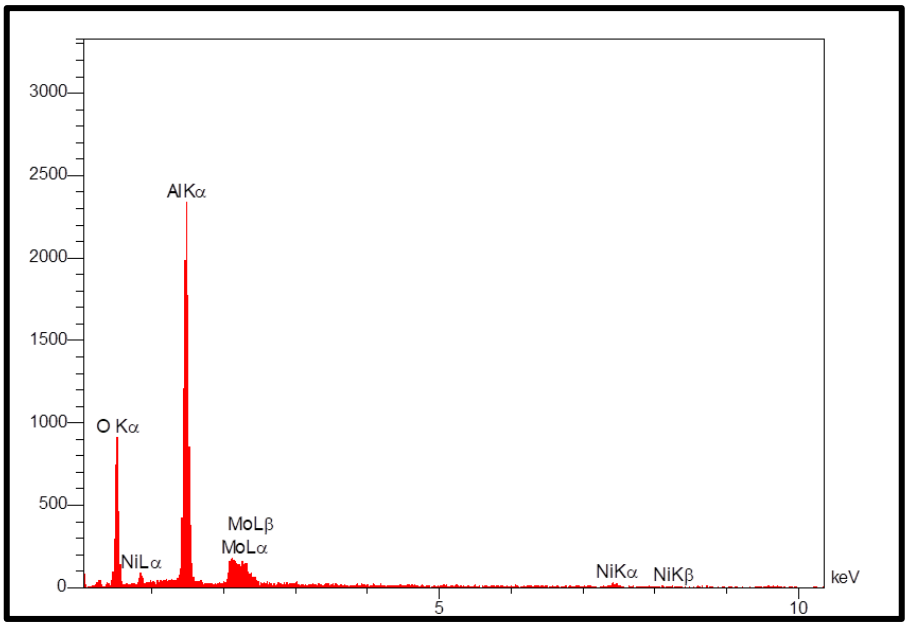

Fig (4.10) . EDX analysis for prepared $NiMo/Al_2O_3$

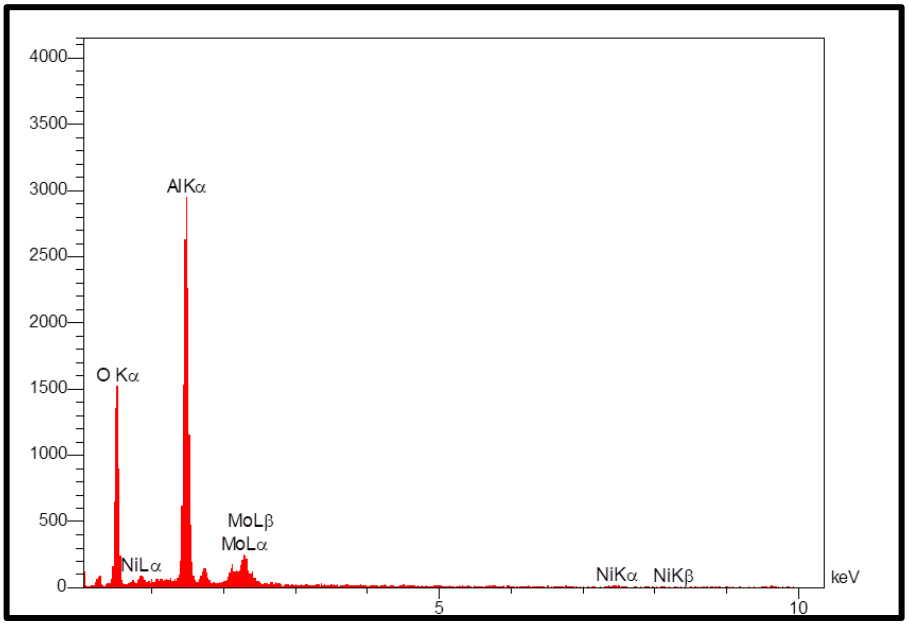

Fig (4.11) . EDX analysis for regenerated $NiMo/Al_2O_3$

Table (4.2) weight percent for element in new , spent ,prepared and regenerated NiMo/Al_2O_3 from EDX .

Element	New catalyst	Spent catalyst	Preparated catalyst	Regenerated catalyst
O	34.88	32.89	49.10	30.92
Ni	1.77	0.86	3.01	2.90
NiO	2.69	1.41	4.34	3.41
Al	29.60	28.43	32.46	47.73
Al_2O_3	67.02	69.84	69.46	82.88
Mo	16,85	14.74	15.43	9.46
MoO_3	30.29	28.74	26.21	13.12

4.1.2 Surface-studies of catalysts.

4.1.2.1 Field emission scanning electron microscopy (FESEM) .

Figure (4.12) represent the (FESEM) images of the new (NiMo/γ-Al_2O_3), which shows its surface morphology and structural properties. From its observation we note that the minimum and maximum and average particle size are (26.05 , 48.38 and 33.80 nm) respectively and that the shape of the particle is spherical or nearly spherical and in the form of clusters distributed on the surface in a regular equal manner indicating that the shape is regular.

Figure (4.13) shows images of spent catalysts, it appears in the form of larger sized nanofibers or nanotubes that clump together, with the minimum , maximum and average particle size of (24.19 , 156.2 and 64.11 nm) respectively as well. This indicates that some metals, sulfur compounds and carbon are deposited and cause fouling of the surface and sintering of pores and are trapped in resulting in particle size rise.

surface morphology and structural properties for the prepared and regenerated catalyst shown in **figures (4.14) ,(4.15)** . the shape of the particle is spherical or nearly spherical and distributed on the surface in a regular equal and it is an approximate in its forms to the new catalyst .

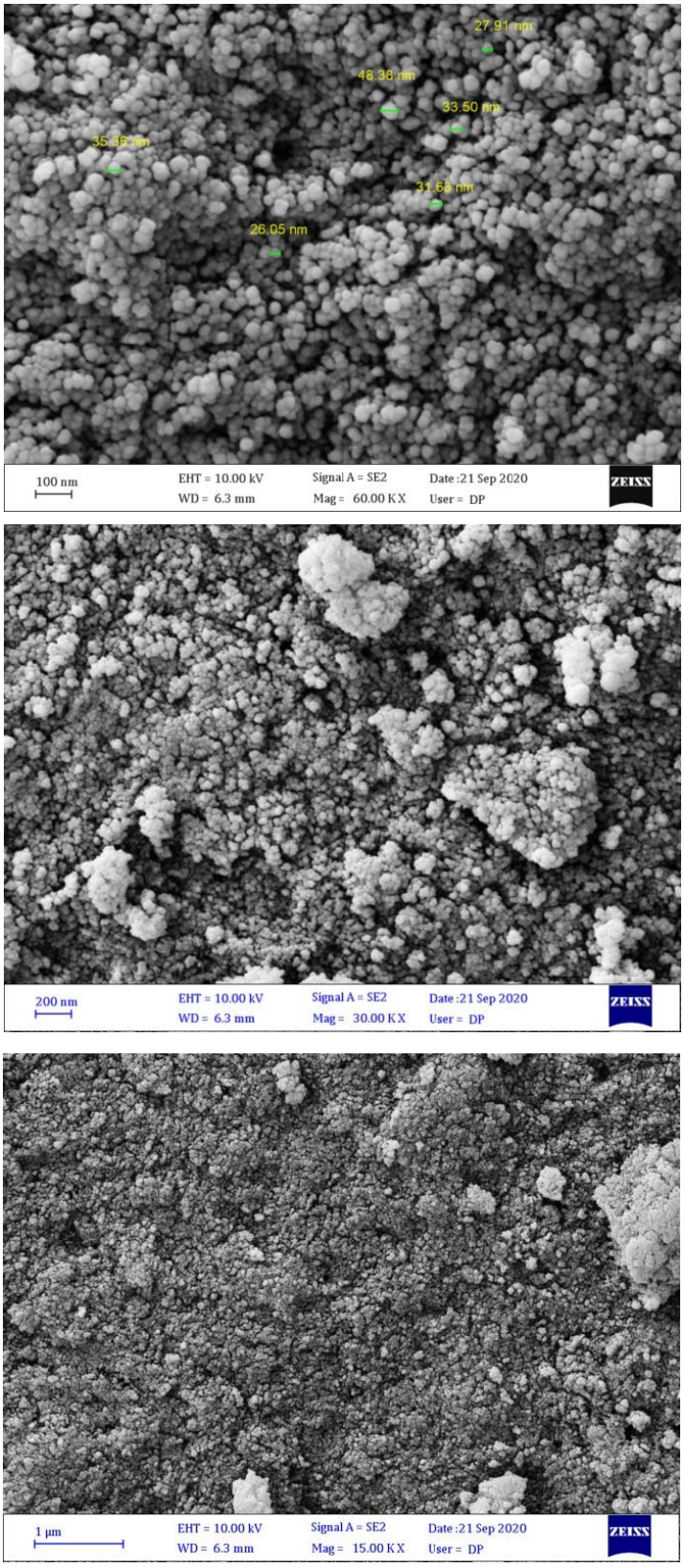

Fig (4.12) . (FESEM) image of the new catalyst (NiMo/γ-Al_2O_3)

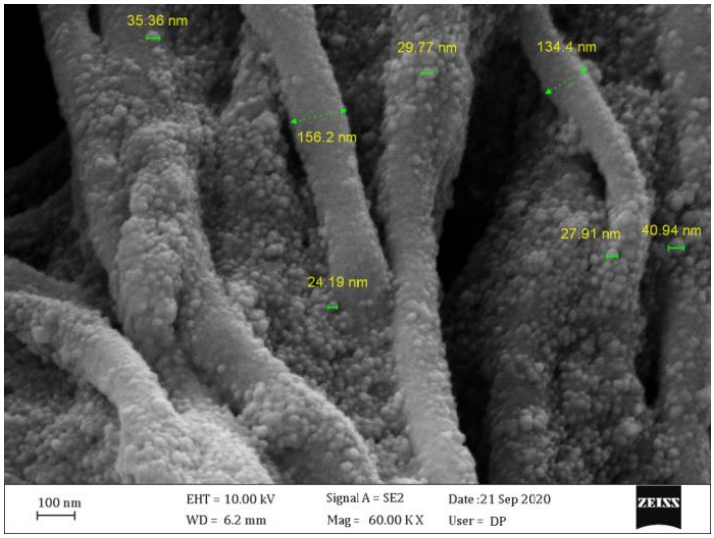

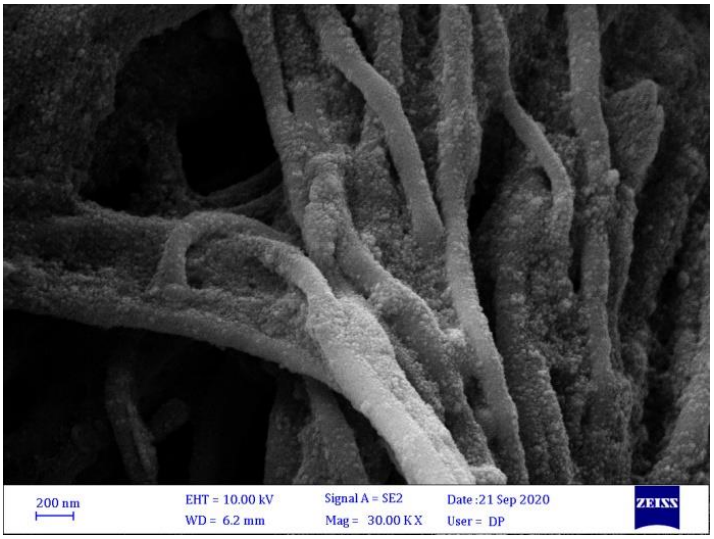

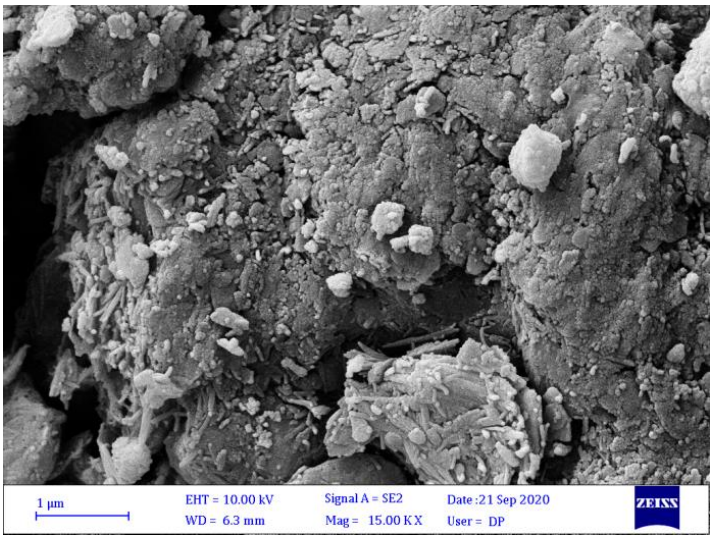

Fig (4.13). FESEM image of the spent catalyst (NiMo/γ-Al_2O_3)

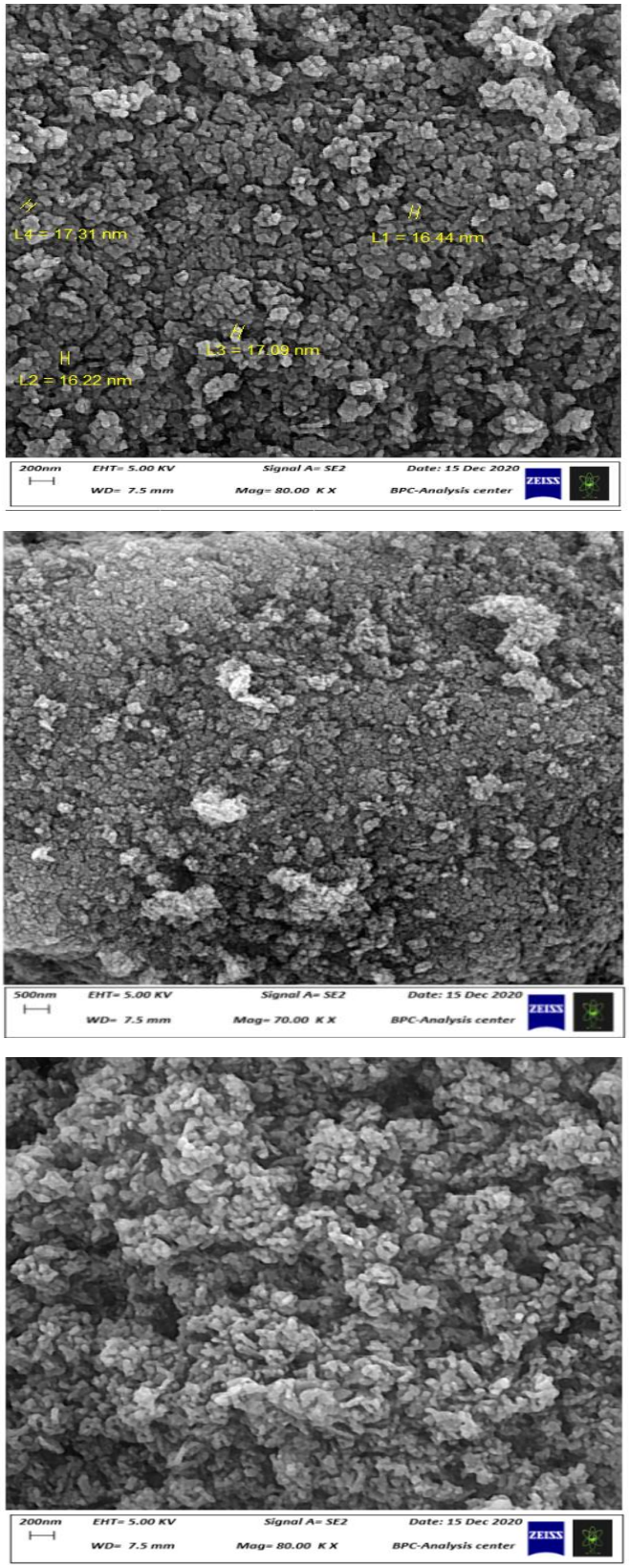

Fig (4.14) FESEM image of the prepared catalyst (NiMo/γ-Al_2O_3) .

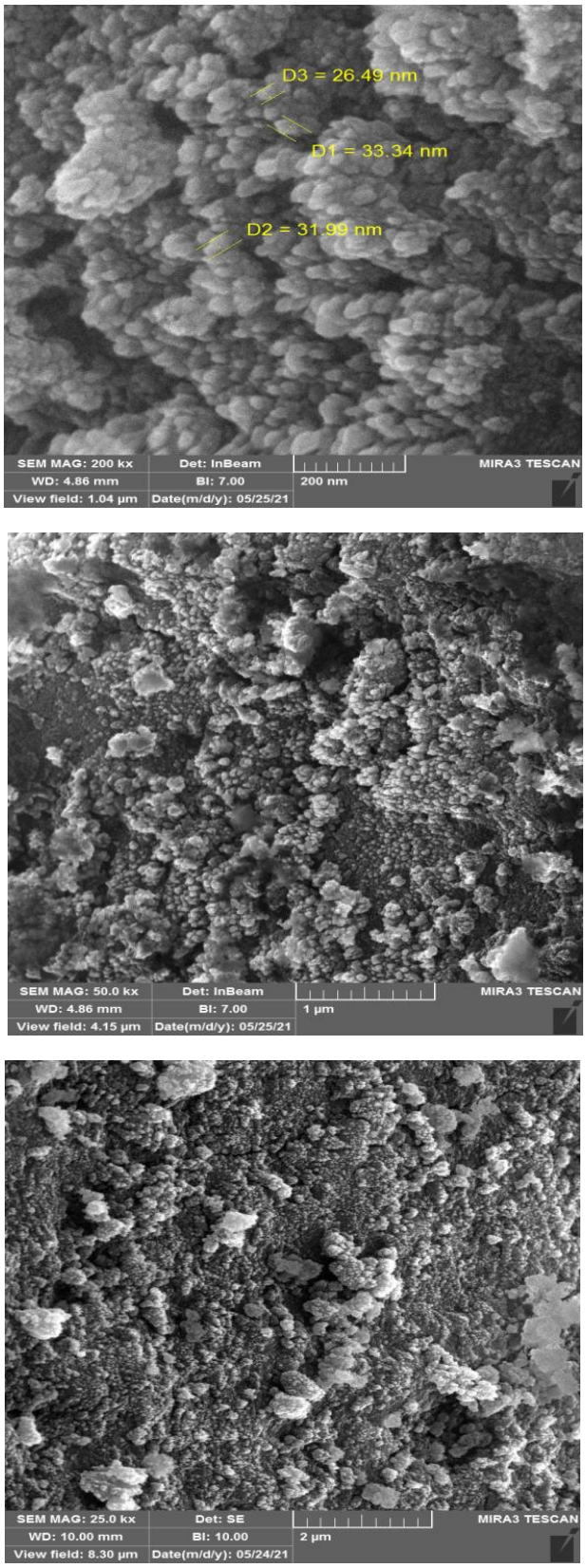

Fig (4.15). FESEM image of the regenerated catalyst (NiMo/γ-Al_2O_3) .

4.1.2.2 Atomic Force Microscopy(AFM) .

AFM is a new technology used to recognize porous nature and surface thickness and the topography and roughness of the surface. **Figures (4.16)** and **(4.18)** show a three-dimensional (3D) and two-dimensional (2D) and nanoscale image of the new and spent NiMo/γ-Al_2O_3 catalysts , and the **figures (4.17)** and **(4.19)** shows the granular distribution diagrams of the new and spent NiMo /γ-Al_2O_3 nanoparticles. The pictures showed spherical shapes and nearly uniform distribution, with some clusters. The AFM images clearly show the small size for nanoparticles of the material, which confirmed that deactivation of the catalyst very affected the surface properties of the catalyst. AFM also showed that the surface is porous. In addition, the average roughness and thickness of the layers increase with the increase in the deactivated [130] .

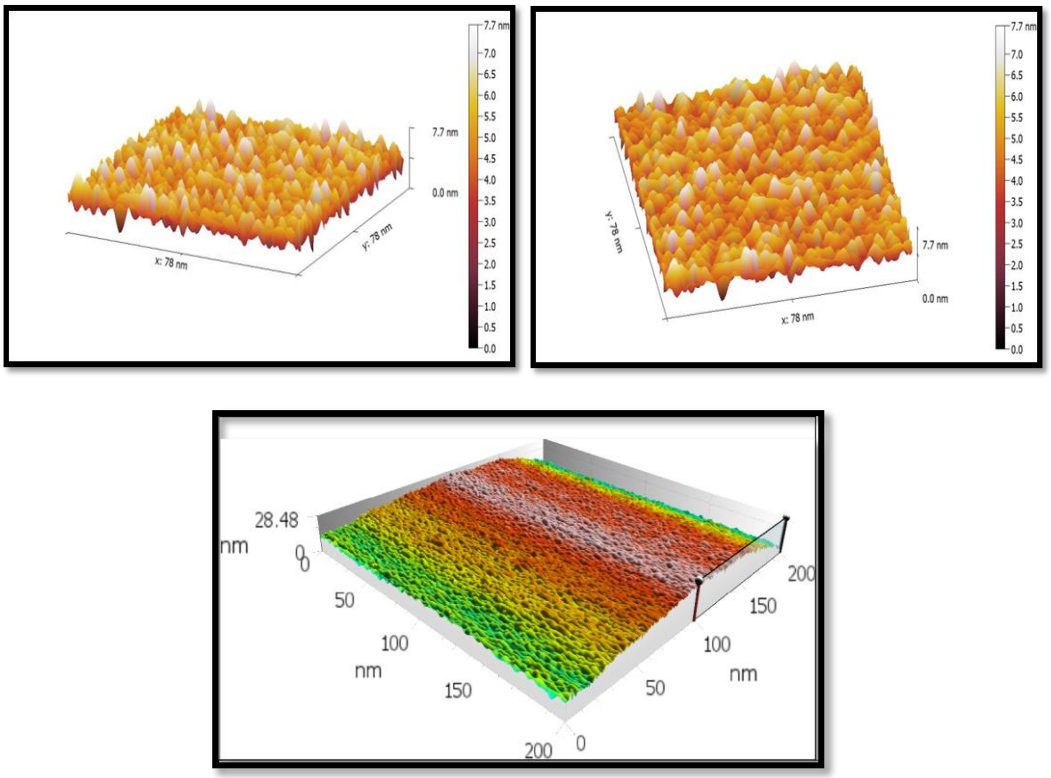

Fig (4.16) AFM 3D and 2D images for new catalyst.

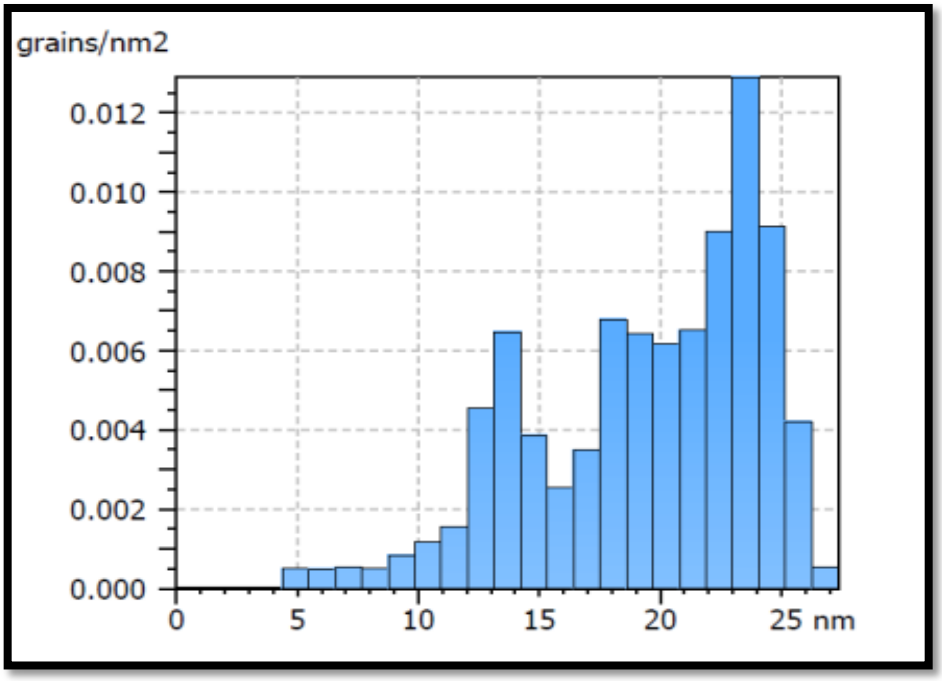

Fig (4.17) Granular distribution diagrams for new catalyst .

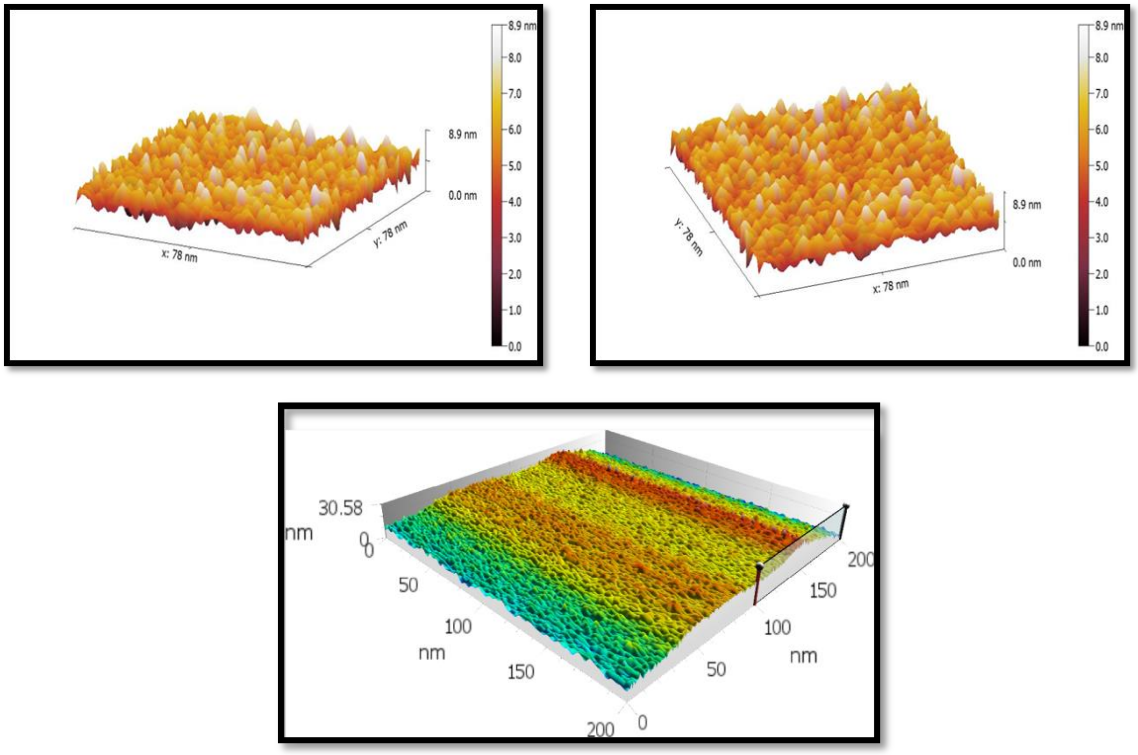

Fig (4.18) AFM 3D and 2D images for spent catalyst .

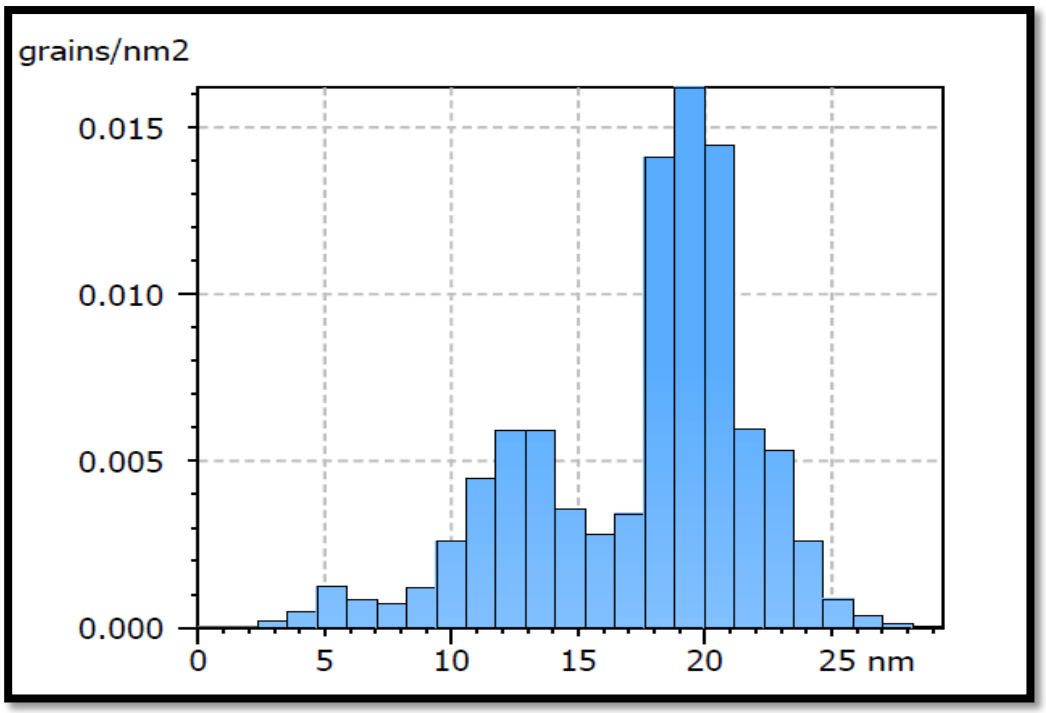

Fig (4.19) Granular distribution diagrams for spent catalyst .

Table (4.3) shows the factors that determine the surface and that the average roughness is high for the spent catalysts . It is also noted that there is in an increase in surface area factor in the spent catalyst , in addition to the thickness or maximum height of particles which increase as well as results of use sintering and agglomeration of carbon .

Table (4.3) Roughness coefficients of the new and spent NiMo/γ-Al_2O_3 catalysts .

Amplitude Factors	New catalyst	Spent catalyst
Thickness or (maximum height)	28.48 nm	30.58 nm
(average diameter)or Particle size	18.56 nm	16.30 nm
Roughness (Sa)	4.261 nm	3.751 nm
Root mean square (RMS)	1.095 nm	1.24 nm
Surface skewenss (R_{sk})	-0.00106	-0.0189
Surface kurtosis (R_{ku})	0.108 nm	0.387 nm
Average roughness (Ra)	0.868 nm	0.98 nm
Surface area	83.9720 *10 $^{-15}$	92.0856 * 10^{-15}

4.2 Thermal studies analysis (TGA) of catalysts .

The (TGA) curves of new and spent catalyst are shown in **Figure (4.20)** and **Figure (4.21)** respectively. According to (TGA) in **Figure (4.20)** there are successive stages of weight loss in the sample .The reason for weight loss at room temperature up to (50-200 ^{o}C) is the elimination of the water physically adsorbed on the surface of the sample and the partial decomposition of nickel and molybdenum , the second reason for weight loss is due to the total decomposition of the salts of nickel and molybdenum as well as the decomposition of the remaining organic additives in the sample [47,130,131]. In nano catalysts, mass loss due to combustion reactions is (6.86 % ,10.96% , and 4.083 %) respectively as shown in **figure (4.20) .**

In accordance with (TGA) there is not loss of weight between (620 and 800 ^{o}C). We can say that at temperatures above (620 °C) , all remaining volatile compounds were removed. The interfering signals in the (DTA) curves may be due to the endothermic evaporation, oxidative decomposition, and thermal adsorption [132]. Because of these interfering signals in the (DTA) curve, it is difficult to determine the endothermic or exothermic peak to a specific temperature [132,133].

Figure (4.21) (TGA) provide information on the nature and evolution of coke deposits as reaction time increased when the temperature reaches (700 ^{o}C), the sample generally loses about (20%) weight (coke) [144]. In the region from (50 to 200 ^{o}C) weight loss occurs due to the evaporation of the physically adsorbed water on the surface of the sample [134,22].

The second weight loss in the range (250-400 ^{o}C) is due to the combustion of coke at higher temperatures [134-136] . The signal in the region between (500 to 600^{o}C) is due to the emission of sulfur in the form of SO_2 [22].

Fig (4.22) and **(4.23)** show (TGA) curve of prepared and regenerated NiMo /γ-Al_2O_3 catalyst with results consistent to the TGA spectrum of the new NiMo /γ-Al_2O_3 .

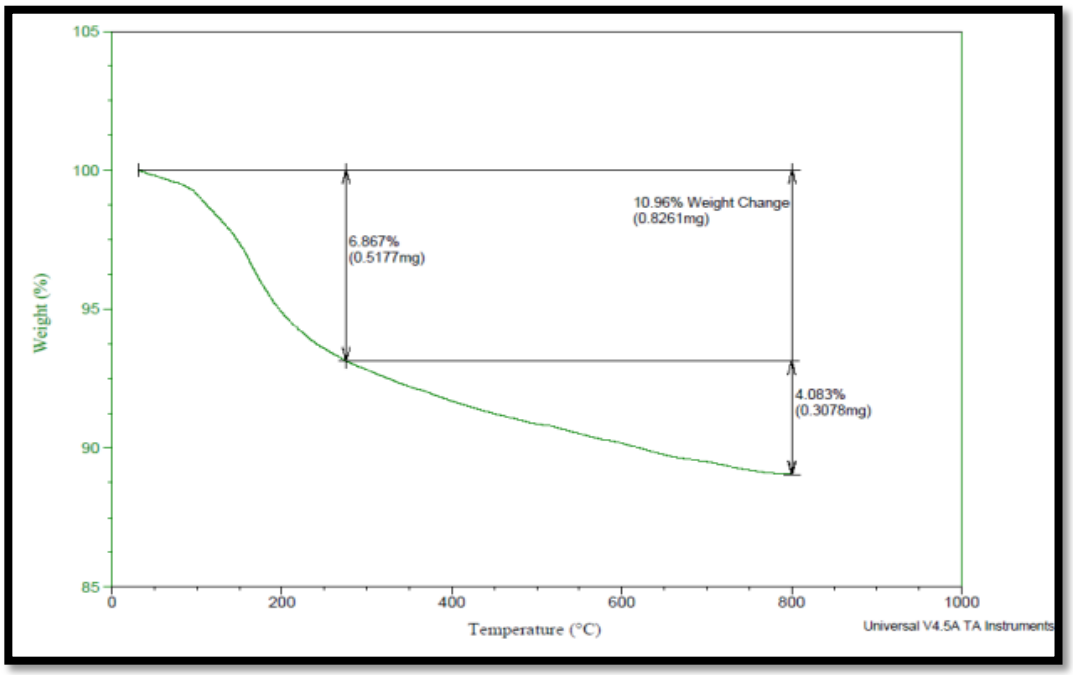

Fig (4.20) . TGA for new NiMo/γ-Al_2O_3 catalys

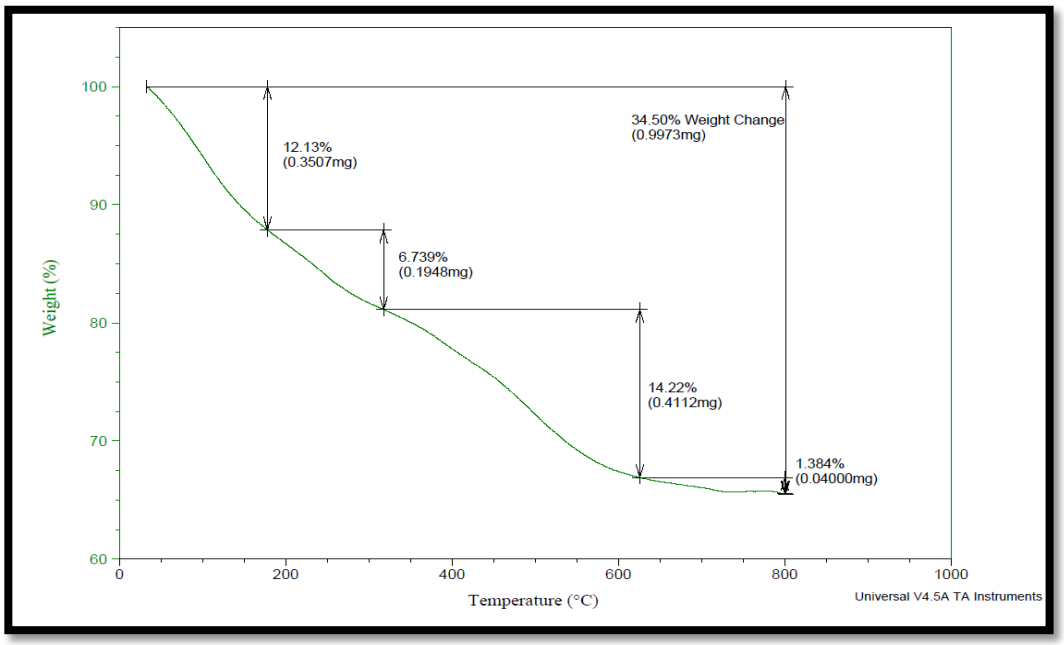

Fig (4.21) . TGA for spent NiMo/γ-Al_2O_3 catalyst

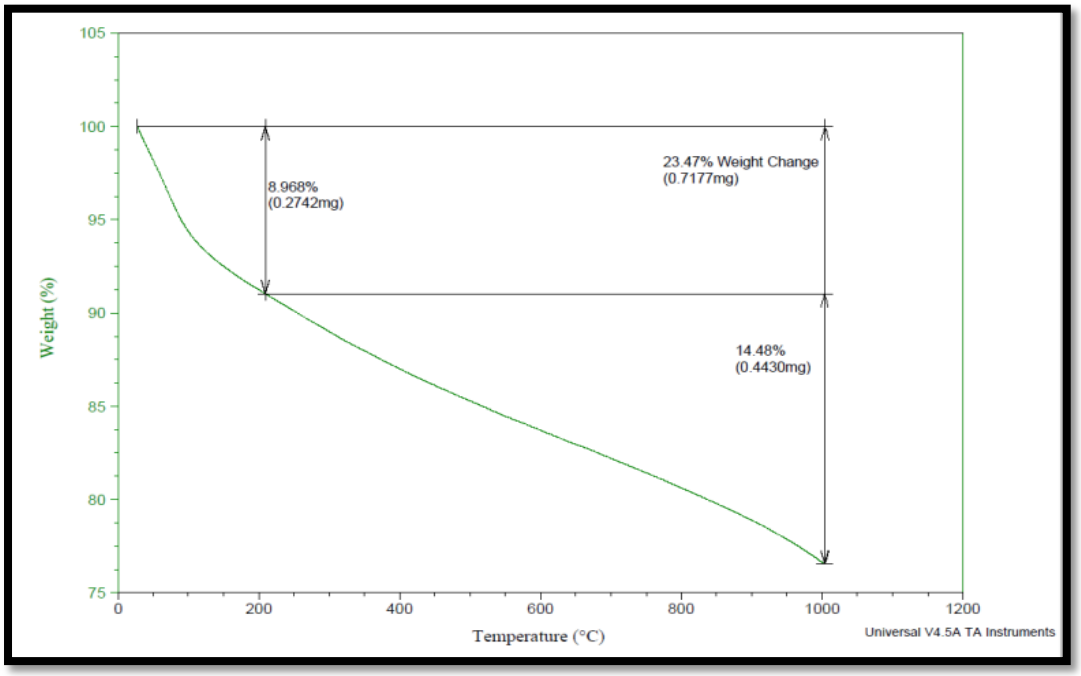

Fig(4.22) . TGA for NiMo/γ-Al_2O_3 catalyst prepared.

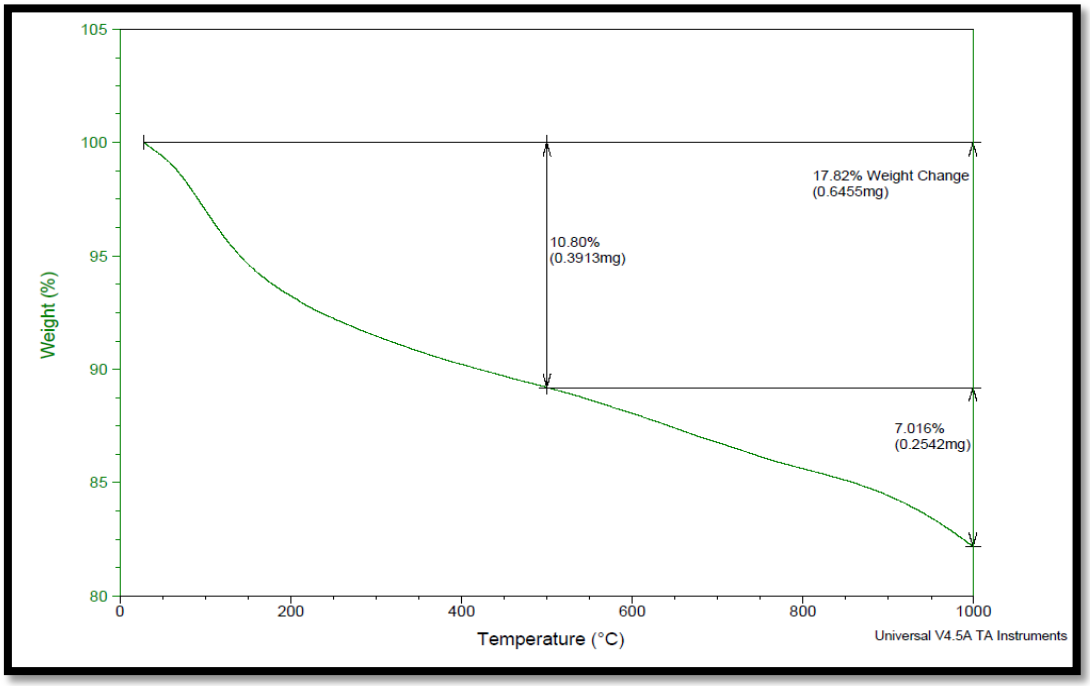

Fig (4.23). TGA for catalyst regenerated (NiMo/γ-Al_2O_3)

4.3 Properties of new and spent catalyst .

4.3.1 physical properties .

The physical and chemical properties of new and spent catalysts are expressed in **table (4.4).** From the changes of the new and spent catalysts, we observe an increase in densities in the spent catalyst due to the increase in the size of the catalyst particles caused from fouling of the material and the filling of pores with carbonaceous materials [85] .

The total size of the material includes particle size, void size, and internal pore size, so the closing of pores as a result of disruption leads to a decrease pore volume, porosity and void fraction [85,86].

Loss on ignition for new catalyst is less than spent catalyst because it does not contain impurities which cause the weight loss to be small , While in the spent catalyst the weight loss is greater due to the deposition of large amounts of impurities inside and outside the pores[87].

Increase in particle density is consistent with data observed from (FESEM) , (AFM)….etc . Finally increase in pH is observed in spent catalysts as during use in HDS process, acidic sulfur compounds will be involved in.

Table (4.4). Physical and chemical properties of commercial virgin and spent catalysts.

Catalyst Property	new catalyst	Spent catalyst
NiO, wt %	2.69	1.41
MoO_3, wt %	30.29	28.74
Al_2O_3, wt %	67.02	69.84
Form	Extrudates	Extrudates / powder
Color	Light green	Dark brown
pH	8	5
Bulk density/gm. cm^{-3}	0.7115	0.8991
Pore volume/ cm^3. gm^{-1}	0.7	0.6
Porosity , %	0.4907	0.4235
Loss on ignition , wt %	1.94	16.34
Void fraction , wt%	0.4175	0.3222
Particle density/gm.cm^{-3}	1.2215	1.3265
Skeletal density/gm.cm^{-3}	2.3985	2.3010

4.3.2. Elemental analysis

For the elements in the new and spent catalysts expressed in **table (4.5) ,**there is a decrease in the values of the elements content (Ni , Al , C , S) in spent catalyst as a result of consumption and use over time [137] . In addition , there is an apparent increase in the metal or element content in the waste catalysts that comes from both the feed and the reactants as well as those that come from the corrosion of reactor materials due to harsh operating conditions and time [137].

Table (4.5). Elements present in new and spent catalysts .

Element property (wt%)	New catalyst	Spent catalyst
Mo	9.46	14.74
Ni	2.90	0.86
Al	47.73	28.43
O	39.92	55.96
C	0.0	14.4
S	0.0	4.05
Na	0.362	0.129
K	0.00043	0.0049
Mg	0.00090	0.046
Fe	0.0195	0.445
Zn	0.0036	0.0047
Si	0.16	0.089

4.4 kinetic of Carbon Removal

The kinetic study of the carbon removal process was performed on spent $NiMo/Al_2O_3$ catalysts using experimental conditions : The initial carbon weight $[C]_o$ of the catalyst was heated at different calcination temperatures (723 , 773 , 823 and 873 K) and different time periods (30 ,60 ,90 and 120 min) .

If the weight of carbon originally presents in (1 gm) catalyst is equal to $[C]_o$= 0.1275gm and then the weight of carbon present in catalysts after being calcined at any time and temperature $[C]_t$ will be calculated from suggested equation **(4.1) .**

$$0.1275 - W_{carbon\ removed} = [C]_t \quad \ldots\ldots\ldots \textbf{(4.1)}$$

Table (4.6) demonstrate the data used to fit 1st and 2nd order **equation (4.2)** and **(4.3)** given below [138] :

$$\ln (C_o / Ct) = k_1 . t \quad \ldots\ldots\ldots \textbf{(4.2)}$$

$$(1 /C_t - 1/C_o) = k_2 . t \quad \ldots\ldots\ldots \textbf{(4.3)}$$

In which (k_1 and k_2) are the rate constants for the first and second order respectively and (t)is the reaction contact time .

The values of half-life ($t_{1/2}$) are estimated from **equation (4.4)**and **(4.5)** for 1st and 2nd order cases respectively [138] .

$$t_{1/2} = (\ln 2/k_1) \quad \ldots\ldots\ldots \textbf{(4.4)}$$

$$t_{1/2} = [1/k_2 . C_o] \quad \ldots\ldots\ldots \textbf{(4.5)}$$

Table (4.6) Data for $[C]_t$, time and temperature for carbon removal from spent $NiMo/Al_2O_3$

Temperature/K	$[C]_t$	t/ min	ln (C_0 / C_t)	(1 /C_t - 1/C_0)
723	0.1012	30	0.231	2.038
	0.0833	60	0.462	4.161
	0.0638	90	0.693	7.831
	0.0506	120	0.924	11.919
773	0.0798	30	0.468	4.688
	0.0501	60	0.936	12.117
	0.0313	90	1.404	24.105
	0.0196	120	1.872	43.177
823	0.0550	30	0.84	10.338
	0.0237	60	1.68	34.351
	0.0085	90	2.7	109.804
	0.0035	120	3.595	277.871
873	0.0446	30	1.05	22.421
	0.0156	60	2.1	56.259
	0.0045	90	3.344	214.379
	0.0015	120	4.4427	658.823

These data was applied by plotting of ln (C_0 / C_t) against values of (t) which give straight lines with slope of k_1 at different temperatures shown in **fig (4.24)** and the plot of (1 /C_t - 1/C_0) against values of (t) give straight lines with slope of k_2 at different temperatures shown in **fig (4.25)** as well .

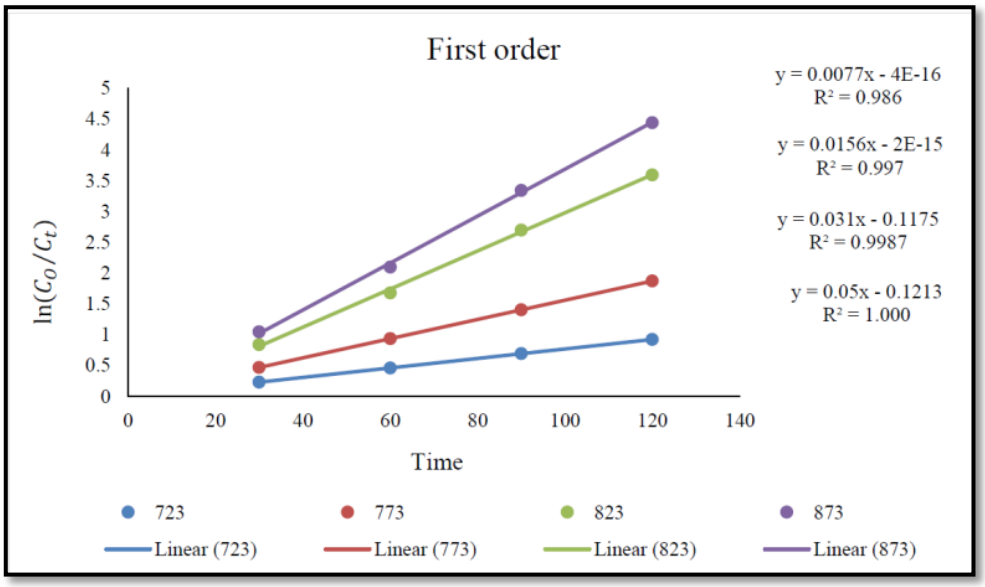

Fig (4.24) First order kinetic model for carbon removal from spent NiMo/Al_2O_3 catalyst

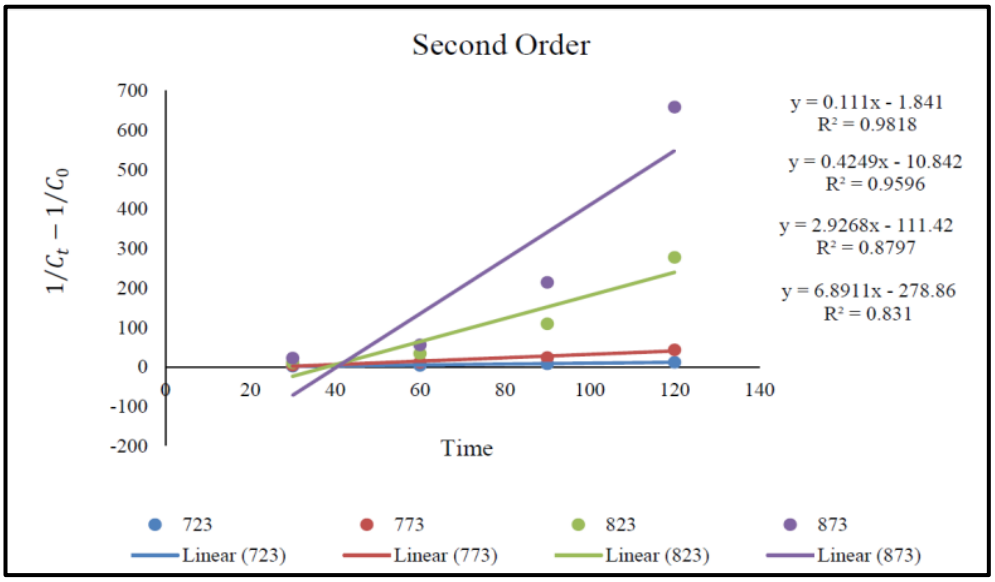

Fig (4.25) Second order kinetic model for carbon removal from spent NiMo/Al_2O_3 catalyst.

Table (4.7) display the values of rate constants and half-life at different temperatures for 1st and 2nd order kinetics models as calculated from slopes of figures above.

Table (4.7) Data for k_1 ,k_2 and $t_{1/2}$

T/ K	1/T	K_1	-ln k_1	-ln(k_1/T)	$t_{1/2}$	K_2	-lnk_2	-ln(k_2/T)	$t_{1/2}$
723	0.001383	0.0077	4.8665	11.4499	5.55	0.111	-2.1982	8.7816343	1.14
773	0.001293	0.0156	4.1605	10.8107	4.85	0.4249	-0.8559	7.50618048	0.30
823	0.001215	0.0310	3.4737	10.1867	4.16	2.9268	1.0739	5.63904652	0.04
873	0.001145	0.0499	2.9977	9.7696	3.69	6.8911	1.9302	4.84170483	0.03

The Arrhenius and free energy equations linearized froms are given in **equations (4.6)** and **(4.7)** [138] **.**

$$\ln k = \ln A - \frac{Ea}{RT} \ldots\ldots\ldots\ldots \textbf{(4.6)}$$

$$\ln (k/T) = (-\Delta H/RT) + [\ln(Kb/h) + \Delta S/R] \ldots\ldots\ldots \textbf{(4.7)}$$

In which :

K : transmission coefficient

A : factor in the Arrhenius equation

Ea : apparent activation energy (KJ. mol $^{-1}$)

R : universal gas constant (J K^{-1}. mol $^{-1}$)

T : absolute reaction temperature (K)

ΔH^{*} : enthalpy of activation (KJ mol^{-1})

ΔS^{*} : entropy of activation (J mol^{-1} K^{-1})

K_b : Boltzmann constant (J K^{-1})

h : plank constant (J. s)

So , from the plot of ln k_1 and ln k_2 against 1/T show in **fig (4.26)** and **(4.28) the** energies activation can be calculated from slopes and from the plots of ln (k_1/T) and ln (k_2/T) ageinst 1/T **fig (4.27)** and **(4.29)** the enthalpies (ΔH) and entropies (ΔS) of activation can be also calculated .

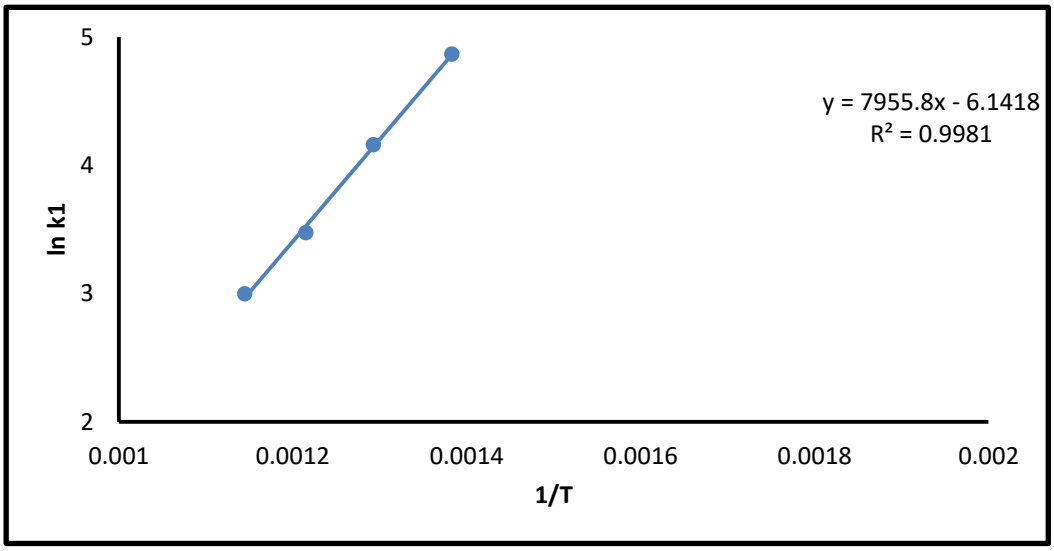

Fig (4.26) . the plot of ln k_1 against 1/T

So from the Arrhenius plot of [ln k_1 vs 1/T] , the slope of 7955.8 represent (E_a/R) , from which the energy of activation can be calculated as 66.144 kJ/mole.

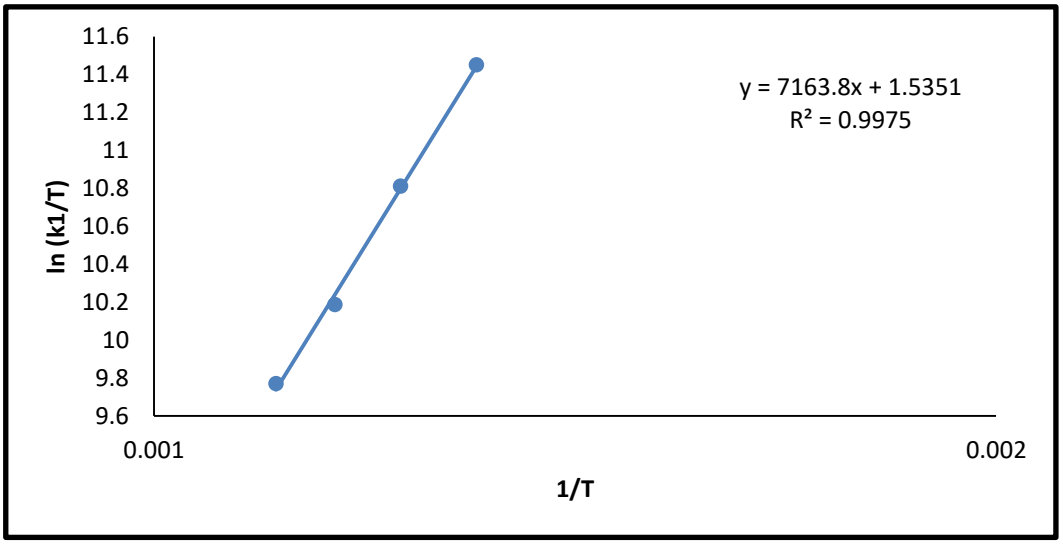

Fig (4.27). the plots of ln (k1/T) ageinst 1/T

Also the linearized plot of [ln(k1/T) vs 1/T] yield slope of (ΔH/R) and intercept of [$\ln(K_b/h) + \Delta S/R$] where enthalpy and entropy change can be calculated from equations (4.8) and (4.9) respectively [139].

$$\text{Slope} = -\Delta H/R \ldots\ldots \textbf{(4.8)}$$

$$\text{Intercept} = [\ln(K_b/h) + \Delta S/R] \ldots\ldots \textbf{(4.9)}$$

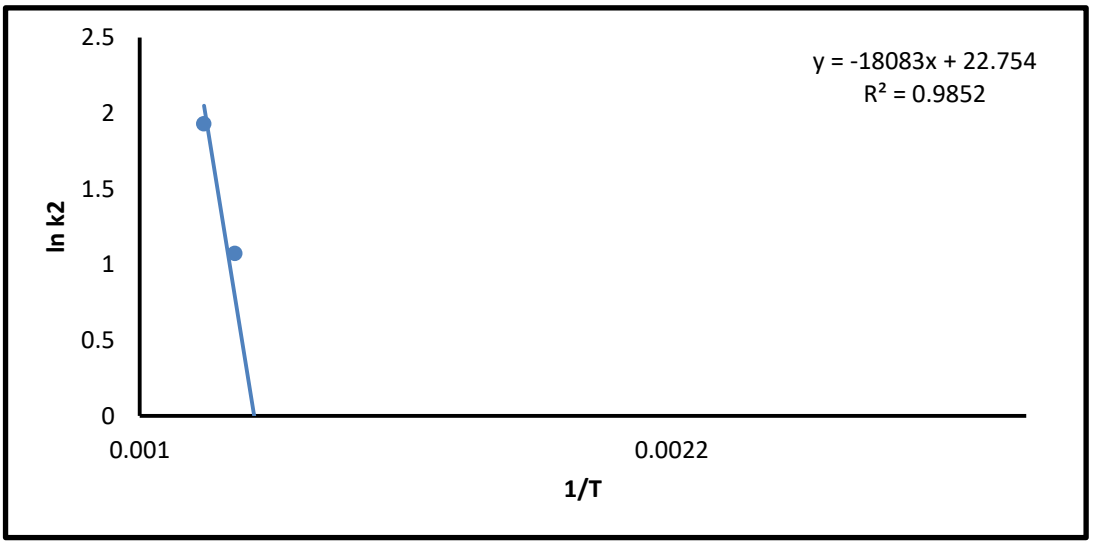

Fig (4.28). the plots of ln (k_2/T) ageinst 1/T

The plot of [ln k_2 vs 1/T] , the slope of -18083 represent (E_a/R) , from which the energy of activation was calculated as 150.34 kJ/mole.

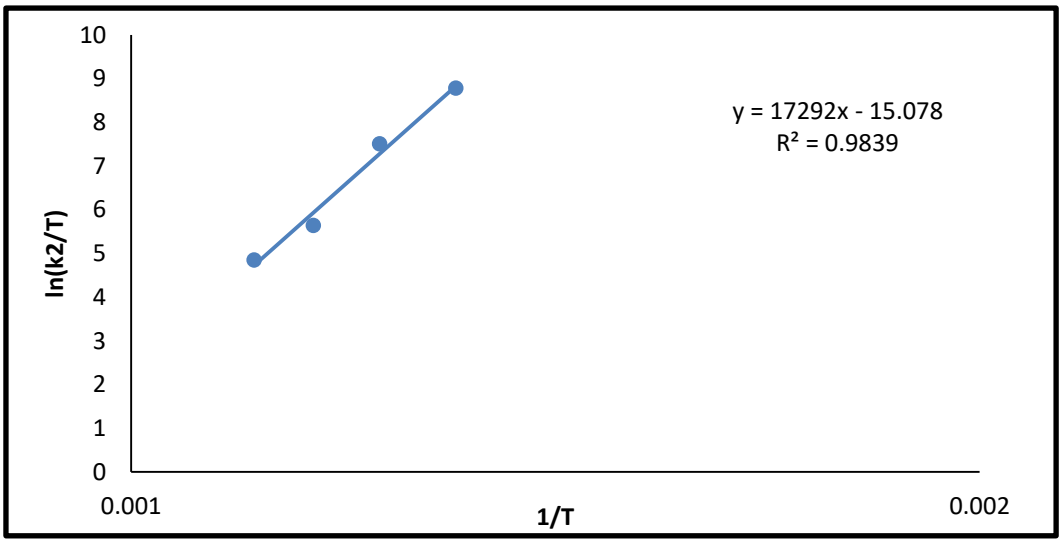

Fig (4.29). the plots of ln (k_2/T) ageinst 1/T

Plot of [ln(k_2/T) vs 1/T] yield slope of (ΔH/R) and intercept of [ln(K_b/h) + ΔS/R] The same method is followed to calculate the enthalpy and entropy energy for the second order **equations (4.8)** and **(4.9)** .

Table (4.8) shows the values of energy of activation and thermodynamic functions ΔH and ΔS being calculated.

Table (4.8) Values of E_a , ΔH and ΔS for spent catalyst carbon removal .

	E_a, kJ/mole	ΔH, kJ/mole	ΔS,kJ/mole
First order	66.144	59.559	-0.184
Second order	150.342	143.765	- 0.322

The results shown as the correlation coefficient R^2 is higher that is mean the reaction is the first order kinetic.

4.5. Conclusions

1- Using impregnation / incipient wetness route is a very good method for preparing ($NiMo/Al_2O_3$) catalyst with small nano size .

2 - X-ray diffraction revealed that the obtained particle size is (11.903 nm) for the prepared ($NiMo/Al_2O_3$) catalyst in the nano range .

3- Some changes in the composition, particle size and shape of the new and spent catalyst were observed when comparing them.

4 - The spent catalyst was deactivated by treatment with toluene , benzene and carbon disulfide, the carbon and some metals were removed from it.

5 - The metal content of the spent catalyst were known and compared with the new catalyst.

6 - There is an increase in the metal content of the spent catalysts.

7 - There are changes in the physical properties such as densities, porosity, pore size, etc. for new and spent catalysts .

8 - The kinetics of carbon removal from spent catalyst follow a first-order model equation.

4.6. Future Studies

1 - Conduct a spectroscopic study on other catalysts such as reforming , cracking , isomerization zeolites and investigate in more causes of catalyst deactivation .

2 - Preparing catalysts in other is easier and faster ways .

3 - Calculation of the carbon removal rate at higher temperatures and other conditions .

4 - Calculating the percentage of carbon removal using the thermo gravimetric analysis (TGA) technique .

5 - Metal recovery from spent catalysts after treatment such as reforming , catalyst .

6 - Intensification of studies on the mechanism of removing carbon and metals from catalysts.

7- The kinetic study of carbon removal from new catalyst .

References

1- Oza, R., Shah, N., & Patel, S. (2011). ***Recovery of nickel from spent catalysts using ultrasonication-assisted leaching.*** Journal of Chemical Technology & Biotechnology, 86(10), 1276-1281.

2- Bezergianni, S., & Kalogianni, A. (2008***). Application of principal component analysis for monitoring and disturbance detection of a hydrotreating process.*** Industrial & engineering chemistry research, 47(18), 6972-6982.

3- Marafi, M., & Stanislaus, A. (2003). ***Studies on rejuvenation of spent residue hydroprocessing catalysts by leaching of metal foulants.*** Journal of Molecular Catalysis A: Chemical, 202(1-2), 117-125.

4- Al-Sheeha, Marafi, M., H., Al-Omani, S., & Al-Barood, A. (2009). ***Activity of hydroprocessing catalysts prepared by reprocessing spent catalysts.*** Fuel processing technology, 90(2), 264-269.

5- Mizuno, N. (Ed.). (2009). ***Modern heterogeneous oxidation catalysis: design, reactions and characterization.*** John Wiley & Sons.

6- Coulier, L. (2001). ***Hydrotreating model catalysts: from characterization to kinetics.*** Eindhoven: Technische Universiteit Eindhoven.

7- Moqadam, S. I., & Mahmoudi, M. (2013). ***Advent of nanocatalysts in hydrotreating process: benefits and developments***. American Journal of Oil and Chemical Technologies, 1(2), 13-21.

8- Centeno, G., Ancheyta, J., Alvarez, A., Marroquín, G., Alonso, F., & Castillo, A. (2012). ***Effect of different heavy feedstocks on the deactivation of a commercial hydrotreating catalyst.*** Fuel, 100, 73-79.

9- Boudart, M. (2014). ***Kinetics of Chemical Processes:*** Butterworth-Heinemann Series in Chemical Engineering. Elsevier.

10- Alonso, G., & Chianelli, R. R. (2004). ***WS2 catalysts from tetraalkyl thiotungstate precursors and their concurrent in situ activation during HDS of DBT.*** Journal of Catalysis, 221(2), 657-661.

11- Marafi, M., Stanislaus, A., & Kam, E. (2008). ***A preliminary process design and economic assessment of a catalyst rejuvenation process for waste disposal of refinery spent catalysts.*** Journal of environmental management, 86(4), 665-681.

12- Valverde Jr, I. M., Paulino, J. F., & Afonso, J. C. (2008). ***Hydrometallurgical route to recover molybdenum, nickel, cobalt and aluminum from spent hydrotreating catalysts in sulphuric acid medium.*** Journal of Hazardous Materials, 160(2-3), 310-317.

13- Jarullah, A. T., Mujtaba, I. M., & Wood, A. S. (2011). ***Kinetic model development and simulation of simultaneous hydrodenitrogenation and hydrodemetallization of crude oil in trickle bed reactor.*** Fuel, 90(6), 2165-2181.

14- Sharma, G., Kripesh, V., Sim, M. C., & Sow, C. H. (2007). ***Synthesis and characterization of patterned and nonpatterned copper and nickel nanowire arrays on silicon substrate.*** Sensors and Actuators A: Physical, 139(1-2), 272-280.

15- Dufresne, P. (2007). ***Hydroprocessing catalysts regeneration and recycling.*** Applied Catalysis A: General, 322, 67-75.

16- Pereira, A. L. D. S., Silva, C. N. D., Afonso, J. C., & Mantovano, J. L. (2011). ***The importance of pre-treatment of spent hydrotreating catalysts on metals recovery.*** Química Nova, 34(1), 145-150.

17- Wang, X., Zhao, Z., Zheng, P., Chen, Z., Duan, A., Xu, C., & Ge, B. (2016). ***Synthesis of NiMo catalysts supported on mesoporous Al2O3 with different crystal forms and superior catalytic performance for the hydrodesulfurization of dibenzothiophene and 4, 6-dimethyldibenzothiophene.*** Journal of Catalysis, 344, 680-691.

18- Soni, K., Rana, B. S., Sinha, A. K., Bhaumik, A., Nandi, M., Kumar, M., & Dhar, G. M. (2009). ***3-D ordered mesoporous KIT-6 support for effective hydrodesulfurization catalysts.*** Applied Catalysis B: Environmental, 90(1-2), 55-63.

19- Corma, A., Martınez, A., & Martınez-Soria, V. (1997). ***Hydrogenation of aromatics in diesel fuels on Pt/MCM-41 catalysts.*** Journal of Catalysis, 169(2), 480-489.

20- Alamoudi, M. (2016). Hydrodesulphurization of dibenzothiophene using carbon supported NiMoS catalysts (Doctoral dissertation, University of British Columbia).

21- Kaluža, L., & Zdražil, M. (2007). ***Preparation of bimetallic CoO-MoO 3/γ-Al 2 O 3 and NiO-MoO 3/γ-Al 2 O 3 hydrodesulfurization catalysts by deposition of Co, Ni and Mo onto α-AlOOH during paste processing.*** Reaction Kinetics and Catalysis Letters, 91(2), 249-255.

22- Guichard, B., Roy-Auberger, M., Devers, E., Rebours, B., Quoineaud, A. A., & Digne, M. (2009). ***Characterization of aged hydrotreating catalysts. Part I: Coke depositions, study on the chemical nature and environment.*** Applied Catalysis A: General, 367(1-2), 1-8.

23- Vakros, J., Lycourghiotis, A., Voyiatzis, G. A., Siokou, A., & Kordulis, C. (2010). ***CoMo/Al2O3-SiO2 catalysts prepared by co-equilibrium deposition filtration: Characterization and catalytic behavior for the hydrodesulphurization of thiophene.*** Applied Catalysis B: Environmental, 96(3-4), 496-507.

24- Ahmed, A. J., Hassan, K. H., & Dawood, A. F. (2018). ***Adsorption of Lead (II) Ions on Rejuvenated NIMo/γAl2O3 Spent Hydrodesulfurization Catalyst.*** Journal of Biochemical Technology, 9(3), 17.

25- Kubicka, D., & Horáček, J. (2011). ***Deactivation of HDS catalysts in deoxygenation of vegetable oils.*** Applied Catalysis A: General, 394(1-2), 9-17.

26- Karim, M. R., Rahman, M. A., Miah, M. A. J., Ahmad, H., Yanagisawa, M., & Ito, M. (2011). ***Synthesis of γ-alumina particles and surface characterization.*** The Open Colloid Science Journal, 4(1),32-36.

27- Pacheco, M. E., Martins Salim, V. M., & Pinto, J. C. (2011). ***Accelerated deactivation of hydrotreating catalysts by coke deposition.*** Industrial & engineering chemistry research, 50(10), 5975-5981.

28- Zhang, J., Zhang, H., Yang, X., Huang, Z., & Cao, W. (2011). ***Study on the deactivation and regeneration of the ZSM-5 catalyst used in methanol to olefins.*** Journal of natural gas chemistry, 20(3), 266-270.

29- Mitozo, P. A., de Souza, L. F., Loch-Neckel, G., Flesch, S., Maris, A. F., Figueiredo, C. P., ... & Dafre, A. L. (2011). ***A study of the relative importance of the peroxiredoxin-, catalase-, and glutathione-dependent systems in neural peroxide metabolism.*** Free Radical Biology and Medicine, 51(1), 69-77.

30- Sun, Y. D., Yang, C. H., & Liu, Z. Y. (2012). ***Properties Analysis of Spent Catalyst for Fixed-Bed Residue Hydrotreating Unit:*** Composition of Deposited Elements Along Catalyst Bed. Energy Science and Technology, 4(1), 34-40.

31- Rahmanpour, O., Shariati, A., & Nikou, M. R. K. (2012).***New Method for Synthesis Nano Size [gamma]-Al2O3 Catalyst for Dehydration of Methanol to Dimethyl Ether.*** International Journal of Chemical Engineering and Applications, 3(2), 125-128.

32- Behnejad, B., Abdouss, M., & Tavasoli, A. (2019). ***Comparison of performance of Ni–Mo/γ-alumina catalyst in HDS and HDN reactions of main distillate fractions.*** Petroleum Science, 16(3), 645-656.

33- Bleken, F. L., Barbera, K., Bonino, F., Olsbye, U., Lillerud, K. P., Bordiga, S., & Svelle, S. (2013). ***Catalyst deactivation by coke formation in microporous and desilicated zeolite H-ZSM-5 during the conversion of methanol to hydrocarbons.*** Journal of catalysis, 307, 62-73.

34- Ahn, C. I., Koo, H. M., Jin, M., Kim, J. M., Kim, T., Suh, Y. W., & Bae, J. W. (2014). ***Catalyst deactivation by carbon formation during CO hydrogenation to hydrocarbons on mesoporous Co3O4.*** Microporous and Mesoporous materials, 188, 196-202.

35- Yi, X., Guo, D., Li, P., Lian, X., Xu, Y., Dong, Y., & Fang, W. (2017). ***One pot synthesis of NiMo–Al 2 O 3 catalysts by solvent-free solid-state method for hydrodesulfurization.*** RSC advances, 7(86), 54468-54474.

36- Tavizón-Pozos, J. A., Suárez-Toriello, V. A., Del Ángel, P., & de Los Reyes, J. A. (2016). ***Hydrodeoxygenation of phenol over sulfided CoMo catalysts supported on a mixed Al2O3-TiO2 oxide.*** International Journal of Chemical Reactor Engineering, 14(6), 1211-1223.

37- Kim, H. K., Lee, C. W., Kim, M., Oh, J. H., Song, S. A., Jang, S. C, & Ham, H. C. (2016). ***Preparation of CoMo/Al2O3, CoMo/CeO2, CoMo/TiO2 catalysts using ultrasonic spray pyrolysis for the hydro-desulfurization of 4, 6-dimethyldibenzothiophene for fuel cell applications.*** International Journal of Hydrogen Energy, 41(41), 18846-18857.

38- Mohamed, A. H. A., & Atta, H. H. (2016). ***Synthesis Of Nano Ni-Mo/γ-Al2O3 CatalystSynthesis Of Nano Ni-Mo/γ-Al2O3 Catalyst.*** Iraqi Journal of Chemical and Petroleum Engineering, 17(4), 11-23.

39- Hassan, K. H., Jarullah, A. A., & Saadi, S. K. (2017). ***Synthesis of copper oxide nanoparticle as an adsorbent for removal of Cd (II) and Ni (II) ions from binary system.*** International journal of applied environmental sciences, 12(11), 1841-1861.

40- Jbara, A. S., Othaman, Z., Ati, A. A., & Saeed, M. A. (2017). Characterization of γ-Al2O3 nanopowders synthesized by Co-precipitation method. Materials Chemistry and Physics, 188, 24-29.

41- Tabesh, S., Davar, F., & Loghman-Estarki, M. R. (2018). ***Preparation of γ-Al2O3 nanoparticles using modified sol-gel method and its use for the adsorption of lead and cadmium ions.*** Journal of Alloys and Compounds, 730, 441-449.

42- Munguía-Guillén, J. L., de los Reyes-Heredia, J. A., Picquart, M., Vera-Ramírez, M. A., & Viveros-García, T. (2018). ***CoMo/γ-Al 2 O 3 Catalysts Prepared by Reverse Microemulsion: Synthesis and Characterization.*** In Microemulsion-a Chemical Nanoreactor. IntechOpen.

43- Pimerzin, A., Roganov, A., Mozhaev, A., Maslakov, K., Nikulshin, P., & Pimerzin, A. (2018). ***Active phase transformation in industrial CoMo/Al2O3 hydrotreating catalyst during its deactivation and rejuvenation with organic chemicals treatment.*** Fuel Processing Technology, 173, 56-65.

44- Stummann, M. Z., Høj, M., Hansen, A. B., Beato, P., Wiwel, P., Gabrielsen, J., & Jensen, A. D. (2019). ***Deactivation of a CoMo Catalyst during Catalytic Hydropyrolysis of Biomass. Part 1. Product Distribution and Composition.*** Energy & Fuels, 33(12), 12374-12386.

45- Liu, Z., Han, W., Hu, D., Sun, S., Hu, A., Wang, Z., ... & Yang, Q. (2020). ***Effects of Ni–Al2O3 interaction on NiMo/Al2O3 hydrodesulfurization catalysts.*** Journal of Catalysis, 387, 62-72.

46- Kohli, K., Prajapati, R., Maity, S. K., & Sharma, B. K. (2020). ***Effect of Silica, Activated Carbon, and Alumina Supports on NiMo Catalysts for Residue Upgrading.*** Energies, 13(18), 4967.

47- Hamidi, R., Khoshbin, R., & Karimzadeh, R. (2020). ***Fabrication of Nimo Nanostructured Catalyst via Ultrasonic-Assisted Combustion Method Used in High Efficiency Thiophene Hydrodesulfurization:*** Influence of Organic Compound Type .

48- Hemalatha, K., Madhumitha, G., Kajbafvala, A., Anupama, N., Sompalle, R., & Mohana Roopan, S. (2013). ***Function of nanocatalyst in chemistry of organic compounds revolution: an overview.*** Journal of Nanomaterials, 2013.

49- Ryoo, R., & Jun, S. (1997). ***Improvement of hydrothermal stability of MCM-41 using salt effects during the crystallization process.*** The Journal of Physical Chemistry B, 101(3), 317-320.

50- Polshettiwar, V., & Varma, R. S. (2010). ***Green chemistry by nano-catalysis.*** Green Chemistry, 12(5), 743-754.

51- Gawande, M. B., Branco, P. S., & Varma, R. S. (2013). ***Nano-magnetite (Fe3O4) as a support for recyclable catalysts in the development of sustainable methodologies.*** Chemical Society Reviews, 42(8), 3371-3393.

52- Farag, H., El-Hendawy, A. N. A., Sakanishi, K., Kishida, M., & Mochida, I. (2009). ***Catalytic activity of synthesized nanosized molybdenum disulfide for the hydrodesulfurization of dibenzothiophene: Effect of H2S partial pressure.*** Applied Catalysis B: Environmental, 91(1-2), 189-197.

53- Kobayashi, Y., Horiguchi, J., Kobayashi, S., Yamazaki, Y., Omata, K., Nagao, D., ... & Yamada, M. (2011). ***Effect of NiO content in mesoporous NiO–Al2O3 catalysts for high pressure partial oxidation of methane to syngas.*** Applied Catalysis A: General, 395(1-2), 129-137.

54- Daroughegi, R., Meshkani, F., & Rezaei, M. (2020). ***Characterization and evaluation of mesoporous high surface area promoted Ni-Al2O3 catalysts in CO2 methanation.*** Journal of the Energy Institute, 93(2), 482-495.

55- Yi, X., Guo, D., Li, P., Lian, X., Xu, Y., Dong, Y., & Fang, W. (2017). ***One pot synthesis of NiMo–Al 2 O 3 catalysts by solvent-free solid-state method for hydrodesulfurization.*** RSC advances, 7(86), 54468-54474.

56- Turányi, T., & Tomlin, A. S. (2014). ***Analysis of kinetic reaction mechanisms***. (Vol. 20). Berlin, Germany: Springer Berlin Heidelberg.

57- Richardson, J. T. (2013). ***Principles of catalyst development.*** Springer.

58- Shi, Y., Chen, J., Chen, J., Macleod, R. A., & Malac, M. (2012). ***Preparation and evaluation of hydrotreating catalysts based on activated carbon derived from oil and petroleum coke.*** Applied Catalysis A: General, 441, 99-107.

59- De León, M. A., Castiglioni, J., Bussi, J., & Sergio, M. (2008). ***Catalytic activity of an iron-pillared montmorillonitic clay mineral in heterogeneous photo-Fenton process.*** Catalysis Today, 133, 600-605.

60- Liu, Q., Gao, J., Gu, F., Lu, X., Liu, Y., Li, H., & Su, F. (2015). ***One-pot synthesis of ordered mesoporous Ni–V–Al catalysts for CO methanation.*** Journal of Catalysis, 326, 127-138.

61- Speight, J. G. (1999). ***The chemistry and technology of petroleum.*** CRC press.

62- Iwamoto, R. (2013). ***Regeneration of Residue Hydrodesulfurization Catalyst.*** Journal of the Japan Petroleum Institute, 56(3), 109-121.

63- An, N., Yuan, X., Pan, B., Li, Q., Li, S., & Zhang, W. (2014). ***Design of a highly active Pt/Al_2O_3 catalyst for low-temperature CO oxidation.*** RSC advances, 4(72), 38250-38257.

64- Abed, A. N., & Sabri, B. A. (2017). ***Microstructure and density characterization for nano and micro alumina-aluminum composites produced by powder metallurgy process.*** Al-Nahrain Journal for Engineering Sciences, 20(5), 1024-1033.

65- Ahmed, A.J. (2012). ***Synthesis and Characterization of Gold, Silver, Copper, and Platinum Nanoparticles by using Anodic Aluminum Oxide Template .*** M.Sc. thesis, College of Science for Women, University of Baghdad, Iraq

66- Chen, F., Jiang, X., Zhang, L., Lang, R., & Qiao, B. (2018). ***Single-atom catalysis: Bridging the homo-and heterogeneous catalysis.*** Chinese Journal of Catalysis, 39(5), 893-898.

67- Murzin, D. Y. (2020). ***Engineering catalysis.*** de Gruyter.

68- Verstraete, J. J., Le Lannic, K., & Guibard, I. (2007). ***Modeling fixed-bed residue hydrotreating processes.*** Chemical engineering science, 62(18-20), 5402-5408.

69- Rana, M. S., Ancheyta, J., Maity, S. K., & Rayo, P. (2007). ***Hydrotreating of Maya crude oil: I. Effect of support composition and its pore-diameter on asphaltene conversion.*** Petroleum science and technology, 25(1-2), 187-199.

70- Bose, D. (2015). ***Design parameters for a hydro desulfurization (HDS) unit for petroleum naphtha at 3500 barrels per day.*** World Scientific News, (9), 99-111.

71- Boniek, D., Figueiredo, D., dos Santos, A. F. B., & de Resende Stoianoff, M. A. (2015). ***Biodesulfurization: a mini review about the immediate search for the future technology.*** Clean Technologies and Environmental Policy, 17(1), 29-37.

72- Chianelli, R. R., Berhault, G., & Torres, B. (2009). ***Unsupported transition metal sulfide catalysts: 100 years of science and application.*** Catalysis Today, 147(3-4), 275-286.

73- Amaya, S. L., Alonso-Núñez, G., Zepeda, T. A., Fuentes, S., & Echavarría, A. (2014). ***Effect of the divalent metal and the activation temperature of NiMoW and CoMoW on the dibenzothiophene hydrodesulfurization reaction***. Applied Catalysis B: Environmental, 148, 221-230.

74- Liu, H., Yin, C., Li, H., Liu, B., Li, X., Chai, Y., & Liu, C. (2014). ***Synthesis, characterization and hydrodesulfurization properties of nickel–copper–molybdenum catalysts for the production of ultra-low sulfur diesel.*** Fuel, 129, 138-146.

75- Walton, A. S., Lauritsen, J. V., Topsøe, H., & Besenbacher, F. (2013). ***MoS2 nanoparticle morphologies in hydrodesulfurization catalysis studied by scanning tunneling microscopy.*** Journal of catalysis, 308, 306-318.

76- Furimsky, E., & Massoth, F. E. (1999). ***Deactivation of hydroprocessing catalysts.*** Catalysis Today, 52(4), 381-495.

77- Fu, W., Zhang, L., Tang, T., Ke, Q., Wang, S., Hu, J., & Xiao, F. S. (2011). ***Extraordinarily high activity in the hydrodesulfurization of 4, 6-dimethyldibenzothiophene over Pd supported on mesoporous zeolite Y.*** Journal of the American Chemical Society, 133(39), 15346-15349.

78- Liu, H., Li, Y., Yin, C., Wu, Y., Chai, Y., Dong, D., ... & Liu, C. (2016). ***One-pot synthesis of ordered mesoporous NiMo-Al2O3 catalysts for dibenzothiophene hydrodesulfurization.*** Applied Catalysis B: Environmental, 198, 493-507.

79- Marafi, M., Stanislaus, A., & Furimsky, E. (2017). ***Handbook of spent hydroprocessing catalysts.*** Elsevier.

80- Rana, M. S., Ancheyta, J., Maity, S. K., & Rayo, P. (2008). ***Heavy crude oil hydroprocessing: A zeolite-based CoMo catalyst and its spent catalyst characterization.*** Catalysis today, 130(2-4), 411-420.

81- Moqadam, S. I., & Mahmoudi, M. (2013). ***Advent of nanocatalysts in hydrotreating process: benefits and developments.*** American Journal of Oil and Chemical Technologies, 1(2), 13-21.

82- Aljamali, N. M., & Ahmed, H. A. (2020). ***Review in Effect of Catalysis in Any Organic Reaction.*** International Journal of Innovations in Scientific Engineering, 7-17.

83- Lee, S. W., Ryu, J. W., & Min, W. (2003). ***SK hydrodesulfurization (HDS) pretreatment technology for ultralow sulfur diesel (ULSD) production.*** Catalysis Surveys from Asia, 7(4), 271-279.

84- Gao, Q., Ofosu, T. N., Ma, S. G., Komvokis, V. G., Williams, C. T., & Segawa, K. (2011). ***Catalyst development for ultra-deep hydrodesulfurization (HDS) of dibenzothiophenes. I: Effects of Ni promotion in molybdenum-based catalysts.*** Catalysis Today, 164(1), 538-543..

85- Richardson, J. T. (2013). ***Principles of catalyst development.*** Springer.

86- Athy, L. F. (1930***). Density, porosity, and compaction of sedimentary rocks.*** Aapg Bulletin, 14(1), 1-24.

87- Robertson, S. (2011). ***Direct estimation of organic matter by loss on ignition: methods.*** SFU Soil Science Lab, 1-11.

88- Narayanasarma, P. (2011). ***Mesoporous carbon supported NiMo catalyst for the hydrotreating of coker gas oil***. (Doctoral dissertation, University of Saskatchewan).

89- Bartholomew, C. H. (2001). ***Mechanisms of catalyst deactivation.*** Applied Catalysis A: General, 212(1-2), 17-60.

90- Thakur, D. S., & Thomas, M. G. (1985). ***Catalyst deactivation in heavy petroleum and synthetic crude processing:*** a review. Applied catalysis, 15(2), 197-225.

91- Furimsky, E., & Massoth, F. E. (1999). ***Deactivation of hydroprocessing catalysts.*** Catalysis Today, 52(4), 381-495.

92- Sahoo, S. K., Ray, S. S., & Singh, I. D. (2004). ***Structural characterization of coke on spent hydroprocessing catalysts used for processing of vacuum gas oils.*** Applied Catalysis A: General, 278(1), 83-91.

93- Argyle, M. D., & Bartholomew, C. H. (2015). ***Heterogeneous catalyst deactivation and regeneration: a review.*** Catalysts, 5(1), 145-269.

94- Ochoa, A., Bilbao, J., Gayubo, A. G., & Castaño, P. (2020). ***Coke formation and deactivation during catalytic reforming of biomass and waste pyrolysis products: A review.*** Renewable and Sustainable Energy Reviews, 119, 109600.

95- Moulijn, J. A., Van Diepen, A. E., & Kapteijn, F. (2001***). Catalyst deactivation: is it predictable?: What to do?.*** Applied Catalysis A: General, 212(1-2), 3-16.

96- Grams, J., & Ruppert, A. M. (2021). ***Catalyst Stability—Bottleneck of Efficient Catalytic Pyrolysis.*** Catalysts, 11(2), 265.

97- Tamm, P. W., Harnsberger, H. F., & Bridge, A. G. (1981). ***Effects of feed metals on catalyst aging in hydroprocessing residuum.*** Industrial & Engineering Chemistry Process Design and Development, 20(2), 262-273.

98- Oh, E. S., Park, Y. C., Lee, I. C., & Rhee, H. K. (1997). ***Physicochemical changes in hydrodesulfurization catalysts during oxidative regeneration.*** Journal of Catalysis, 172(2), 314-321.

99- Yung, M. M., Magrini-Bair, K. A., Parent, Y. O., Carpenter, D. L., Feik, C. J., Gaston, K. R., & Phillips, S. D. (2010). ***Demonstration and characterization of Ni/Mg/K/AD90 used for pilot-scale conditioning of biomass-derived syngas.*** Catalysis letters, 134(3), 242-249.

100- Kuhn, J. N., Zhao, Z., Senefeld-Naber, A., Felix, L. G., Slimane, R. B., Choi, C. W., & Ozkan, U. S. (2008). ***Ni-olivine catalysts prepared by thermal impregnation: Structure, steam reforming activity, and stability.*** Applied Catalysis A: General, 341(1-2), 43-49.

101- Sadeek, S. A., Ahmed, H. S., ElShamy, E. A., El Sayed, H. A., & Abd El Rahman, A. A. (2014). ***Hydrotreating of waste lube oil by rejuvenated spent hydrotreating catalyst.*** Egyptian Journal of Petroleum, 23(1), 53-60.

102- Dufresne, P. (2007). ***Hydroprocessing catalysts regeneration and recycling.*** Applied Catalysis A: General, 322, 67-75.

103- Eijsbouts, S. (1999). ***Life cycle of hydroprocessing catalysts and total catalyst management.*** In Studies in surface science and catalysis , (21-36). Elsevier.

104- Hauser, A., Marafi, A., Almutairi, A., & Stanislaus, A. (2008). ***Comparative study of hydrodemetallization (HDM) catalyst aging by Boscan feed and Kuwait atmospheric residue.*** Energy & fuels, 22(5), 2925-2932.

105- Gao, D., Duan, A., Zhang, X., Zhao, Z., Hong, E., Li, J., & Wang, H. (2015). ***Synthesis of NiMo catalysts supported on mesoporous Al-SBA-15 with different morphologies and their catalytic performance of DBT HDS.*** Applied Catalysis B: Environmental, 165, 269-284.

106- Dufresne, P., & Brahma, N. (1995). ***Off-site Regeneration of Hydroprocessing Catalysts.*** Bulletin des Sociétés Chimiques Belges, 104(4-5), 339-346.

107- Teixeira da Silva, V. L. S., Frety, R., & Schmal, M. (1994). ***Activation and regeneration of a $NiMo/Al_2O_3$ hydrotreatment catalyst.*** Industrial & engineering chemistry research, 33(7), 1692-1699.

108- Khodayari, R., & Odenbrand, C. I. (2001). ***Regeneration of commercial SCR catalysts by washing and sulphation: effect of sulphate groups on the activity.*** Applied Catalysis B: Environmental, 33(4), 277-291.

109- Khodayari, R., & Odenbrand, C. I. (2001). ***Regeneration of commercial TiO2-V2O5-WO3 SCR catalysts used in bio fuel plants.*** Applied Catalysis B: Environmental, 30(1-2), 87-99.

110- Lambrou, P. S., Christou, S. Y., Fotopoulos, A. P., Foti, F. K., Angelidis, T. N., & Efstathiou, A. M. (2005). ***The effects of the use of weak organic acids on the improvement of oxygen storage and release properties of aged commercial three-way catalysts.*** Applied Catalysis B: Environmental, 59(1-2), 1-11.

111- Christou, S. Y., Birgersson, H., & Efstathiou, A. M. (2007). ***Reactivation of severely aged commercial three-way catalysts by washing with weak EDTA and oxalic acid solutions.*** Applied Catalysis B: Environmental, 71(3-4), 185-198.

112- Rasmussen, S. B., Kustov, A., Due-Hansen, J., Siret, B., Tabaries, F., & Fehrmann, R. (2006). ***Characterization and regeneration of Pt-catalysts deactivated in municipal waste flue gas.*** Applied Catalysis B: Environmental, 69(1-2), 10-16.

113- Bui, N. Q., Geantet, C., & Berhault, G. (2015). ***Maleic acid, an efficient additive for the activation of regenerated CoMo/Al2O3 hydrotreating catalysts.*** Journal of Catalysis, 330, 374-386.

114- Müller, S., Liu, Y., Vishnuvarthan, M., Sun, X., van Veen, A. C., Haller, G. L., & Lercher, J. A. (2015). **Coke formation and deactivation pathways on H-ZSM-5 in the conversion of methanol to olefins.** Journal of Catalysis, 325, 48-59.

115- Rodríguez, J. A., Hanson, J. C., & Chupas, P. J. (Eds.). (2013). ***In-situ characterization of heterogeneous catalysts.*** John Wiley & Sons.

116- Ma, Z., & Zaera, F. (2006). ***Characterization of heterogeneous catalysts.*** Surface and Nanomolecular Catalysis, 1-37.

117- Griffiths, P. R., & De Haseth, J. A. (2007). ***Fourier transform infrared spectrometry (Vol. 171).*** John Wiley & Sons.

118- Graves, P. R. G. D. J., & Gardiner, D. (1989). ***Practical raman spectroscopy.*** Springer.

119- Coats, A. W., & Redfern, J. P. (1963). ***Thermogravimetric analysis.*** A review. Analyst, 88(1053), 906-924.

120- Walsh, A. (1955). ***The application of atomic absorption spectra to chemical analysis.*** Spectrochimica Acta, 7, 108-117.

121- Stokes, D. (2008). ***Principles and practice of variable pressure/environmental scanning electron microscopy (VP-ESEM).*** John Wiley & Sons.

122- Goldstein, J. (Ed.). (2012). ***Practical scanning electron microscopy: electron and ion microprobe analysis.*** Springer Science & Business Media.

123- Lang, K. M., Hite, D. A., Simmonds, R. W., McDermott, R., Pappas, D. P., & Martinis, J. M. (2004). ***Conducting atomic force microscopy for nanoscale tunnel barrier characterization.*** Review of scientific instruments, 75(8), 2726-2731.

124- Liu, F., Xu, S., Cao, L., Chi, Y., Zhang, T., & Xue, D. (2007). ***A comparison of NiMo/Al2O3 catalysts prepared by impregnation and coprecipitation methods for hydrodesulfurization of dibenzothiophene.*** The Journal of Physical Chemistry C, 111(20), 7396-7402.

125- Y. Song, H. Liu, S. Liu, D. He,(2009). ***Partial oxidation of methane to syngas over Ni/Al2O3 catalysts prepared by a modified sol-gel method***, Energy Fuels 23 ,1925–1930.

126- Moghny, T. A., Mohamed, A. M. G., Saleem, S. S., & Fathy, M. (2017). ***Abu Zenima synthetic zeolite for removing iron and manganese from Assiut governorate groundwater, Egypt.*** Applied Water Science, 7(6), 3087-3094.

127- Digne, M., Marchand, K., & Bourges, P. (2007). ***Monitoring hydrotreating catalysts synthesis and deactivation using Raman spectrometry.*** Oil & Gas Science and Technology-Revue de l'IFP, 62(1), 91-99.

128- Wang, X. L., Zhao, Z., Chen, Z. T., Li, J. M., Duan, A. J., Xu, C. M., & Fan, J. Y. (2017). ***Effect of synthesis temperature on structure-activity-relationship over NiMo/γ-Al2O3 catalysts for the hydrodesulfurization of DBT and 4, 6-DMDBT.*** Fuel processing technology, 161, 52-61.

129- Asadi, A. A., Alavi, S. M., Royaee, S. J., and Bazmi, M. (2018). ***Ultradeep Hydrodesulfurization of Feedstock Containing Cracked Gasoil through NiMo/γ-Al2O3 Catalyst Pore Size Optimization.*** Energy and Fuels, 32(2) : 2203-2212.

130- Maksumov, A., Vidu, R., Palazoglu, A., & Stroeve, P. (2004). ***Enhanced feature analysis using wavelets for scanning probe microscopy images of surfaces.*** Journal of colloid and interface science, 272(2), 365-377.

131- Gonzalez-Cortes, S. L., Rodulfo-Baechler, S. M., Xiao, T., & Green, M. L. (2006). ***Rationalizing the catalytic performance of γ-alumina-supported Co (Ni)–Mo (W) HDS catalysts prepared by urea-matrix combustion synthesis.*** Catalysis letters, 111(1), 57-66.

132- Huang, Y., Zhou, Z., Qi, Y., Li, X., Cheng, Z., & Yuan, W. (2011). ***Hierarchically macro-/mesoporous structured Co–Mo–Ni/γ-Al2O3 catalyst for the hydrodesulfurization of thiophene.*** Chemical Engineering Journal, 172(1), 444-451.

133- Ibrahim, D. M., & Abu-Ayana, Y. M. (2009). ***Preparation of nano alumina via resin synthesis.*** Materials Chemistry and Physics, 113(2-3), 579-586.

134- Tanimu, A., & Alhooshani, K. (2019). ***Advanced hydrodesulfurization catalysts: a review of design and synthesis.*** Energy & Fuels, 33(4), 2810-2838.

135- González, G. C., Murciano, R., Perales, A. V., Martínez, A., Vidal-Barrero, F., & Campoy, M. (2019). ***Ethanol conversion into 1, 3-butadiene over a mixed Hf-Zn catalyst: A study of the reaction pathway and catalyst deactivation.*** Applied Catalysis A: General, 570, 96-106.

136- Koizumi, N., Urabe, Y., Inamura, K., Itoh, T., & Yamada, M. (2005). ***Investigation of carbonaceous compounds deposited on NiMo catalyst used for ultra-deep hydrodesulfurization of gas oil by means of temperature-programmed oxidation and Raman spectroscopy.*** Catalysis today, 106(1-4), 211-218.

137- Menoufy, M. F., & Ahmed, H. S. (2008). ***Treatment and reuse of spent hydrotreating catalyst.*** Energy Sources, Part A, 30(13), 1213-1222.

138- Mohammed, A. H. A., & Hankish, K. (1985). ***Interpretation of hydrogenation kinetics of spent oil distillate from uv spectroscopy.*** Fuel, 64(7), 921-924.

139- Mutlag,. R.H. (2014). ***Characterizations of Nanostructure of Bucky Paper***. M.Sc. thesis, College of Science, University of Baghdad.

الخلاصة

تناولت هذه الرسالة دراسة فيزيائية وكيميائية واجراء مقارنة المحفز **$NiMo/\gamma\text{-}Al_2O_3$** الجديد والمستهلك والتحقيق والتعرف على ظاهرة فقدان الفعالية وتعطيل المحفزات باستخدام بعض من التقنيات والقياسات مثل استخدام التحليل الحراري الوزني (**TGA**)و تشتت الطاقة بالأشعة السينية (**EDX**) والمجهر الإلكتروني لمسح الانبعاث (**FESEM**) ومجهر القوة الذرية (**AFM**) و مطيافية الأشعة تحت الحمراء(**FTIR**) وتحليل رامان (**RAMAN**). حيث تم ملاحضة بعض التغييرات في تركيب وحجم الجسيمات وشكلها نتيجة الاستهلاك .

تم تحضير **nano $NiMo/\gamma\text{-}Al_2O_3$** باستخدام طريقة التشريب من كلوريد النيكل (كمصدر للنيكل) ومولبيدات الامونيوم (كمصدر للمولبيديوم) على الالومينا الجاهزة وتحت الكلسنة عند درجة حرارة ٥٠٠ درجة مئوية تم استخدام تقنية طيف الاشعة تحت الحمراء (**FTIR**) وتحليل رامان (**RAMAN**) والتحليل الحراري الوزني (**TGA**) و والمجهر الإلكتروني لمسح الانبعاث الميداني (**FESEM**) و تم تشخيص هذه العوامل المساعدة من خلال طيف حيود الاشعة السينية (**XRD**) حيث اظهرت النتائج ان حجم الجسيمات كانت (١١.٩٠٣) نانومتر للمحفز المحضر **nano $NiMo/\gamma\text{-}Al_2O_3$** .

تم اعادة تنشيط العامل المساعد المستهلك (**$NiMo/\gamma\text{-}Al_2O_3$**) عن طريق غسل المحفز بالبنزين اولا ثم بالتلوين عند درجة حرارة ٢٥ درجة مئوية ، ثم تعريض المحفز المجفف لثنائي كبريتيد الكاربون لمدة ١٢ ساعة و التكليس عند درجة حرارة ٤٥٠ درجة مئوية لإزالة كل الكاربون والكبريت المزال بالغسل المتبقي .تم تشخيص تركيب السطح باستخدام تقنية طيف الاشعة تحت الحمراء (**FTIR**) وتحليل رامان (**RAMAN**) والتحليل الحراري الوزني (**TGA**) و والمجهر الإلكتروني لمسح الانبعاث الميداني (**FESEM**) تشتت الطاقة بالأشعة السينية (**EDX**) .

تم تحديد المحتوى المعدني بطريقة الامتصاص الذري (**AAS**)حيث كانت هناك زيادة واضحة في محتوى العناصر في محفزات المستهلكة التي تأتي من التغذية للمفاعل والمواد المتفاعلة بالإضافة إلى تلك التي تأتي من تآكل المفاعل بسبب ظروف التشغيل القاسية والوقت.

وقد لوحظ ان هنالك تغيرات واضحة في الخواص الفيزيائية مثل الكثافة والمسامية للمحفزات الاولية مع استخدامها نتيجة لترسب الكربون والكبريت وبعض المعادن والتغير في مكوناته الهيكلية .

تم إجراء الدراسة الحركية لعملية إزالة الكربون على محفزات **$NiMo / Al_2O_3$** المستهلكة باستخدام ظروف عند درجات حرارة تكليس مختلفة (٧٢٣ ، ٧٧٣ ، ٨٢٣ و ٨٧٣ كلفن) وفترات زمنية مختلفة (٣٠ و ٦٠ و ٩٠ و ١٢٠ دقيقة).عند حساب قيم الدوال الثرموداينميكية لحركية ازالة الكاربون (**E_a,ΔH,ΔS**)،تبين انه تفاعل ماص للحرارة ،تم استخدام معادلتين حركية وهي معادلة من الدرجة الاولى ومعادلة من الدرجة الثانية وقد اشارت النتائج الى ان حركية ازالة الكاربون تخضع لمعادلة من مرتبة الاولى لان معامل الارتباط (**R^2**) قد اعطى افضل قيمة من معادلة المرتبة الثانية .

وزارة التعليم العالي والبحث العلمي

جامعة ديالى

كلية العلوم

قسم الكيمياء

الدراسة الطيفية والسطحية للعوامل المحفزة المعطلة والنانوية

رسالة مقدمة الى

مجلس كلية العلوم – جامعة ديالى

وهي جزء من متطلبات نيل شهادة الماجستير في علوم الكيمياء

من قبل الطالبة

براء اسعد لطوف

بكالوريوس في علوم الكيمياء 2018

بأشراف

أ.د. كريم هنيكش حسن

1443هجرية **العراق** **2021 ميلادية**